2012-12-12

Acoustic Emission Assessment of Steel Bridge Details Subjected to Fatigue

Navid Nemati
University of Miami, n.nemati@umiami.edu

UNIVERSITY OF MIAMI

ACOUSTIC EMISSION ASSESSMENT OF STEEL BRIDGE DETAILS SUBJECTED TO FATIGUE

By

Navid Nemati

A DISSERTATION

Submitted to the Faculty
of the University of Miami
in partial fulfillment of the requirements for
the degree of Doctor of Philosophy

Coral Gables, Florida

December 2012

UNIVERSITY OF MIAMI

A dissertation submitted in partial fulfillment of
the requirements for the degree of
Doctor of Philosophy

ACOUSTIC EMISSION ASSESSMENT OF STEEL BRIDGE DETAILS SUBJECTED TO FATIGUE

Navid Nemati

Approved:

Antonio Nanni, Ph.D. Professor and Chair of Civil, Architectural and Environmental Engineering	M. Brian Blake, Ph.D. Dean of the Graduate School
Brian Metrovich, Ph.D. Associate Professor of Civil, Architectural and Environmental Engineering	Paul Ziehl, Ph.D. Associate Professor of Civil & Environmental Engineering, University of South Carolina
Carol Hays, Ph.D Associate Professor of Civil, Architectural and Environmental Engineering	

NEMATI, NAVID (Ph.D., Civil Engineering)

Acoustic Emission
Assessment of Steel
Bridge Details Subjected To Fatigue

(December 2012)

Abstract of a dissertation at the University of Miami.

Dissertation supervised by Professor Antonio Nanni.
No. of pages in text. (111)

Acoustic Emission (AE) fatigue crack monitoring has the potential to provide early fatigue crack detection and assessment required to develop a rational prognostics methodology and can provide insight to assess the integrity of structures such as bridges. Most steel structures develop fatigue cracks at the transverse weld toe of stiffeners, attachments, and cover plates. The cracks develop from a combination of initial conditions (e.g. weld toe geometry, discontinuities, residual stress fields) that are difficult to accurately quantify, thus rendering fracture mechanics models for the prediction of fatigue crack growth exceedingly difficult without experimental verification.

Single edge notches provide a very well defined load and fatigue crack size and shape environment for estimation of the stress intensity factor K, which is not found in welded structures. ASTM SE(T) specimens do not appear to provide ideal boundary conditions for proper recording of acoustic wave propagation and crack growth behavior observed in the field, but do provide standard fatigue crack growth rate data. A modified version of the SE(T) specimen has been examined to provide small scale specimens with improved AE characteristics while still maintaining accuracy of fatigue crack growth rate da/dN versus stress intensity factor ΔK. The configuration of the modified SE(T) specimen maintains the similitude with the orientation of crack propagation in flanges of steel

bridge members. Testing of small scale single edge notch tension specimens is considered to assess load ratio (R ratio) and initial crack size effects on fatigue life of specimens. Fatigue tests are conducted at various R ratios to investigate the effect of load ratio on acoustic emission data. Stress Intensity Factor (SIF) models are extended to include expressions for crack tip opening displacement measured experimentally with a clip gauge. Correlation between fatigue crack growth, stress intensity factor and AE data is developed. Analytical and numerical studies of stress intensity factor are developed for single edge notch test specimens consistent with the experimental program. ABAQUS finite element software is utilized for stress analysis of crack tips.

Cruciform specimens consisting of a single tension pull plate with transverse fillet welded plates attached at midspan are tested. The transverse plates represent stiffeners and/or short attachments typical of steel bridge details. The specimen provides realistic initial conditions of fatigue crack initiation and growth from high stress concentration regions. Realistic AE waveform characteristics representative of those expected on bridge structures is produced. Accurate stress intensity factor values are more difficult to obtain due to the small, non-uniform crack growth conditions at the weld toe. Additional Finite Element Models for welded geometries capturing stress fields at the weld toe of stiffeners and attachment details is performed to examine crack depth, limited base plate thickness and weld toe angle effects on the relationship between stress intensity factor K and crack size, a. Numerical results are incorporated into an existing analytical stress intensity factor framework to minimize required computational costs.

As a result, the validity of Acoustic Emission (AE) as a parameter to assess, monitor and predict the structural health of infrastructure was verified. A methodology to combine AE

data and loading data with fracture models was developed to identify and evaluate existing condition (size and shape) and predict future behavior of fatigue cracks on a structure subject to well defined detail types. This will provide the ability to do prognostic using AE and will allow the prediction for the remaining life of the member based on the AE data.

To my fiancé Tala,

and my parents Kobra and Ahmad

with love and gratitude

ACKNOWLEDGEMENTS

This thesis would have remained a dream had it not been for love, support, friendship and guidance of many individuals that have shared the past three and half years with me.

I would like to give my love and thanks to my dear fiancé, Tala Shokri, for being there for me and giving me love and support every step of the way. Pursuit of my Ph.D. would not have been possible let alone joyful without her. I would like to thank my wonderful parents who made me who I am. I cannot thank them enough for supporting me and believing in me during hard times.

It is with immense gratitude that I acknowledge the support and help of my committee members. It gives me great pleasure in acknowledging the support and help of Professor Nanni who guided me through my research and taught me to think outside the box. His leadership and friendship made it possible. I owe my deepest gratitude to Dr. Metrovich who supported me and gave me great guidance and confidence whenever I needed it. Appreciation and gratitude also goes to Dr. Ziehl and Dr. Hays for their valuable technical contributions during my Ph.D. research.

This work was performed with the support of the U.S. Department of Commerce, National Institute of Standards and Technology, Technology Innovation Program, Cooperative Agreement Number 70NANB9H9007. I would like to thank them for their support and I hope my research has been worthy of their investment.

TABLE OF CONTENTS

LIST OF TABLES

LIST OF FIGURES

CHAPTER 1, INTRODUCTION

The majority of civil infrastructure (highways and bridges) in the US were constructed in the 1960's with a 50-year design life. Over the same time period, the average daily traffic and live load magnitude has increased significantly. According to the Federal Highway Administration (FHWA) National Bridge Inventory (NBI) of 2011 (FHWA, 2011), the number of structurally deficient and functionally obsolete bridges is 67,526 and 76,363 respectively. According to a study conducted by the ASCE Committee on Fatigue and Fracture Reliability (ASCE 1982), 80–90% of failures in steel bridges are related to fatigue and fracture. Fatigue cracks commonly develop at the transverse weld toe of stiffeners, attachments, and cover plates in steel bridge members (Fisher et al., 1979), (Metrovich et al., 2012). The cracks develop from a combination of initial conditions (e.g., weld toe geometry, discontinuities, and residual stress fields) that are difficult to accurately quantify, thus rendering fracture mechanics models for the prediction of fatigue crack growth exceedingly difficult without experimental verification (Metrovich and Fisher, 2005, 2006).

Non-destructive evaluation (NDE) of the crack extension is desirable to provide information to aid decision making for bridge management. NDE techniques such as visual inspection, ultrasonics, x-ray radiography, eddy current, magnetic particle and dye penetrant are unable to quantify the initial conditions of crack growth. In addition, most of the fatigue life is consumed while the fatigue crack is too small to be detected via such NDE techniques. Acoustic Emission (AE) monitoring of fatigue cracks has the potential to provide early fatigue crack detection and assessment required to develop a rational

prognostics methodology and can provide insight to assess the integrity of structures such as bridges (Gong and Nyborg, 1992), Martin et al., 1995), (Hamstad and Mccolskey, 1997) and (Ziehl, 2008). Acoustic emission (AE) is defined by (ASTM E1316, 2011) as "the class of phenomena whereby transient stress/displacement waves are generated by the rapid release of energy from localized sources". AE sources are defect-related processes such as crack extension and plasticization of material in the highly stressed zone adjacent to the crack tip (Roberts and Talebzadeh, 2003).

This research aims to develop a prognostic model that relates acoustic emission (AE) data to crack growth rate for steel specimens that are representative of details prone to fatigue and fracture in steel bridges. Studies on well-defined fatigue crack shapes have shown good correlation between AE and crack growth parameters, indicating that AE can assist in understanding the state of the crack and predicting its behavior due to fatigue loads (Roberts and Talebzadeh, 2003) and (Yu et al., 2011). To be able to develop a viable solution for AE assessment and prognosis of fatigue cracks initiated from transverse weld toes in steel bridge details, as a first step, a single edge notched tension (SE(T)) specimen is designed to provide a simplified situation in which AE and fracture mechanics parameters could be associated. The designed specimen provides a shallow, wide crack which better simulates fatigue cracks occurring in the flanges or early stage cracks in webs of steel bridge members. The testing protocol allows for the examination of small versus large crack depth influence on AE data for surface cracks. In order to properly understand the correlation between AE and fracture mechanics features in the modified SE(T) specimen, the effect of test parameters on the stress state of the crack is of significance. Both clevis and hydraulic wedge grips are used to apply the cyclic loading

to the specimen. Clevis grips can provide an ideal pin-pin condition for fatigue tests while hydraulic wedge gripping condition is commonly used in lab environment. Effects of gripping condition on correlation crack growth evolution was quantified and accounted for.

A test matrix of SE(T) specimens was designed to take into account the effects of variables as material, load ratio (R ratio), gripping conditions and different initial notch depths in specimen and the possible effects of these variables on AE data recorded during the fatigue crack growth. The AE data was used to develop a fundamental relationship between absolute energy rate of the AE signals and crack growth rate for through-thickness crack growth. Using this relationship, for the simplified case of SE(T) specimen, the fatigue life of a typical specimen is predicted by means of AE signal features.

As a final step, cruciform specimens are designed to provide realistic initial conditions of fatigue crack initiation and growth from high stress concentration regions. Cruciform specimens consisting of a single tension pull plate with transverse fillet welded plates attached at midspan are manufactured and fatigue tested. The transverse plates represent stiffeners and/or short attachments typical of steel bridge details. Realistic AE waveform characteristics representative of those expected on bridge structures was produced. The geometry of pull plate was chosen to be identical to the SE(T) specimens to provide consistency in wave path of AE signals.. FEM Models for welded geometries capturing stress fields at the weld toe of stiffener details were performed and numerical results were incorporated into an existing analytical stress intensity factor framework. The developed

fundamental relationship between absolute energy rate of the AE signals and crack growth rate using SE(T) tests is evaluated and refined for cruciform specimens.

The outcome of this research is a framework developed to combine AE data and loading data with fracture models to identify and evaluate existing condition (size and shape) and predict future behavior of fatigue cracks on a structure subject to well defined detail types. This will provide the ability to do prognostic using AE and will allow us to predict the remaining life of the member based on the AE data, thus reducing the dramatic uncertainty inherent into any inspection plan. The framework can be used to prioritize resources more efficiently, and to improve the decision making for maintenance and repair of bridges.

CHAPTER 2, STUDY 1 – EFFECTS OF TEST PARAMETERS ON FRACTURE AND FATIGUE CHARACTERISTICS OF A SE(T) STEEL SPECIMEN

SUMMARY

The understanding of crack behavior under fatigue remains a critical issue in addressing the performance of steel bridge structures. In this study, effects of test parameters on the stress intensity factor (K) of a modified single edge notched tension (SE(T)) steel specimen with a through width notch was experimentally, analytically and numerically investigated. Equations were developed to include the effects of fixed boundary condition on K and crack mouth opening displacement (CMOD) of the crack. Effects of axial and angular misalignments on K along the crack were examined and a progressively decreasing influence on K was observed when the crack size increased. Two dimensional (2D) and three dimensional (3D) Finite Element Method (FEM) was used to evaluate the effect of the two end bounding conditions on K value of non-uniform crack fronts. Influence of ungripped length of the specimen on K was evaluated and showed to be more substantial for short specimens. Finally, for a modified SE(T) specimen with initial crack inclination, a framework was proposed to map the crack front evolution through high cycle fatigue tests.

OUTLINE

Fatigue cracks develop at the transverse weld toe of stiffeners, attachments, and cover plates in steel bridge members. The cracks develop from a combination of initial conditions (e.g. weld toe geometry, discontinuities, residual stress fields) that are difficult

to accurately quantify, thus rendering fracture mechanics models for the prediction of fatigue crack growth exceedingly difficult without experimental verification ((Metrovich and Fisher, 2005, 2006). Single edge notches provide a very well defined load and fatigue crack size and shape environment, which is not found in welded structures, for estimation of the stress intensity factor (K). Nondestructive evaluation of the crack extension is desirable to provide information to decision making for bridge management. Acoustic emission (AE) fatigue crack monitoring has the potential to provide early fatigue crack detection and can provide insight to assess the integrity of structures such as bridges (Gong and Nyborg, 1992), Martin et al., 1995), (Hamstad and Mccolskey, 1997) and (Ziehl, 2008). Studies on well-defined fatigue crack shapes have shown good correlation between AE and crack growth parameters, indicating that AE can assist in understanding the state of the crack and predicting its behavior due to fatigue loads (Roberts and Talebzadeh, 2003) and (Yu et al., 2011). ASTM SE(T) specimens (ASTM E647-11e1, 2011) do provide standard fatigue crack growth rate data but do not appear to provide ideal boundary conditions for proper recording of acoustic wave propagation for through thickness crack growth behavior observed in the field. In steel bridge members, AE transducers are commonly attached to the same surface of plates from which the crack is initiated, hence producing a crack with through thickness growth monitored by the transducer. A modified version of the SE(T) specimen has been examined in order to maintain similitude with the orientation of crack propagation with reality. The specimen provides a crack with through thickness growth that simulates fatigue cracks through the flanges or early stage of crack growth in webs of steel bridge members.

The modified SE(T) specimen is designed to offer improved acoustic emission (AE) characteristics while still maintaining accuracy of fatigue crack growth rate (da/dN) versus stress intensity factor range (ΔK). In order to properly understand the correlation between AE and fracture mechanics features for the modified SE(T) specimen, the effect of test parameters on the stress state of the crack is of significance. Clevis and hydraulic wedge grips ideally apply pin-pin and fix-fix boundary condition to the specimen. Clevis grips can provide an ideal pin-pin condition for fatigue tests; however, in many cases fatigue crack growth, shear or bearing failure is likely to occur by the clevis hole in the specimen. The stress intensity factor for pin-pin condition is given by standard handbook solutions (Tada et al., 2000). Fix-fix gripping condition is equivalent to a uniform displacement condition at the ends of the specimen. Solutions for the stress intensity factor for the uniform displacement condition have been previously developed by (John et al., 1995), and (John and Rigling, 1998). Stress intensity factor (K) is used in linear elastic fracture mechanics (LEFM) to describe the stress state near the tip of a crack. Relationships for the stage II stable crack growth with stress intensity factor range ΔK was first developed by (Paris et al., 1961) and later modified by (Forman, 1967) to make better allowance for the mean stress. Fix gripping condition modifies the state of stress in the specimen, therefore K value changes. Due to the power law correlating between the crack growth rate and the stress-intensity factor range as seen in Paris' law, even a small change in ΔK may result in a considerable change in the predicted number of cycles to failure. Consequently, effects of boundary condition on K need to be quantified and accounted for.

In this paper the effects of test parameters as gripping conditions (pin-pin and fix-fix), axial and angular misalignments on *K* value of the modified SE(T) specimen is investigated using experimental and numerical solutions. Moreover, the effect of crack inclination with respect to specimen surface is investigated using 3D FEM models. Non-uniform cracking can happen due to misaligned fatigue loading, fabrication imperfection or non-uniform crack initiation in the specimens. This leads to a range of *K* values along the crack front for a given applied stress. In order to predict the behavior of a non-uniform crack during a fatigue test, accurate values of *K* need to be known for any mean crack size and any crack slope. To accomplish this, for modified SE(T) specimen geometry with an initial crack inclination, a framework is proposed to map the crack front evolution in high cycle fatigue tests.

For brevity, pin-pin and fix-fix boundary conditions are called "pin" and "fix" conditions here. Linear elastic finite element method (LEFEM) was utilized to calculate *K* values. This paper only deals with the effects of test parameters on mode I stress intensity factor which is labeled as "*K*" here. Stress of 1 ksi (6.895 MPa) was applied to all FEM models therefore *K* needs to be multiplied by the magnitude of a given stress for different cases. Collapsed quarter-point elements suggested by (Henshell and Shaw, 1975) and (Barsoum, 1976) were used to obtain accurate solution around crack tip.

2.1 EXPERIMENTATION

Quasi static tests were performed to understand the state of stress in the specimen on both pin and fix conditions. Modified SE(T) specimens were fabricated from ASTM A572

Grade 50 steel. Two specimen types with different notch depths were instrumented with 12 strain gages. The load was applied with rate of 0.2 kip/s (0.89 kN/s) in 1kip (4.448 kN) steps, with a 5 second pause between steps. The process was continued to maximum load of 10 kips (44.48 kN).

2.1.1 Geometry

Two specimen types (SE(T)-0.1 and SE(T)-0.15) with notch depths of 0.1 in. (2.54e-3 m) and 0.15 in. (3.81e-3 m) were used for the experiments. Electric Discharge Machining (EDM) was employed to fabricate the 0.006 in. (1.52e-4 m) wide notches in the specimens. Specimen geometry loading conditions and strain gage locations are shown in Figure 2-1. A total of 8 quasi-static tests were performed on two specimen types as shown in Table 2-1. To investigate misalignment the specimens were clamped using hydraulic grips in both angularly and axially misaligned fashions as demonstrated in Figure 2-2.

2.1.2 Tests RESULTS

Strain gage measurements at applied stress of 5 ksi are seen in Figure 2-3. Strain gage locations are seen in Figure 2-1 as stated before. Comparing the results of QS1 to QS2 and QS5 to QS6, little change is seen in the specimen with 0.1 in. (2.54e-3 m) crack while in SE(T)-0.15 with larger crack size, the difference in strains with two gripping conditions is more evident. The surface far from the crack shows to be in compression in both fix and pin gripped cases but the existence of the applied moment due to hydraulic gripping is evident while comparing the results of QS5 to QS6. Based on the comparison

between results from strain gages near the grips of the specimens (strain gages 1&2 vs. 5&6), it is observed that fix boundary condition applies higher moment to the specimen when the crack is larger.

QS3 and QS7 test results show that even though the strain considerably varies on two sides (A and B) of the specimen close to the grips, angular misalignment lead to similar strains on two sides of the crack in midspan of the specimen. Thus, angular misalignment showed minor effect on the stress distribution around the crack for this test setup. On the other hand axial misalignment did have a more significant effect on the stress field in two sides of the crack as observed in Figure 3 (QS4 and QS8).

2.2 FRACTURE MECHANICS CONSIDERATIONS

A straight forward method to determine the stress intensity factor in fix condition is proposed here. In linear elastic fracture mechanics (LEFEM), stress intensity factor for a fix boundary condition case can be calculated by using superposition in which K due to moment is decreased from that of in pin case (Figure 2-4).

Empirical equations for single edge crack subjected to tension (pin condition) is as follow (Tada et al., 2000):

$$K = \sigma\sqrt{\pi a} * F\left(\frac{a}{b}\right) \qquad 2-1$$

where

$$F\left(\frac{a}{b}\right) = \sqrt{\frac{2b}{\pi a}\tan\frac{\pi a}{2b}} * \frac{0.752 + 2.02\frac{a}{b} + 0.37(1-\sin\frac{\pi a}{2b})^3}{\cos\frac{\pi a}{2b}} \qquad 2-2$$

K is the mode I stress intensity factor, σ is the uncracked body applied stress, a is the crack length, b is the plate thickness corresponding to maximum possible crack size and the crack mouth opening displacement (CMOD) is:

$$\delta = \frac{4\sigma a}{E'} V_1\left(\frac{a}{b}\right) \qquad 2-3$$

where

$$V_1\left(\frac{a}{b}\right) = \frac{1.46 + 3.42(1-cos\frac{\pi a}{2b})}{(cos\frac{\pi a}{2b})^2} \qquad 2-4$$

E' is equal to E (modulus of elasticity) for plain stress case and $E/(1-\upsilon^2)$ for plain strain case where υ is the poisson's ratio of the material.

Empirical equations for single edge crack subjected to pure moment are as follow (Tada et al., 2000):

$$K = \sigma\sqrt{\pi a} * F\left(\frac{a}{b}\right) \qquad 2-5$$

where σ is the uncracked body extreme fiber tensile stress ($\sigma = \frac{6M}{b^2}$) and

$$F\left(\frac{a}{b}\right) = \sqrt{\frac{2b}{\pi a}\tan\frac{\pi a}{2b}} * \frac{0.923 + 0.199(1-\sin\frac{\pi a}{2b})^4}{\cos\frac{\pi a}{2b}} \qquad 2-6$$

Crack mouth opening displacement for this loading case is

$$\delta = \frac{4\sigma a}{E'} V_2\left(\frac{a}{b}\right) \qquad 2-7$$

where

$$V_2\left(\frac{a}{b}\right) = 0.8 - 1.7\left(\frac{a}{b}\right) + 2.4\left(\frac{a}{b}\right)^2 + \frac{0.66}{\left(1 - {}^{a}/_{b}\right)^2} \qquad 2-8$$

FEM modeling was used to calculate K and CMOD for different crack sizes (a). Moments applied to the specimen ends with different crack sizes are calculated for fix boundary condition. As seen in Table 2-2 value of K from FEM results shows less than 0.6% difference when compared to K due to moment (K_m) decreased from K in pin loading case (K_{pin}).

To simplify the process of calculating K and CMOD for fix boundary condition for any value of a/b, Eq. 2-9 and Eq. 2-12 are proposed based on least squares fitting of the FEM results for $0.2 \leq (a/b) \leq 0.9$ in a similar fashion to Eq. 2-1:

$$K = \sigma\sqrt{\pi a} * F_f\left(\frac{a}{b}\right) \qquad 2-9$$

where

$$F_f\left(\frac{a}{b}\right) = F\left(\frac{a}{b}\right) * \gamma_1\left(\frac{a}{b}\right) \qquad 2-10$$

where

$$\gamma_1\left(\frac{a}{b}\right) = 1.0623 - 0.9954\left(\frac{a}{b}\right) + 5.7306 - 16.133\left(\frac{a}{b}\right)^3 + 20.885\left(\frac{a}{b}\right)^4 - 10.866\left(\frac{a}{b}\right)^5 \quad 2-11$$

and Eq. 2-3 is modified to

$$\delta = \frac{4\sigma a}{E'} * V_f\left(\frac{a}{b}\right) \quad 2-12$$

where

$$V_f\left(\frac{a}{b}\right) = V_1\left(\frac{a}{b}\right) * \gamma_2\left(\frac{a}{b}\right) \quad 2-13$$

where

$$\gamma_2\left(\frac{a}{b}\right) = 1.0093 - 0.1341\left(\frac{a}{b}\right) + 1.7783\left(\frac{a}{b}\right)^2 - 8.0182\left(\frac{a}{b}\right)^3 + 12.717\left(\frac{a}{b}\right)^4 - 7.6847\left(\frac{a}{b}\right)^5 \quad 2-14$$

Accuracy of the proposed equations is demonstrated in Tables 2-3 and 2-4 and Figure 2-5. Both *K* and CMOD calculated from the equations are in close agreement with FEM results thus similar to LEFEM results.

2.2.1 LEFM Validity for Fatigue

Based on ASTM E561 for the compact tension (CT) specimen, to ensure that a given calculated value of *K* in a fatigue test is considered valid, the remaining uncracked ligament must remain predominantly elastic (ASTM E561-10e1, 2010). This condition is considered to be met in this method as long as the length of the remaining uncracked

ligament, b - a_p, at that point in the test is greater than or equal to eight plastic zone sizes. For plain stress condition this is met with the condition given in Eq. 2-15.

$$(b - a_p) \geq \frac{4}{\pi}\left(\frac{K_{max}}{\sigma_{YS}}\right)^2 \qquad 2-15$$

b is the specimen thickness, a_p is the physical crack size corresponding to the K point being considered, and σ_{YS} is the 0.2 % offset yield strength of the material. The span of validity for LEFM in these specimens should be further investigated using Elastic Plastic Finite Element Method (EPFEM) especially for fix-fix boundary condition case. Limited linear elastic crack propagation and K_{max} can be experienced by the specimens. This problem is more evident in case of the specimens with high R ratio ($load_{min}/load_{Max}$). Figure 2-6 and Figure 2-7 show the limitations of the specimen in fix-fix and pin-pin gripped conditions in terms of maximum valid K value and crack size based on Eq. 2-15. These graphs are representing the limits in plain stress and 50 ksi (345 MPa) yield strength of the material. The higher is the applied maximum sigma the higher will be the achievable valid K_{max} and the lesser the valid crack size and consequently shorter fatigue life. Comparing Figure 2-6 and Figure 2-7 reveals that higher valid K values at lower 'a' can be achieved using pin-pin gripping. In any case of gripping conditions the test specimen proves to be limited to K_{max} of 30 ksi.in.$^{1/2}$ (33 MPa.m$^{1/2}$). Figure 2-8 shows that if a 0.75 in. (0.019 m) thick specimen is used higher valid K_{max} and crack size can be reached. Even with the above-said limitations performing fatigue tests on these specimens are of significance and interest since it can illuminate if the AE has the ability

to verify the state of the crack and predict its behavior in early stages of through thickness crack growth.

2.3 NUMERICAL ANALYSYS

FEM analysis was utilized to understand the state of stress and the effect of pin and fix gripping conditions on characteristics of the crack in 2D and 3D. Effects of installment human errors as change in ungripped length (Figure 2-1) and specimen misalignments were investigated. LEFEM was used to capture *K* value which is a linear elastic parameter. FEM models had an applied stress of 1 ksi (6.89 MPa) thus for different load magnitudes the *K* values can be calculated by multiplication due to linear elastic nature of models. Collapsed quarter-point elements were used in order to achieve accurate solutions around crack tip.

2.3.1 Effect of ungripped length

The effect of ungripped length of the specimen (Figure 2-1) on K factor of the modified SE(T) specimen was investigated. For pin case, FEM results for K value due to various ungripped lengths were constant for a given crack size as expected. The results of FEM analysis confirmed that by increasing the ungripped length, the values for *K* in pin and fix boundary conditions converge and the effect of gripping length is more evident when the specimen is very short. Effect of ungripped length on *K* value in the specimen for different crack sizes is demonstrated in Figure 2-9. Numerical comparison of the results indicates that in an extreme case of installment error, if ungripped length of the specimen

is changed by an inch (say from 26 to 25 in. (0.635 to 0.660 m)), K value is affected by only 0.4 percent.

2.3.2 Effects of misalignments on K value

Misalignments can cause the experiment to differ from the ideal case for which the solution for *K* is developed. 3D FEM was used to understand the effects of misaligned gripping conditions on *K* along the crack. Under fatigue loading these imperfections can cause a crack to grow with non-uniform rates along the crack thus creating a non-uniform crack front as seen in Figure 2-10. Figure 2-2 shows extreme cases in which the specimen can be gripped with angular and axial misalignments. Both configurations were modeled in 3D FEM for range of crack sizes of 0.1 to 0.4 in. (2.54e-3 to 1.02e-2 m) and the effect of these misalignments on the *K* are presented in Figure 2-11. The angular misalignment has insignificant effect on the stress distribution in mid-section of the specimen thus stress intensity of the crack front is not affected. However, FEM results show that angular misalignment introduces modes two and three of crack opening. When the specimen is loaded in fatigue this can cause an out of surface crack propagation yet in test setup under study the magnitude of the K_{II} and K_{III} is around 0.1 percent of K_I and is overlooked. Axial misalignment, as seen in Figure 2-11, has a more prominent effect on the stress distribution at mid span of the specimen and the slope of the *K* curve (m_k) in width of the specimen increases as crack gets larger.

Tables 2-5 and 2-6 show the percentile effect of misalignments on *K* value for these two cases. As seen the contribution of misalignments decreases while the crack size is

increased. The extreme cases of misalignment are studied here and when the proper care is given for installation, effect of misalignments is reduced. These effects can be further reduced using strain gages on sides of the specimen.

2.3.3 Effects of crack inclination on K value

3D FEM was used to investigate the effects of non-uniform crack front on *K* value along the crack (Figure 2-10). During the fatigue tests, non-uniform cracking can occur due to misaligned installation of the specimen. Variable stress intensity factor of the crack needs to be calculated and accounted for since the K value is no longer constant due to variable crack depths along crack front. Table 2-7 shows 28 3D FEM models that were investigated with variables of crack inclinations, mean crack size and boundary condition (fix and pin) for the proper *K* values to be calculated. m_C $((a\_A - a\_mean)/(w/2))$ is defined as the slope of the crack front with respect to the specimen surface (Figure 2-10).

Distribution of *K* along the crack front for all models is presented in Figure 2-12. *K* value for crack with zero inclination (mc = 0) passes through the mean of *K* (*K_mean*) for incline cracks with similar *a_means*. The results of FEM analyses, investigating the effects of crack inclination on the stress intensity factor along the crack, are summarized in Figure 2-13 where m_K is the slope of the stress intensity curve along the crack front. Using the results from FEM analysis a chart is developed in which an estimate for all cases with non-uniform crack front can be achieved as long as LEFM is applicable (Figure 2-13).

The FEM results show that the crack inclination has a significant effect on the stress intensity of the crack front. Table 2-8 and Table 2-9 show the effect of crack slope of mc = 0.05 on *K* and it is observed that this effect is more prominent when crack size is small.

2.3.4 Effect of crack inclination on fatigue

In high cycle fatigue tests, crack growth behavior varies from ideal case when the crack front is inclined. To account for the initial crack inclination in fatigue crack growth behavior, a procedure is proposed as follow. Assuming that axial and angular misalignments have insignificant effects on *K* value of the crack front and given an initial crack size mean (*a_mean*) and an initial crack inclination (mc) for a specimen, average *K_means* can be calculated considering crack size of *a_mean* for a fix or pin boundary condition using Eq. 2-1 and Eq. 2-9. Then the value of m_k for the crack is obtained from Figure 2-13. Therefore range of *K* value on two sides of the crack is calculated for given applied stress range. Consequently, using Paris' law or similar equations, crack sizes on the sides of the specimen (*a_A* and *a_B*) are calculated for a limited number of cycles. Then using the updated *a_mean* and mc, values for updated *K_mean* and mk is obtained and the process repeats iteratively as long as LEFM is valid. Thus the crack front evolution is mapped by connecting *a_A* and *a_B* in each iteration.

2.4 CONCLUSION

Effects of test parameters on Stress intensity factor of a modified SE(T) specimen representing early stage cracks in flanges and webs of steel bridge members are investigated. Equations to include the effects of fix boundary condition on *K* and CMOD

of the crack are developed. Experimental and numerical procedures show that fix boundary condition applies progressively increasing moment to the specimen as the crack size increases. The effects of misalignments on *K* value along the crack front are investigated numerically and experimentally. Less than 3% change on *K* is observed along the crack even in extreme cases of angular and axial misalignments. Angular misalignment is seen to introduce mode II and III of crack opening. The contribution of misalignments on the magnitude of *K* decreases considerably for larger crack sizes hence the problem most likely affects the initiation of the crack growth. Influence of ungripped length of the specimen on *K* was evaluated and shown to be insignificant for an extreme case of installation error. In addition, effects of pin and fix boundary conditions on *K* value of non-uniform crack fronts were investigated and a framework is proposed to map the crack front evolution in high cycle fatigue tests for the modified SE(T) specimen with initial crack inclination. Plasticity and its effects on the span of validity for LEFM were investigated based on existing equations in literature and further investigation is required using Elastic Plastic Finite Element Method (EPFEM).

To summarize, for the given geometry of modified SE(T) specimen representing a crack with through-thickness growth, a framework is proposed to accurately compute *K* values with test setup variables taken into account. The results can be used as a foundation to understand the crack behavior during high cycle fatigue tests performed on the specimen.

FIGURES

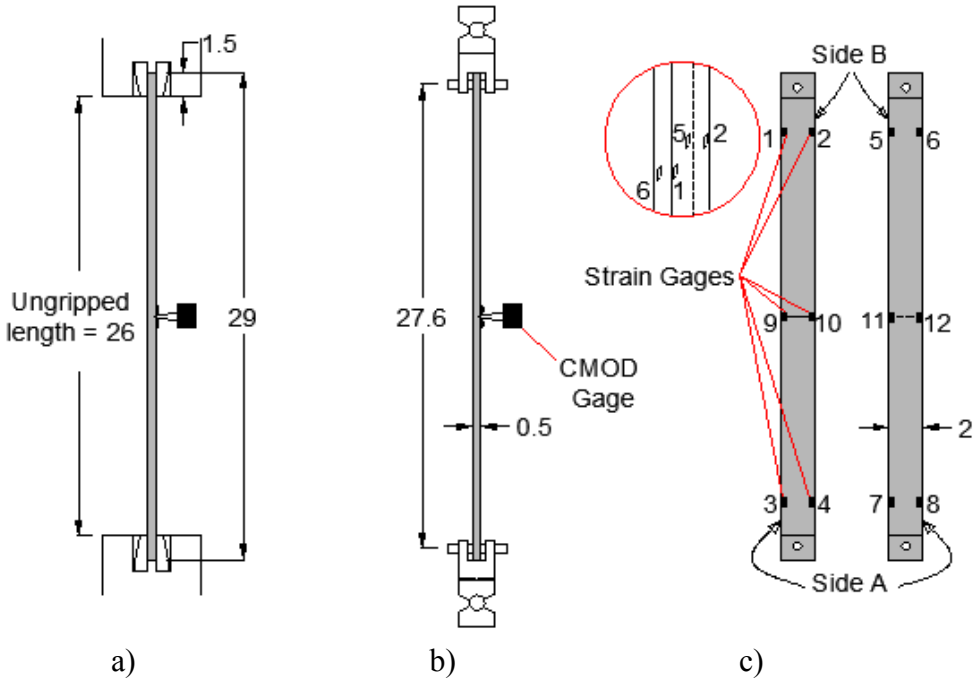

Figure 2-1- Test Setup and Specimen Geometry a) Fix Gripping b) Pin griping c) strain gage locations

(dimensions in in. (1 in.= 0.0254 m))

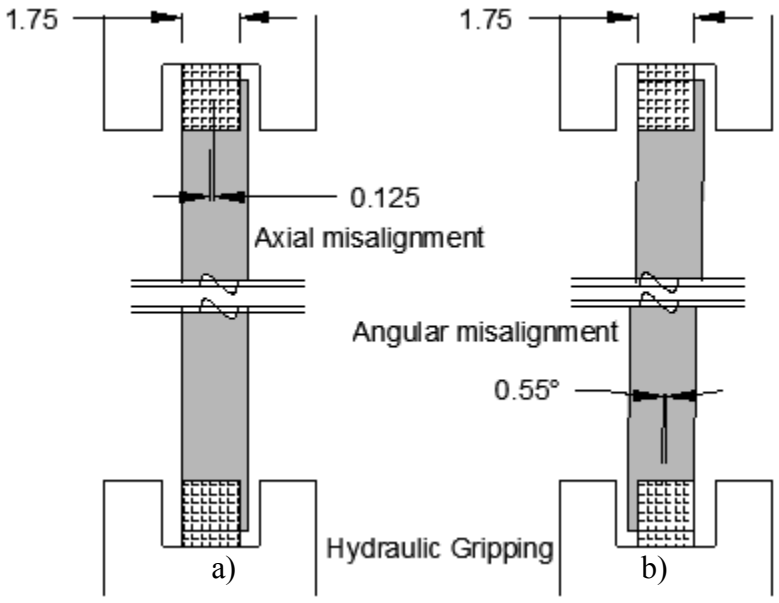

Figure 2-2- Misalignments in Installation a) Axial b) Angular (dimensions in in. (1 in.= 0.0254 m))

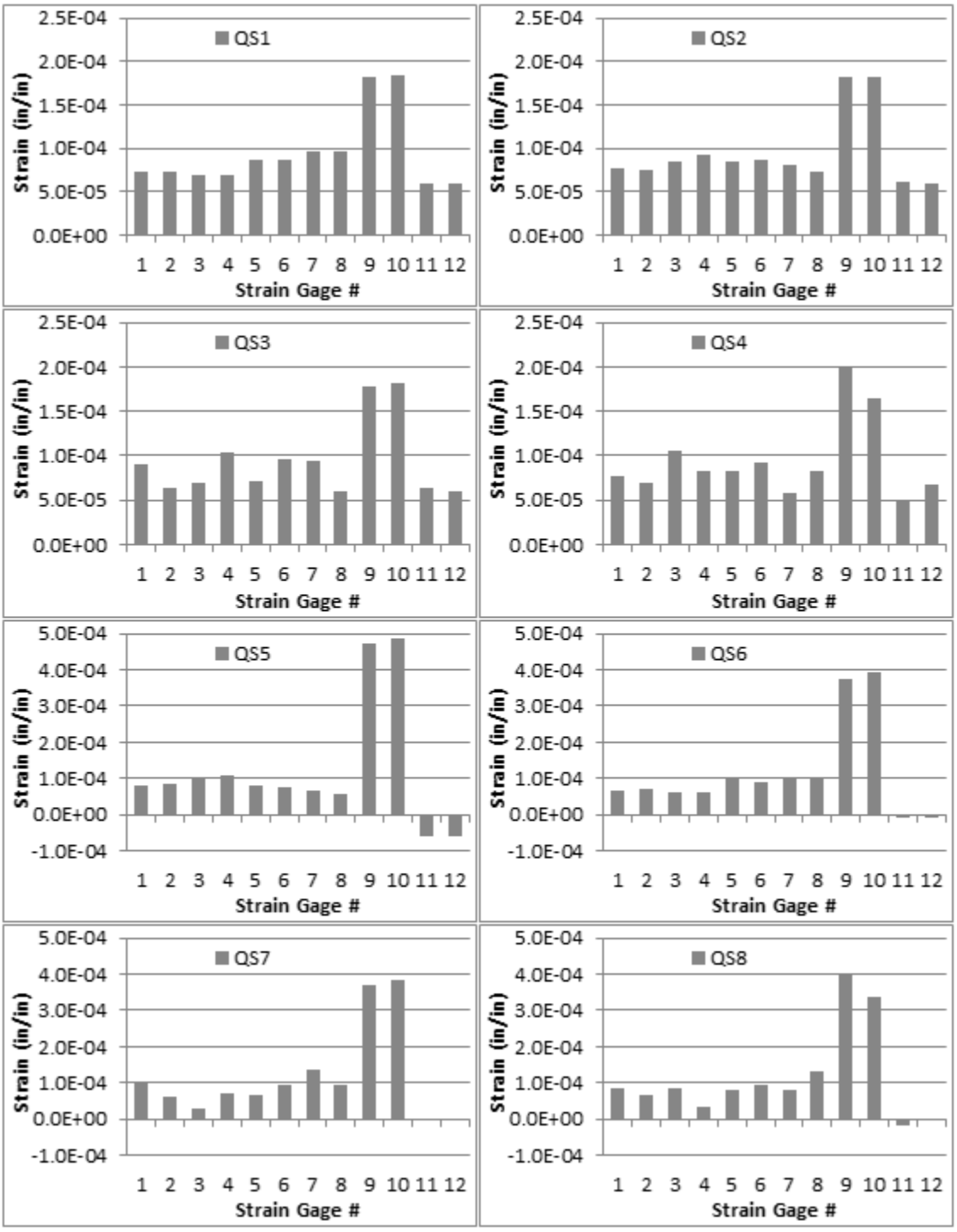

Figure 2-3- Strain Results for Tests QS1 to QS4 on SE(T)-0.1 and Test QS5 to QS8 on SE(T)-0.15 for Applied Load of 5000 lbs (1 lb = 4.448 N, 1 in. = 0.0254 m)

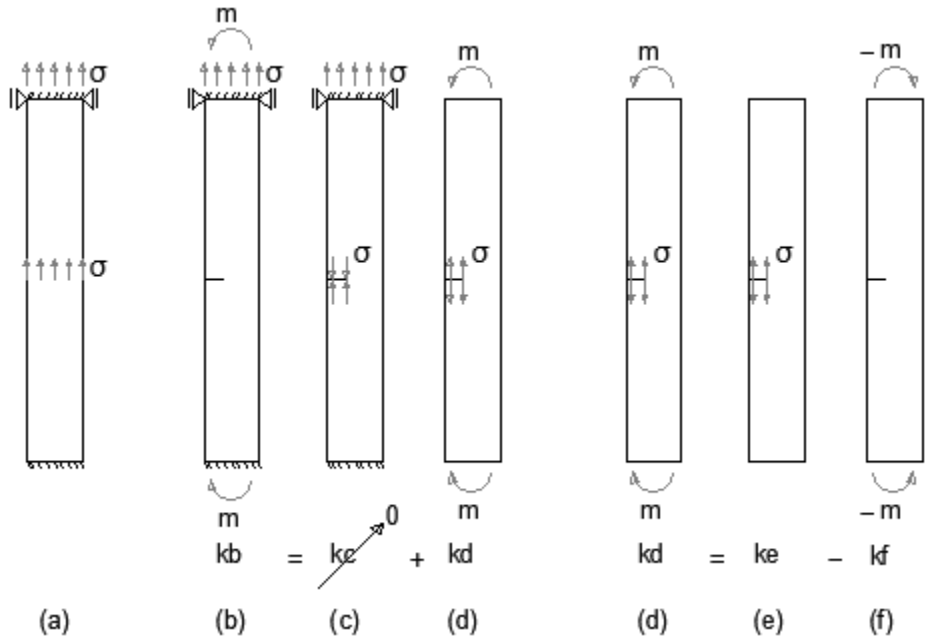

Figure 2-4- Superposition to Calculate K Factor for fix-fix case

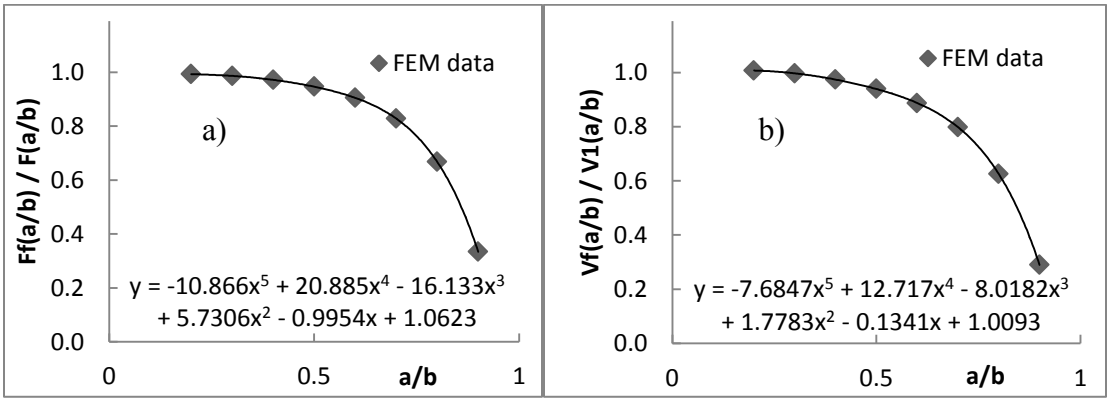

Figure 2-5- a) γ_1 for Various a/b Values. b) γ_2 for Various a/b Values

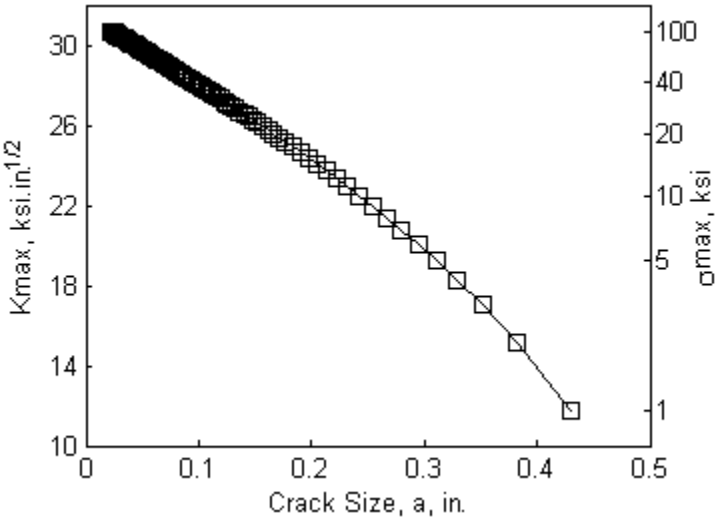

Figure 2-6- Specimen Valid Limits based on ASTM for fix-fix case

(1 in. = 0.0254 m, 1ksi=6.89MPa, 1ksi.in.1/2=1.1MPa.m1/2)

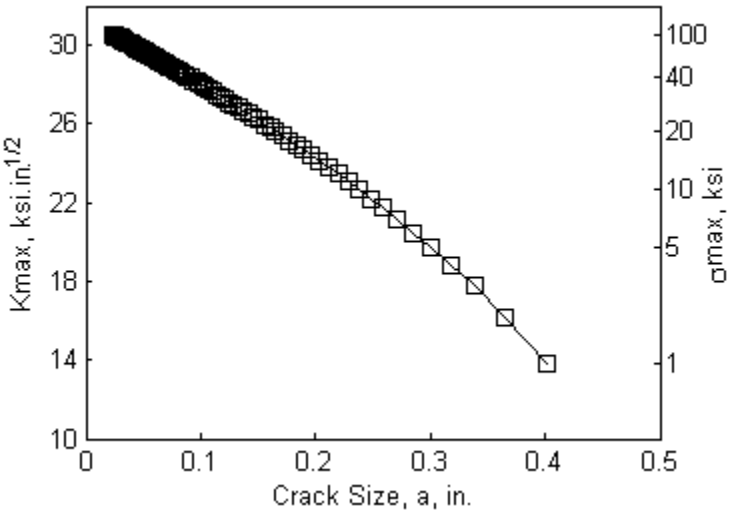

Figure 2-7- Specimen Valid Limits based on ASTM for pin-pin case

(1 in. = 0.0254 m, 1ksi=6.89MPa, 1ksi.in.1/2=1.1MPa.m1/2)

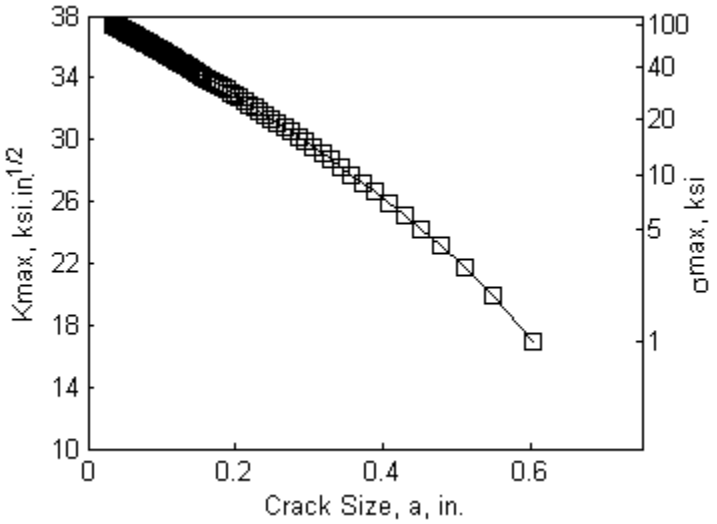

Figure 2-8- Valid Limits for 0.75 in. thick specimen based on ASTM for pin-pin case

(1 in. = 0.0254 m, 1ksi=6.89MPa, 1ksi.in.1/2=1.1MPa.m1/2)

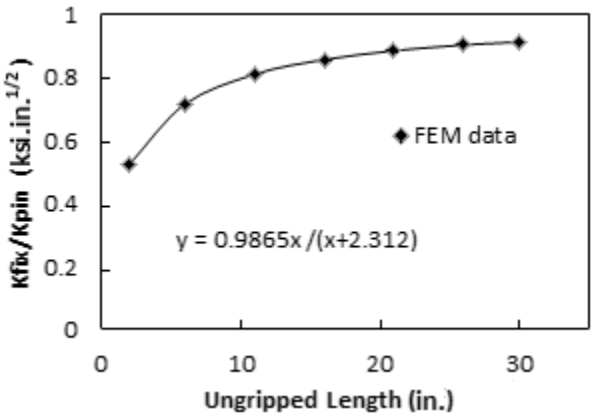

Figure 2-9- Effect of Ungripped Length of the Specimen on K for case of a=0.3 in.

(1 lb = 4.448 N, 1 in. = 0.0254 m)

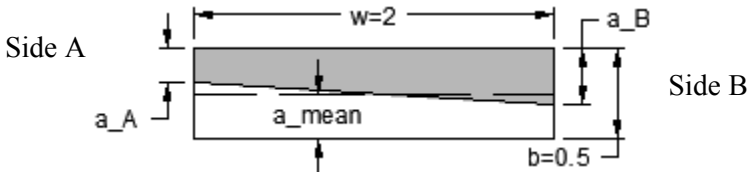

Figure 2-10- Non-uniform Crack Surface

(dimensions in in., 1 in. = 0.0254 m)

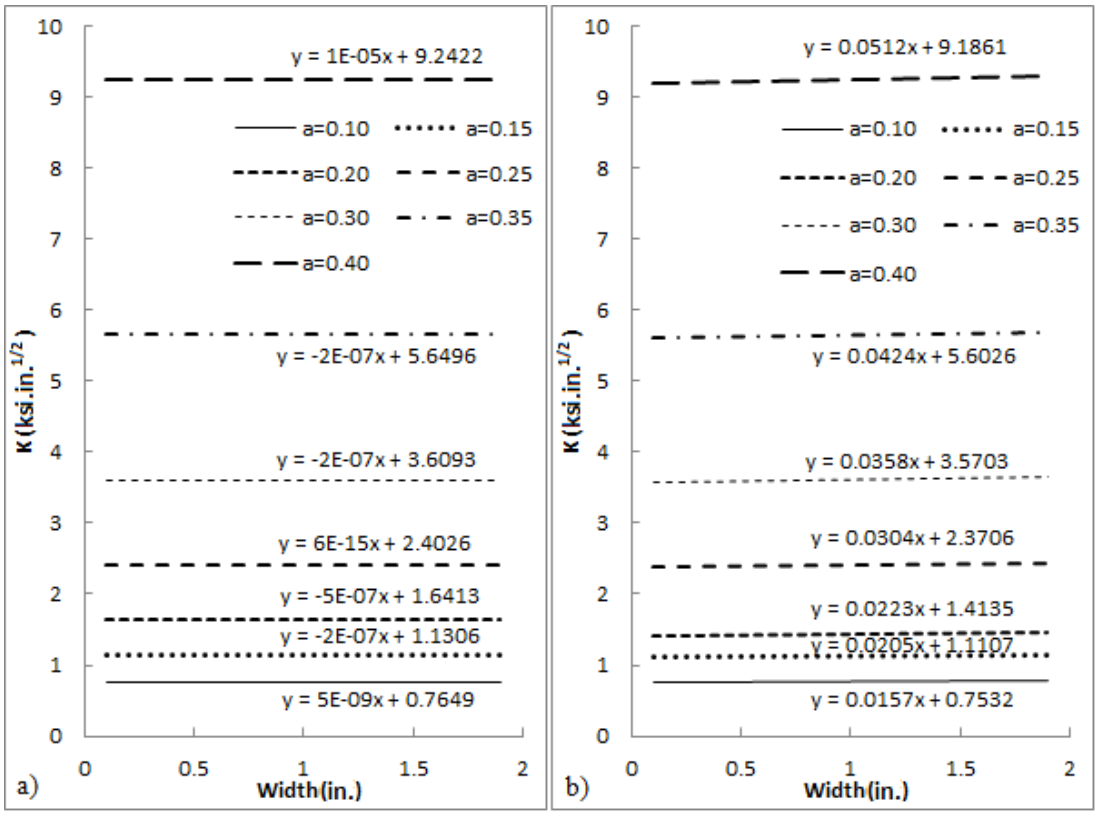

Figure 2-11- K Value along the Crack Front a) Angular Misalignment case b) Axial Misalignment case

(applied stress= 1ksi, 1 lb = 4.448 N, 1 in = 0.0254 m)

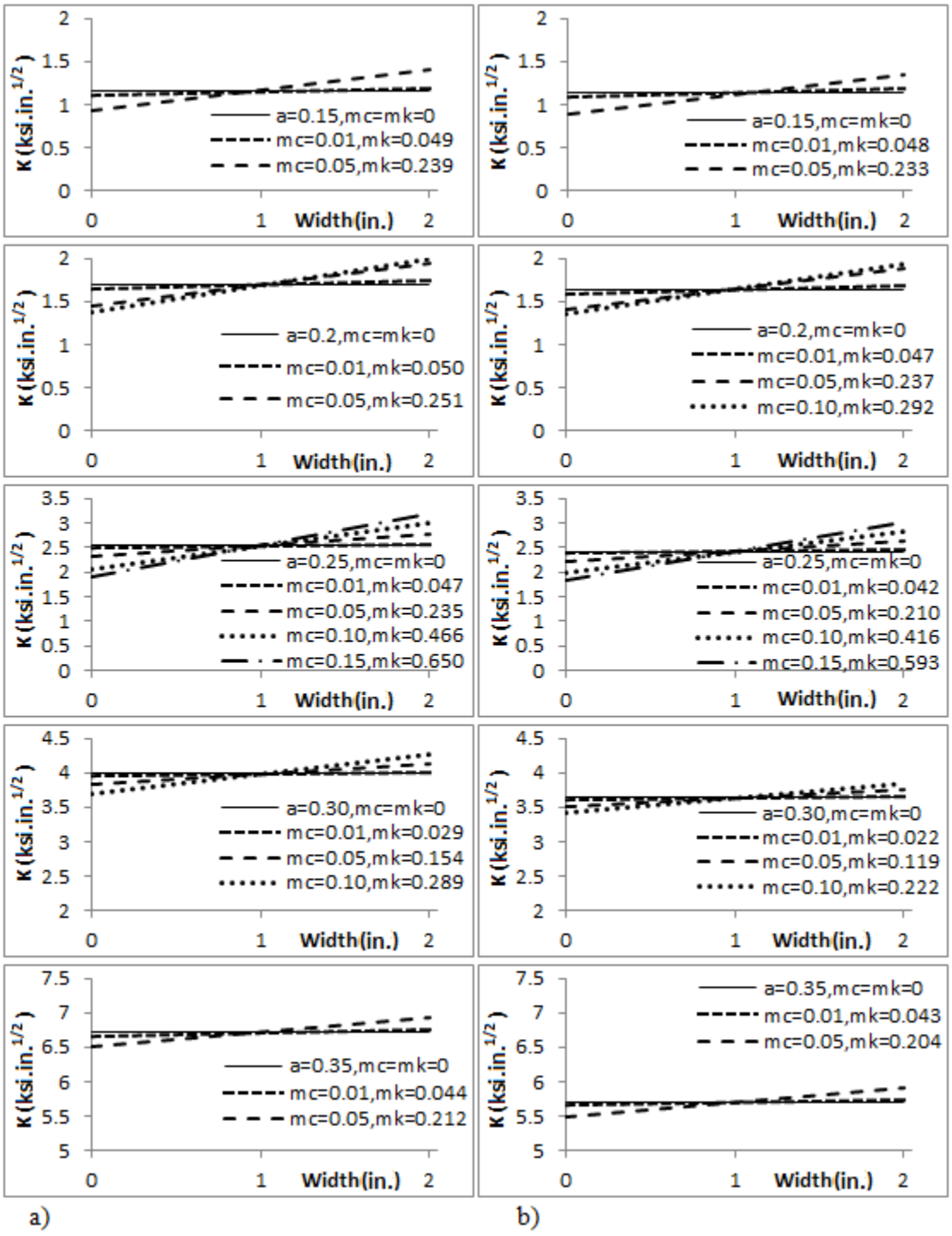

Figure 2-12- K along the Crack Front for various a_means a) Pin B.C. b) Fix B.C.

(applied Stress= 1 ksi, 1 lb = 4.448 N, 1 in. = 0.0254 m)

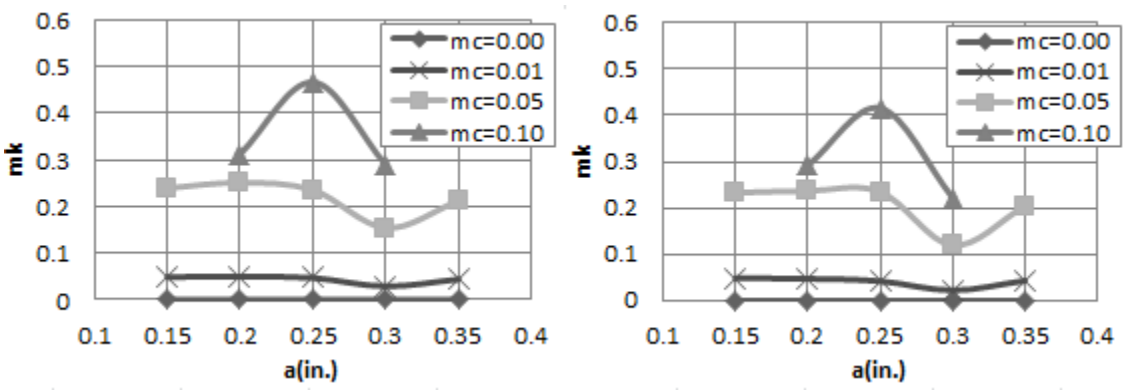

Figure 2-13- mk vs. a_mean for Different Crack Inclinations (applied Stress= 1ksi, , 1 lb = 4.448 N, 1 in. = 0.0254 m)

a) pin B.C. b) fix B.C.

TABLES

Table 2-1- Quasi-Static Test Matrix

Test	Specimen	Gripping
QS1	SE(T)-0.1	Pin
QS2	SE(T)-0.1	Fix
QS3	SE(T)-0.1	Fix / Angular misalignment
QS4	SE(T)-0.1	Fix / Axial misalignment
QS5	SE(T)-0.15	Pin
QS6	SE(T)-0.15	Fix
QS7	SE(T)-0.15	Fix / Angular misalignment
QS8	SE(T)-0.15	Fix / Axial misalignment

Table 2-2- Analytical and FEM Results Comparison for K vs. a/b (1 lb = 4.448 N, 1 in. = 0.0254 m)

a/b	Moment (kips-in.)	Km (ksi*in.$^{1/2}$)	Kpin (ksi*in.$^{1/2}$)	Kfix(FEM) (ksi*in.$^{1/2}$)	Kpin - Km (ksi*in.$^{1/2}$)	% diff. (KfixFEM and Kpin - Km)
0.2	7.742E-04	0.0055	0.7660	0.7609	0.7605	0.06
0.3	1.967E-03	0.0184	1.1362	1.1210	1.1177	0.29
0.4	4.174E-03	0.0506	1.6709	1.6240	1.6203	0.23
0.5	8.281E-03	0.1325	2.5050	2.3710	2.3725	0.06
0.6	1.623E-02	0.3612	3.9252	3.5530	3.5640	0.31
0.7	3.281E-02	1.1200	6.6854	5.5380	5.5654	0.49
0.8	7.036E-02	4.4119	13.4437	8.9760	9.0319	0.62
0.9	1.540E-01	27.4103	41.2805	13.7900	13.8702	0.58

Table 2-3- Proposed Equations and FEM Comparison for K vs. a/b (1 lb = 4.448 N, 1 in. = 0.0254 m)

			Ff(a/b) / F(a/b)		
a/b	K fix (ksi*in.$^{1/2}$)	K pin (ksi*in.$^{1/2}$)	FEM	γ_1	% diff
0.2	0.76	0.77	0.9933	0.9935	0.00
0.3	1.12	1.14	0.9866	0.9867	0.00
0.4	1.62	1.67	0.9719	0.9719	0.00
0.5	2.37	2.50	0.9465	0.9464	0.01
0.6	3.55	3.93	0.9052	0.9053	0.01
0.7	5.54	6.69	0.8284	0.8285	0.03
0.8	8.98	13.44	0.6677	0.6679	0.04
0.9	13.79	41.28	0.3341	0.3344	0.12

Table 2-4- Proposed Equations and FEM Comparison for CMOD vs. a/b (1 in. = 0.0254 m)

	CMOD fix (in.)		CMOD pin (in.)		Vf(a/b) / V1(a/b)		
a/b	Plane Stress	Plane Strain	Plane Stress	Plane Strain	FEM	γ_2	% diff
0.2	2.50E-05	2.29E-05	2.48E-05	2.27E-05	1.0074	1.0074	0.00
0.3	4.76E-05	4.36E-05	4.78E-05	4.37E-05	0.9969	0.9970	0.01
0.4	8.67E-05	7.94E-05	8.91E-05	8.16E-05	0.9739	0.9739	0.00
0.5	1.59E-04	1.46E-04	1.70E-04	1.55E-04	0.9393	0.9392	0.01
0.6	3.05E-04	2.79E-04	3.44E-04	3.15E-04	0.8873	0.8877	0.04
0.7	6.22E-04	5.70E-04	7.79E-04	7.14E-04	0.7986	0.7983	0.04
0.8	1.38E-03	1.27E-03	2.21E-03	2.02E-03	0.6254	0.6256	0.03
0.9	3.19E-03	2.92E-03	1.10E-02	1.01E-02	0.2896	0.2897	0.01

Table 2-5- Effect of Angular Misalignment on K along the Crack Front (1 lb = 4.448 N, 1 in. = 0.0254 m)

a (in.)	K_mean (ksi*in.$^{1/2}$)	K_Max (ksi*in.$^{1/2}$)	% diff
0.10	0.765	0.773	1.02
0.15	1.131	1.139	0.74
0.20	1.641	1.648	0.41
0.25	2.403	2.408	0.23
0.30	3.609	3.615	0.14
0.35	5.650	5.655	0.09
0.40	9.242	9.251	0.10

Table 2-6- Effect of Axial Misalignment on K along the Crack Front (1 lb = 4.448 N, 1 in. = 0.0254 m)

a (in.)	K_mean (ksi*in.$^{1/2}$)	K_Max (ksi*in.$^{1/2}$)	% diff
0.10	0.768	0.788	2.63
0.15	1.130	1.155	2.17
0.20	1.436	1.459	1.62
0.25	2.402	2.430	1.17
0.30	3.608	3.639	0.86
0.35	5.647	5.684	0.65
0.40	9.238	9.288	0.54

Table 2-7- 3D FEM Modeles Created for Incline Cracks (1 in. = 0.0254 m)

Model #	B.C.	Model #	B.C.	a_mean (in.)	a_A (in.)	a_B (in.)	mc
I_P1	Pin	I_F1	Fix	0.15	0.14	0.16	0.01
I_P2	Pin	I_F2	Fix	0.15	0.1	0.2	0.05
I_P3	Pin	I_F3	Fix	0.2	0.19	0.21	0.01
I_P4	Pin	I_F4	Fix	0.2	0.15	0.25	0.05
I_P5	Pin	I_F5	Fix	0.2	0.1	0.3	0.1
I_P6	Pin	I_F6	Fix	0.25	0.24	0.26	0.01
I_P7	Pin	I_F7	Fix	0.25	0.2	0.3	0.05
I_P8	Pin	I_F8	Fix	0.25	0.15	0.35	0.1
I_P9	Pin	I_F9	Fix	0.25	0.1	0.4	0.15
I_P10	Pin	I_F10	Fix	0.3	0.29	0.31	0.01
I_P11	Pin	I_F11	Fix	0.3	0.25	0.35	0.05
I_P12	Pin	I_F12	Fix	0.3	0.2	0.4	0.1
I_P13	Pin	I_F13	Fix	0.35	0.34	0.36	0.01
I_P14	Pin	I_F14	Fix	0.35	0.3	0.4	0.05

Table 2-8- Effect of Non-uniform Crack Front on Range of K (mc=0.05, Pin B.C., 1 lb = 4.448 N, 1 in. = 0.0254 m)

a_mean (in.)	mk	K_mean (ksi*in.$^{1/2}$)	K_Max (ksi*in.$^{1/2}$)	% diff
0.15	0.239	1.170	1.409	20.42
0.20	0.251	1.687	1.938	14.88
0.25	0.235	2.542	2.777	9.25
0.30	0.154	3.982	4.136	3.87
0.35	0.212	6.715	6.927	3.16

Table 2-9- Effect of Non-uniform Crack Front on Range of K (mc=0.05, Fix B.C., 1 lb = 4.448 N, 1 in. = 0.0254 m)

a_mean (in.)	mk	K_mean (ksi*in.$^{1/2}$)	K_Max (ksi*in.$^{1/2}$)	% diff
0.15	0.233	1.121	1.354	20.79
0.20	0.237	1.640	1.877	14.45
0.25	0.210	2.416	2.626	8.69
0.30	0.119	3.634	3.753	3.27
0.35	0.204	5.698	5.902	3.58

CHAPTER 3, STUDY 2 - ACOUSTIC EMISSION ASSESSMENT OF THROUGH-THICKNESS FATIGUE CRACK GROWTH IN STEEL MEMBERS

SUMMARY

The understanding of crack behavior under fatigue remains a critical issue in addressing the performance of steel bridges. Single edge notches in general provide a very well defined load and fatigue crack size and shape environment for estimation of the stress intensity factor *K*, which is not found in welded elements. ASTM-E647 SE(T) specimens do not appear to provide ideal boundary conditions for proper recording of acoustic wave propagation and crack growth behavior observed in steel bridges, but do provide standard fatigue crack growth rate data. Acoustic emission (AE) has been increasingly used for assessment and prediction of fatigue cracks in steel bridge members. In steel bridge members, AE transducers are commonly attached to the surface of the plate from which the crack is initiated, hence producing a through-thickness crack growth monitored by the transducer. A modified version of the SE(T) specimen was developed in order to maintain similitude with the field crack propagation orientation and to provide a small-scale specimen with improved AE characteristics while maintaining accuracy of fatigue crack growth rate (*da/dN*) versus stress intensity factor range (ΔK). The specimen simulates fatigue cracks in flanges or early stage of crack growth in webs of steel bridge members. Effects of load ratio (R) and material on AE data recorded during the crack growth was addressed. Applicability of AE to capture, locate and predict the behavior of the growing crack was positively verified. R ratio showed to have a significant effect on evolution of AE data captured during the test.

OUTLINE

Acoustic emission (AE) has been increasingly used for assessment and prediction of fatigue cracks in steel bridge members (Sinclair et al., 1977), (Bassim, et al., 1994), (Oh, et al., 2004), (Ohira, et al., 1980), (Chen and Choi, 1980), (Ziehl, et al., 2009), (Yu, et al., 2011), (Yu, et al., 2012). Fatigue cracks develop at the transverse weld toe of stiffeners, attachments, and cover plates in steel bridge members. The cracks develop from a combination of initial conditions (e.g., weld toe geometry, discontinuities, and residual stress fields) that are difficult to accurately quantify, thus rendering fracture mechanics models for the prediction of fatigue crack growth exceedingly difficult without experimental verification (Metrovich and Fisher, 2005, 2006). Accurate assessment of the early fatigue crack growth characteristics is essential for the implementation of any rational prognostics methodology. Fatigue cracks, which are large enough to be detected by ordinary NDE inspection techniques, typically require extensive repair efforts (Fisher et al., 1979), (Roy et al., 2003). This level of crack detection is not suitable to develop efficient prognostic tools.

Single edge notches, as used in traditional laboratory test coupons, provide a very well defined load and fatigue crack size and shape environment for estimation of the stress intensity factor (K), which is not found in welded structures. Nondestructive evaluation of the crack extension is desirable to provide information to decision making for bridge management. To this end AE fatigue crack monitoring has the potential to provide early fatigue crack detection and insight to assess the structural integrity (Gong and Nyborg, 1992), (Ziehl, et al., 2009). AE sources are defect-related processes such as crack extension and plasticization of material in the highly stressed zone adjacent to the crack

tip (Roberts and Talebzadeh, 2003). Studies on well-defined fatigue crack shapes have shown good correlation between AE and crack growth parameters, indicating that AE can assist in understanding the state of the crack and predicting its behavior due to fatigue loads (Roberts and Talebzadeh, 2003), (Yu, et al., 2011).

Typical ASTM-E647 (ASTM E647-11e1, 2011) specimens require AE sensors to be located on edge surfaces which contain the crack tip and do not represent field configurations for crack initiation and early propagation stages. To overcome this limitation a small scale specimen is designed to develop uniform stress perpendicular to the plane of fatigue crack growth (Figure 3-1). Specimen design allows for AE sensors to be oriented on the same surfaces as anticipated in the field. Influence of sensor surface with respect to crack orientation has thus been minimized and the similitude with field condition is maintained. As a result the specimen provides a shallow, wide crack which better simulates fatigue cracks occurring in the flanges or early stage of crack growth in webs of steel bridge members. The testing protocol also allows for the examination of small versus large crack depth influence on AE data for surface cracks. In addition, the modified SE(T) specimen provides an ideal geometry for which the benefit of location and extraneous noise filtering techniques are maximized.

The test matrix used in this paper consists of seven specimens referenced in Table 3-1. The matrix takes into account the effect of the material, R ratio, gripping conditions and different initial notch depths in the specimen and the possible effects of these variables on AE data recorded during the fatigue crack growth. The AE data was used to develop a fundamental relationship between absolute energy rate of the AE signals and crack

growth rate for through-thickness crack growth. Using this relationship, the fatigue life of a typical specimen is predicted by means of AE signal features.

3.1 THEORETICAL PROCEDURE

Association of fatigue crack parameters with AE data forms the basis for AE structural damage evaluation (Yu, et al., 2011). Parameters commonly used in linear elastic fracture mechanics (LEFM) such as crack length, a, crack growth rate, da/dN, and stress intensity factor, K, can be used as indicators of fatigue damage and assessment of remaining fatigue life in terms of load cycles (Yu, et al., 2011). Four major causes are postulated to contribute to AE when an element is subject to cyclic loading: plastic flow ahead of the crack tip, crack growth, grating from fracture surfaces, and extraneous noise (Sinclair et al., 1977), (Lindley et al., 1978). The spatial filtering techniques based on source location, guard sensors and time of arrival (Gong and Nyborg, 1992) can be employed to separate extraneous noise from crack related signals in laboratory testing.

In former studies, count rate of AE signals was employed to set up the theoretical relationship between AE data characteristics and crack growth behavior. (Harris and Dunegan, 1974) presented a model to describe the relationship between AE count rate, dn/dN and stress intensity range, ΔK, by relating the energy released during crack extension to AE counts. Researchers then focused on obtaining the relationship between dn/dN and ΔK for the materials of interest (Hamel, et al., 1981), (Daniel, et al., 1998), (Roberts and Talebzadeh, 2003a&b).

In AE, “energy” and “signal strength” features represent the area under the rectified signal envelope with the former having a higher resolution and “absolute energy” is

obtained from the integration of the squared voltage signal divided by a reference resistance over the duration of an AE waveform (DiSP User's Manual, 2001). When used for processing burst type emissions, out of the three features, "absolute energy" provides the greatest prominence to larger signals (higher voltage and longer duration).

AE signals accumulate with the crack growth, and therefore it is reasonable to investigate the relationship between "cumulative counts" and "cumulative absolute energy" rates and "crack growth rate" and "stress intensity" (Yu, et al., 2011).

Assuming that absolute energy of acquired AE signals, U, is proportional to the crack-released energy [$\Delta K^2/(E'(1-R)^2)\, t\, a$], the following equation has been presented (Yu, et al., 2011):

$$\frac{dU}{dN} = \frac{B.t}{E'} \cdot \frac{\Delta K^2}{(1-R^2)} \cdot \frac{da}{dN} \qquad 3-1$$

where a is the crack size, t is the width of specimen along the crack, B is a proportional constant for a specific material, N is the number of load cycles, E' is equal to E (modulus of elasticity) for plane stress case and $E/(1-\upsilon^2)$ for plane strain case where υ is the poisson's ratio of the material and dU/dN and da/dN are AE absolute energy rate and crack growth rate, respectively. For a given set of loading conditions, stable crack growth behavior (Stage II) in a material is usually characterized by the Paris Law (Paris and Erdogan, 1963).

$$\frac{da}{dN} = C(\Delta K)^m \qquad 3-2$$

where *C* and *m* are material constants. The relationship between AE absolute energy rate and stress intensity range is set up by introducing Eq. 3-1 into Eq. 3-2 (Yu, et al., 2011).

$$\frac{dU}{dN} = B_e(\Delta K)^p \qquad 3-3$$

where $B_e = BtC/(E'(1-R)^2)$, $p = m+2$

Using similar approach and assuming that number of threshold crossing of acquired AE signals, count, represented as *n*, is also proportional to the crack-released energy leads to the following equation:

$$\frac{dn}{dN} = B_c(\Delta K)^q \qquad 3-4$$

For a component under specific loading conditions, B_e (or B_c) can be considered as a material constant. In engineering applications, assuming that "absolute energy" (or "count") of acquired AE signals is proportional to the crack-released energy, *p* (or *q*) may be less than (*m+2*) due to attenuation of the AE signals filtering or high recording threshold level.

Combining Eq. 3-2 and Eq. 3-3 leads to:

$$\frac{da}{dN} = B_g\left(\frac{dU}{dN}\right)^r \qquad 3-5$$

where $B_g = C/Be^{m/p}, r = m/p$

Using Eq. 3-5, crack size at any stage of fatigue life can be calculated by absolute energy feature of the AE signals. As when an AE signal is recorded after a certain number of cycles, the only unknown in Eq. 3-5 becomes the extension of "*a*". This method for

calculating the crack size is especially useful when correlation between "a" and K is unknown or difficult to obtain.

Fatigue tests in combination with AE monitoring are necessary to obtain the values of material constants in Eq. 3-1 through 5. As an equation exists to describe the relationship between K and "a" for a given load and geometry, number of cycles required for an extension of Δa can be calculated. dU/dN is attained by AE monitoring of the specimen and the constants B_e and p are calculated for a segment of fatigue life. Thus, dU/dN for any crack size can be obtained using Eq. 3-3. Assuming that at the end of this segment crack size is "a_i", after "N_i" number of cycles, numerical integration techniques can be employed to calculate N_{i+1} for a given a_{i+1} using Eq. 3-5.

It is observed that AE signals do not appear in a per cycle basis in fatigue tests. In fact, series of events (sometimes referred to as a cascade, or waterfall (Fowler et al., 1989)) are seen in different stages of the test. Therefore, historic index ($H(I)$) and severity (S_r) as good indicators of onset of significant damage are investigated.

The historic index is used for identification of onset of significant emissions and is defined as a measure of the change in "signal strength" throughout the test (Golaski et al., 2002), (Nair and Cai, 2010a&b). Historic index is a form of trend analysis with the objective of locating significant changes in the slope of the cumulative signal strength versus time curve. It aims at comparing the signal strength of the most recent signals to all the signals, and is calculated as follows (Gostautas et al., 2005):

$$H(I) = \frac{N}{N-F}\left(\frac{\sum_{i=F+1}^{N} S_{oi}}{\sum_{i=1}^{N} S_{oi}}\right) \qquad 3-6$$

Similarly, the severity index is the average signal strength for a certain number of events having the largest value of signal strength (Gostautas et al., 2005). It is calculated as follows:

$$S_r = \frac{\sum_{g=1}^{J} S_{og}}{J} \qquad 3-7$$

In Eq. 3-6 and 7, *H(I)* = historic index at time t, *N* =number of signals up to and including time (*t*), *F and J* = empirically derived constants based on material type, S_{oi} (S_{og}) = signal strength of the i_{th} (g_{th}) signal. *F* values for metals depend on *N* and are given in [26]. For metals, *F* values are related to *N* by the relations: $N \leq 15$, $F = 0$; $16 \leq N \leq 75$, $F = N\text{-}15$; $76 \leq N \leq 1000$, $F = 0.8\,N$; $N \geq 1001$, $F = N\text{-}200$ as well as *J* values for $N < 10$; $J = 0$ and $N \geq 10$; $J = 10$ (Chotickai, 2001).

The values of historic index and severity index are commonly plotted on intensity charts for quantitative damage assessment (Chotickai, 2001) (Figure 3-2).

In this study the relevance of historic index and severity in fatigue tests is investigated in order to verify if these parameters could be of significance for early crack detection and diagnostics.

(Gong and Nyborg, 1992) devised a way to categorize crack into five different levels, as shown in Figure 3-3. The concept of classifying fatigue cracks in bridge steels into safety index levels, based on the range of ΔK determined by AE monitoring is used in this study and the tests are divided to intervals of 10 ksi-in.$^{1/2}$ for both K_{max} and ΔK parameters. This is to verify if a certain band of K_{max} or ΔK in the test can be associated to an AE feature as

H(I). This approach can be valuable in understanding the safety of the crack and decision making for a repair strategy.

3.1.1 LEFM validity

Based on ASTM-E561 (ASTM E561-10, 2011) for the compact tension (CT) specimen, in order to ensure that a given calculated value of *K* is valid, the remaining uncracked ligament must remain predominantly elastic. This condition is considered to be met as long as the length of the remaining uncracked ligament, $b - a_p$, at that point in the test is greater than or equal to eight plastic zone sizes. For plane stress condition this is met with the condition given in Eq. 3-8.

$$\left(b - a_p\right) \geq \frac{4}{\pi}\left(\frac{K_{max}}{\sigma_{YS}}\right)^2 \qquad 3-8$$

where b is the maximum achievable crack size, a_p is the physical crack size corresponding to the *K* for point being considered, and σ_{YS} is the 0.2 % offset yield strength of the material. This equation is assumed to be valid for the modified SE(T) specimen and a band of validity is developed for the plane stress condition. Assuming that the specimen is in plane strain condition and the remaining ligament stays greater than or equal to 8 plastic zone sizes, another band is developed to include more AE data. Experimental test results indicated that the Paris curve stays linear even after the plane strain valid band. Elastic-plastic FEM models will be required to fully verify the validity of the assumptions.

3.2 EXPERIMENTAL PROCEDURES

Modified SE(T) specimens were fabricated from A36 structural steel and ASTM A572 Grade 50 steel with final dimension of 29 by 2 by 0.5 in. (0.7366 by 0.0508 by 0.0127 m) representative of materials widely used in steel bridge construction. Cyclic tension loads with different R ratios were applied to the specimens using a servo-hydraulic mechanical testing machine under load-controlled mode and a constant amplitude cyclic load frequency of 2 Hz. A clip gage was employed to measure the crack mouth opening displacement (CMOD) and from it crack length, "*a*", was calculated during the test. The CMOD gage was mounted at the edge of the crack as shown in Figure 3-1. The surface of the crack was also monitored optically with two recording microscopes from the sides. Load and CMOD were recorded every 10 msec, which permitted 50 data points to be collected in a load cycle.

The test matrix used for this paper consisted of 7 specimens referenced in Table 3-1. Specimens were designed to take into account the effect of the R-ratio, initial crack size and gripping conditions (clevis and hydraulic wedge grips). The effect of gripping is thoroughly investigated in [30]. At mid-height of each specimen, a machined notch of initial depth 0.1 or 0.15 in. (2.54e-3 or 3.81e-3 m) was fabricated by the electric discharge machining (EDM) method, resulting in a sharp initial crack tip radius of 0.003 in. (7.62e-5 m). Geometries of both Clevis and hydraulic gripped specimens are shown in Figure 3-1.

3.2.1 AE Setup

Noise precautions were implemented in the test setup by attaching modeling clay to the specimen as acoustic damper. In addition, isolation shims between the grips and specimen were used in case of wedge gripped specimens (Figure 3-1-d). Before each test, a verification test was performed to identify the extraneous noise level and choose an appropriate threshold for AE signal recording. In this test, the minimum load in the cycles was increased to a higher level resulting in an insufficient ΔK for crack to grow. The AE signals obtained with this loading condition were assumed to be due to non-relevant emission. The AE threshold was then set to a level higher than the constant extraneous noise. Occasional extraneous noise with higher amplitudes was observed and filtered in post processing. The thresholds for sensors numbered 3 and 4 in the tests are given in Table 3-2. Sensors closer to the grips (numbered 1, 2, 5 and 6) were used as guard sensors to discriminate the extraneous noise coming from the grips. The guard sensor technique is a commonly used way of filtering the non-relevant signals based on the sequence of arrival times for AE signals at different sensors.

The AE technology has the notable advantage that the sensors together with appropriate algorithms are capable of locating active crack activity (Yu et al., 2012). AE location technique is based on triangulation and time of arrival of signals. At least two sensors are required to locate an event on the line connecting the sensors. Each event in a 1D case includes two signals captured by two sensors. Signals from events located further than 2 in. (0.0508 m) away from the notch were regarded as extraneous noise and filtered out. Of the relevant events, only one of two signals composing each event (signal with first time of arrival) was kept in the database.

Velocity of the acoustic wave was calculated in a pretest in which signals generated using standard Hsu–Nielsen pencil lead breaks (ASTM E976, 2010) at specimen mid-height on the opposite surface of the notch and along its length. This data was used in a location error minimization algorithm to calculate the optimal average velocity of wave propagation. After location filtering, AE signals with absolute energy and duration of zero magnitude were assumed insignificant and discarded. Post filtering protocol also included modified Swansong II filtering procedure (Railroads A. A. (1999)). In this step signals with low amplitude and high duration were filtered out using the amplitude and duration parameters described in Table 3-2.

AE data was recorded by Sensor Highway II-Remote Asset Integrity Monitor system. Six resonance sensors of type R15I-AST with integral 40 dB pre-amplification were utilized and the band pass of the analogue filter was set to 100 kHz to 300 kHz.

The sensors were attached to each specimen with vacuum grease and were fixed with clamps. Sensors other than sensors no. 3 and 4 had various threshold level based upon the extraneous noise level at the sensor location. Rate of recorded signals per sensor was kept similar or slightly higher for the guard sensors allowing for optimal use of the guard sensor technique.

3.3 RESULTS AND DISCUSSIONS

Only typical outcomes are shown in this study while details can be found in the appendix. The span in which LEFM is valid for plane stress condition (Eq. 3-8) was used to calculate Paris constants (Figure 3-4). It is observed that the experimental data is scattered in early stage and approach a line even beyond the plane strain limit of validity.

The early scatter can be due to initiation caused by the crack initiating from the round notch tip and the low initial applied ΔK. In order to calculate the material constants for Eq. 3-2 to 3-4 a minimum ΔK was chosen to exclude the initiation portion of the data. The valid bands of crack growth along with the corresponding Paris constants for each specimen are given in Table 3-3.

Representative plots of amplitude vs. duration and amplitude vs. absolute energy from the filtered dataset for a typical specimen are shown in Figure 3-5. The "banded region" data distribution in these two plots has been associated with genuine emission in previous studies (Yu et al., 2011), (Fowler et al., 1989b). Thus, Figure 3-5 supports the assumption that the majority of the signals after filtering are genuine and related to crack growth.

Captured AE events did not appear in a certain ranges of load in load cycles. However, at late stages of the test, AE signals appeared more commonly in highest quarter of the load range. As the early stage of the test is of interest here, all AE data in loading range is used for the further analysis.

In all specimens AE was able to detect and locate the crack at an early stage (e.g., for S4 when the crack was less than 0.12 in. (3.05e-3 m) long, ΔK was 8 ksi-in.$^{1/2}$ (8.79 MPa-m$^{1/2}$) and K_{max} was 9 ksi-in.$^{1/2}$ (9.89 MPa-m$^{1/2}$)).

Cumulative absolute energy and cumulative counts increased exponentially similar to crack length as the number of load cycles increased (Figure 3-6). As seen in Figure 3-6, cumulative absolute energy and cumulative counts can determine the critical level of crack growth.

The constants for Eq. 3-3 and 3-4 are calculated using the filtered AE data for each test. Linear least squares regression was performed to obtain the constants for Eq. 3-2 to 3-4 (*m, C, p, B_e, q, and B_n*) using crack growth and the filtered AE datasets. Figure 3-7 illustrates the data and regression results for a typical specimen using the two valid bands. Differently from Figure 3-5 that is not explicitly related to time, Figure 3-7 shows the scatter in the AE data during the test. Using the plane strain valid band leads to a more suitable curve as shown in Figure 3-7-b and Table 3-4. As seen in Figure 3-7-a, limited AE data is available in plane stress valid band, thus regression results are not representative of the clear trend that exist in the graph. The constants derived from plane strain limits as presented in Table 3-5 are used for further analysis. Table 3-5 shows that in each test result *p* is much closer than q to the theoretical value of (*m*+2). Hence, "absolute energy rate" may be more suitable than "count rate" in the prediction of crack extension and remaining fatigue life. As stated in Table 3-5 and illustrated in Figure 3-8, the value of q for the specimens with high R ratio is noticeably larger than the theoretical value of *m*+2. "B_e" is also considerably larger as theoretically expected ($B_e \sim 1/(1-R)^2$). This reveals that R ratio is critical when AE is used for assessment and prognostics of fatigue cracks. The constants derived from Table 3-5 were used in Eq. 3-5 to assess the crack size using only absolute energy feature for a typical specimen (Figure 3-9-a). To do this, the process of measuring crack size started after the initiation phase for a known a_i after N_i number of cycles. Then, Eq. 3-5 was used to compute "a_{i+1}" when a new AE signal was recorded after a certain number of cycles. Assuming that the material constants for Eq. 3-5 are known, the only unknown in the equation, a, is calculated using "absolute energy" value of the AE signals. This procedure is useful if the relationship

between K and "a" is not clearly defined or the crack is not visible or measurable. In these cases regardless of K, a crack size can be estimated when an AE signal is recorded. Figure 3-9-a indicates that AE can be used to predict the crack size regardless of the value of K. Large scatter or lack of data, however, can lead to inaccurate calculations. Data filtering, appropriate threshold for recording and proper choice of timing parameters of the signal measurement process as HDT (Hit Definition Time) and PDT (Peak Definition Time) becomes exceedingly important when crack propagation prediction is performed using AE. For thorough description of these parameters refer to (DiSP User's Manual, 2001).

Eq. 3-5 is incapable of predicting the crack growth behavior in future since the absolute energy value for a future AE signal is unknown. Thus, for a given number of cycles, a and U remain unknown and the problem stays unsolved. The relationship between K and a needs to be known for the problem to be mathematically solvable.

In the tested specimens, equations exists to correlate K to a for each case of gripping. dU/dN is attained by AE monitoring and the constants Be and p are calculated for the plane strain valid segment of the of fatigue life. Thus, dU/dN for any crack size can be obtained using Eq. 3-3. Assuming that at the end of this segment the crack size is a_i, after N_i number of cycles, dU/dN is numerically integrated over the segment a_i to a_{i+1} to calculate N_{i+1} using Eq. 3-5. The crack propagation prediction for a typical specimen is seen in Figure 3-9-b. Using count instead of absolute energy leads to identical results. The predicted curve closely follows the experimental curve as the constants are derived from the same test. More experiments are necessary for field validation, yet the proposed

methodology with which the relationship between fatigue and AE is established and its prediction is of general use.

The capability of AE to pinpoint significant damage is investigated as the next step. To do this, *H(I)* vs. load cycle, *N* and *ΔK* graphs are developed in order to see if *H(I)* can be used as warning when a certain level of damage is reached. As stated before, a jump in *H(I)* is recognized as a clear indication of damage occurrence. As presented in Figure 3-10, early oscillation in *H(I)* was observed in initiation stage in all tests. Assuming that LEFM is valid throughout each test, *H(I)* shows a major jump when *ΔK* is between 30 to 40 ksi-in.1/2 (33 to 44 MPa-m1/2) for tests with low R for the A572-Gr50 steel. A36 steel shows similar behavior but the ΔK value for the *H(I)* jump is less than 20 ksi-in.1/2 (22 MPa-$m^{1/2}$) (Figure 3-11). Also in specimens with high R ratio (S3 and S4), *H(I)* shows a jump while *ΔK* is between 10 and 20 ksi-$in.^{1/2}$ (11 and 22 MPa-$m^{1/2}$) and K_{max} is between 30 and 40 ksi-$in.^{1/2}$ (33 and 44 MPa-$m^{1/2}$). It is assessed that the jump for *H(I)* is seen at the limit of the plane strain valid band while in A36 steel the *H(I)* shows a jump at the border of valid plane stress limit. Literature suggests that a jump in *H(I)* represents the onset of significant damage. Table 3-6 shows that regardless of load value, steel type and R ratio, when the applied stress is roughly 40 to 60 percent of the yielding capacity of the remaining cross section, a jump appears in *H(I)*. This could be due to change in the nature of damage and the onset of plastic crack growth for which *K* is no longer characterizing the crack tip condition. Figure 3-12 shows the *Sr* vs. *H(I)* plot for a typical specimen. A similar trend of a jump in both *H(I)* and *Sr* is seen in all specimens. Intensity charts are normally plotted as point plots of *H(I)* vs. *Sr* derived from meaningful spans of time. Thus, the data from all tests is divided to intervals of 10 ksi-$in.^{1/2}$ (11 MPa-$m^{1/2}$)

using both K_{max} and ΔK parameters. Figure 3-13 illustrates an intensity chart for a typical specimen and each data point represents a 10 ksi-in.$^{1/2}$ (11 MPa-m$^{1/2}$) interval in ΔK and K_{max}, while the intervals are annotated sequentially. As observed in this figure, ΔK between 30 and 40 ksi-in.$^{1/2}$ (33 and 44 MPa-m$^{1/2}$) shows a significant jump in both axis of the graph. Referring to the data given in Figure 3-13, this jump in *H(I)* and *Sr* values can be designated as Crack Safety Index of 4 indicating "Dangerous" state. A similar concept can be used as a warning mechanism in bridge health monitoring to understand the severity of a crack for maintenance and decision making for repair.

3.4 CONCLUSIONS

Modified SE(T) specimens were tested under high cycle fatigue load while AE activity was monitored. The purpose of these tests was to understand if AE is capable of assessing, locating and predicting through-thickness crack growth in steel members. The specimen provides a simplified case of through-thickness crack growth that simulates fatigue cracks through the flange or early stage of crack growth in the web of steel bridge members. Guard sensor, location and modified Swanson II techniques were used to filter the extraneous noise. Hydraulic gripping condition provided lower noise levels compared to clevis griping. The effect of hydraulic grip condition on the stress intensity factor was accounted for in the stress intensity factor expressions. AE proved to identify and locate the crack at initiation stage and early stage of propagation. In initiation and LEFM valid propagation, limited numbers of signals were recorded and scatter in absolute energy and count of signals was observed. The calculated constant q to correlate absolute energy to crack growth rate was very close to the analytical value of $m+2$ based on the assumption that the absolute energy feature is representative of the released energy released from

crack extension. For specimens with high R ratio, the value of constant p was notably higher than $m+2$. This is important when considering that High R ratios exist in welded members. This also implies that K_{max} has an important role in fatigue assessment of cracks using AE. In the performed tests, the AE signals after filtering were not necessarily created close to peak load as reported in the literature (Roberts and Talebzadeh, 2003), (Yu et al., 2011).

AE absolute energy was used to predict the crack size after the test and the prediction results were compared to the experimental results. AE and crack growth constants were obtained based on the experimental data and procedures for predicting crack length and remaining fatigue life were demonstrated.

The validity of *H(I)* for fatigue crack propagation was evaluated and it is observed that regardless of initial crack size, R ratio and gripping condition, *H(I)* significantly increases when K_{max} reaches 30 to 40 ksi-in.$^{1/2}$ (33 to 44 MPa-m$^{1/2}$) in A572-Gr50 steel and 15-20 ksi-in.$^{1/2}$ (16.5 to 22 MPa-m$^{1/2}$) in A36 steel. The jump in *H(I)* happened when the applied stress was about half of the capacity to yielding of the net cross section of crack plane.

FIGURES

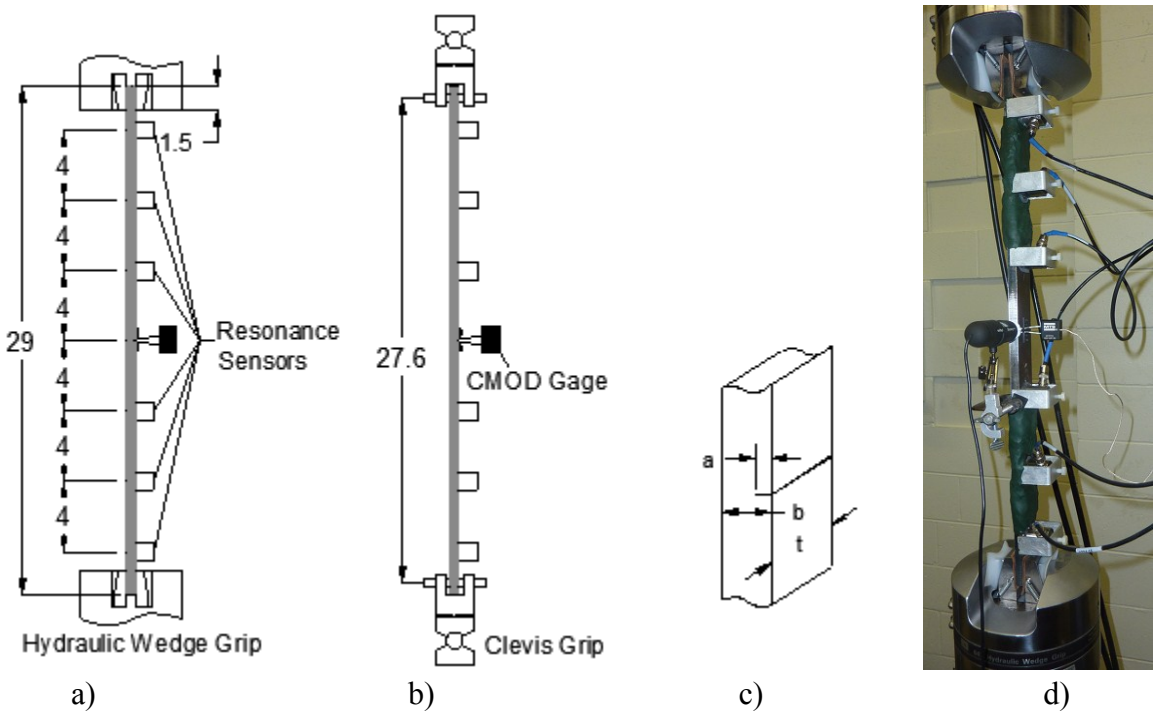

Figure 3-1. SE(T) specimen test setup and sensor layout (dimensions in in., 1 in.=2.54e-2 m) a) Test with Hydraulic wedge gripping b) Tests with clevis gripping c) Notch in the middle of the specimen d) Experiment setup details

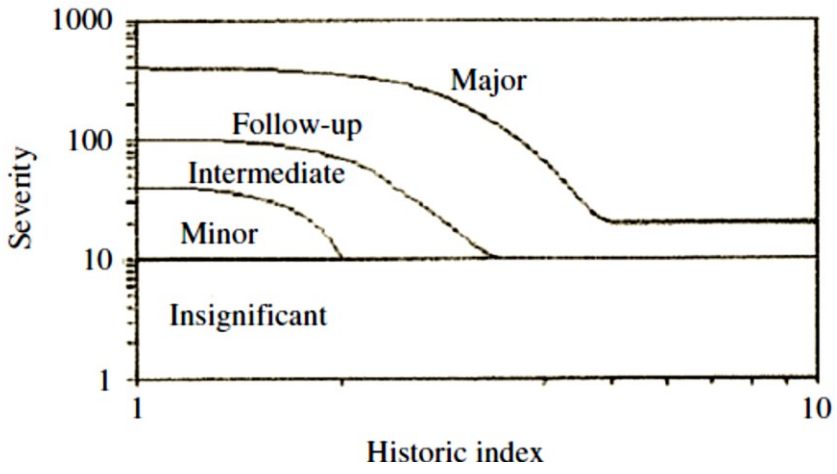

Figure 3-2. Intensity charts used for quantitative damage assessment

Range of ΔK	Crack Safety Index	Crack Description
$0 < \Delta K < 10$	1	Minor defect
$10 \leq \Delta K < 20$	2	Slow crack growth
$20 \leq \Delta K < 30$	3	Requires repair
$30 \leq \Delta K < 40$	4	Dangerous
$40 \leq \Delta K$	5	Imminent failure

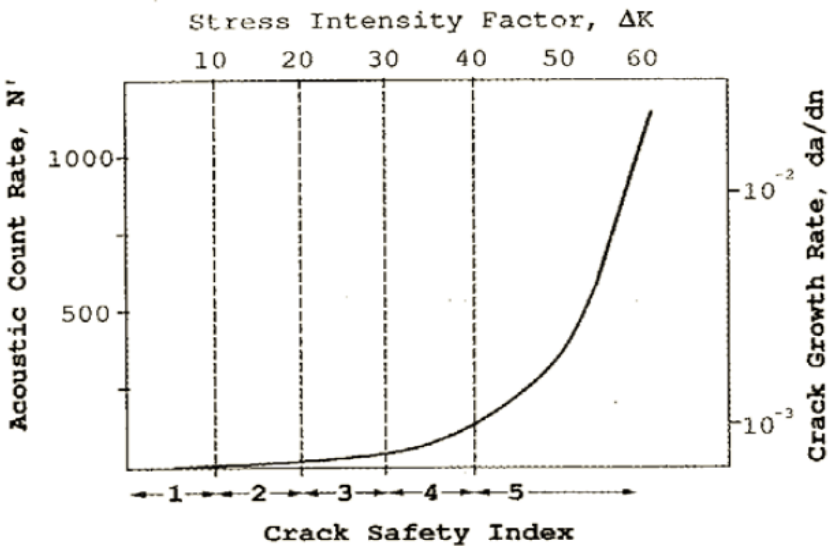

Figure 3-3. Typical relationships among crack safety index, crack growth rate, count rate and *ΔK* for bridge steels

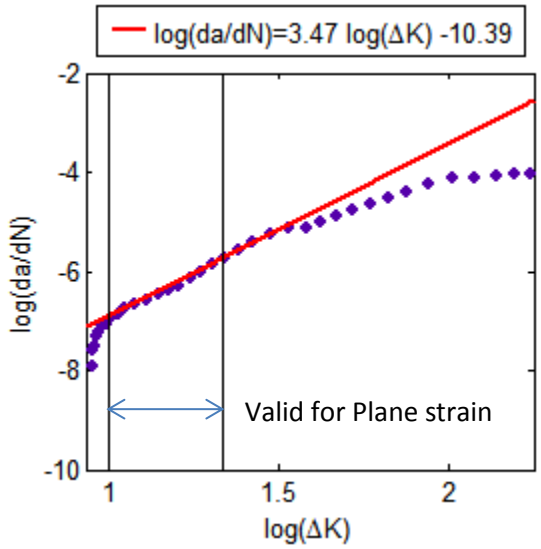

Figure 3-4. Typical experimental and regression results for valid reign of crack growth (specimen S2)

(ΔK in ksi-in.$^{1/2}$, 1 in.=2.54e-2 m, 1 ksi-in.$^{1/2}$=1.1 MPa-in.$^{1/2}$)

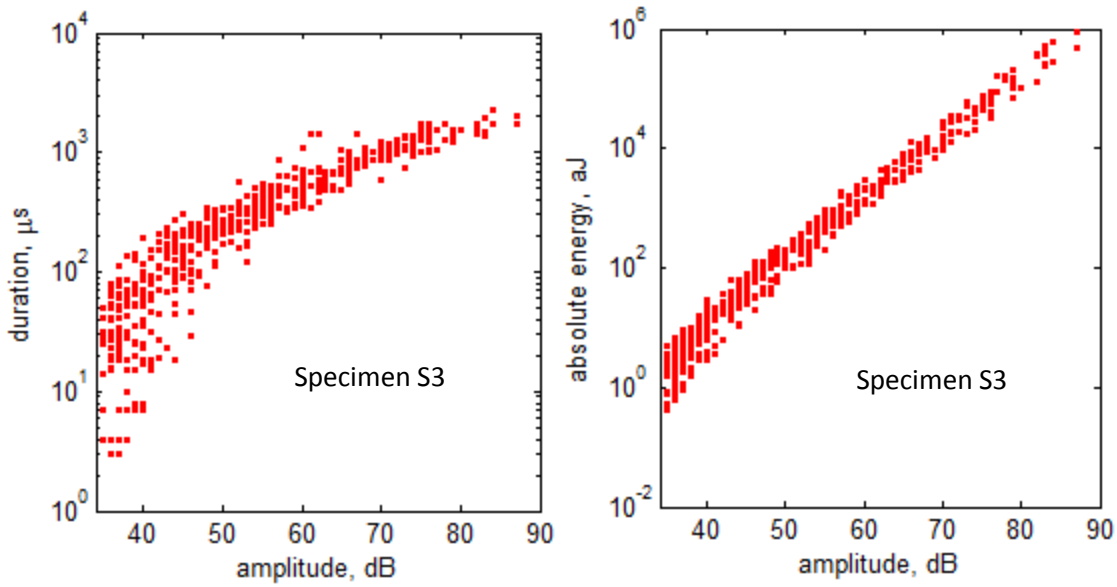

Figure 3-5. Data quality graphs for a typical specimen (after filtering)

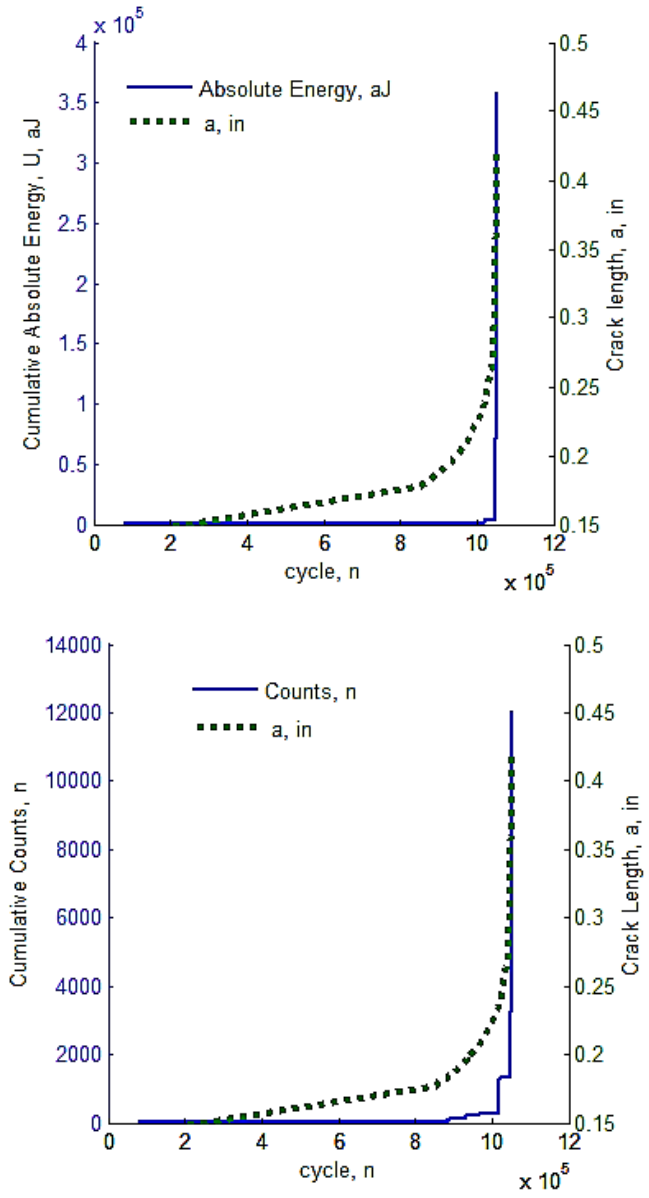

Figure 3-6. a) Cumulative absolute energy and rack length versus load cycles; b) Cumulative counts and crack length versus load cycles

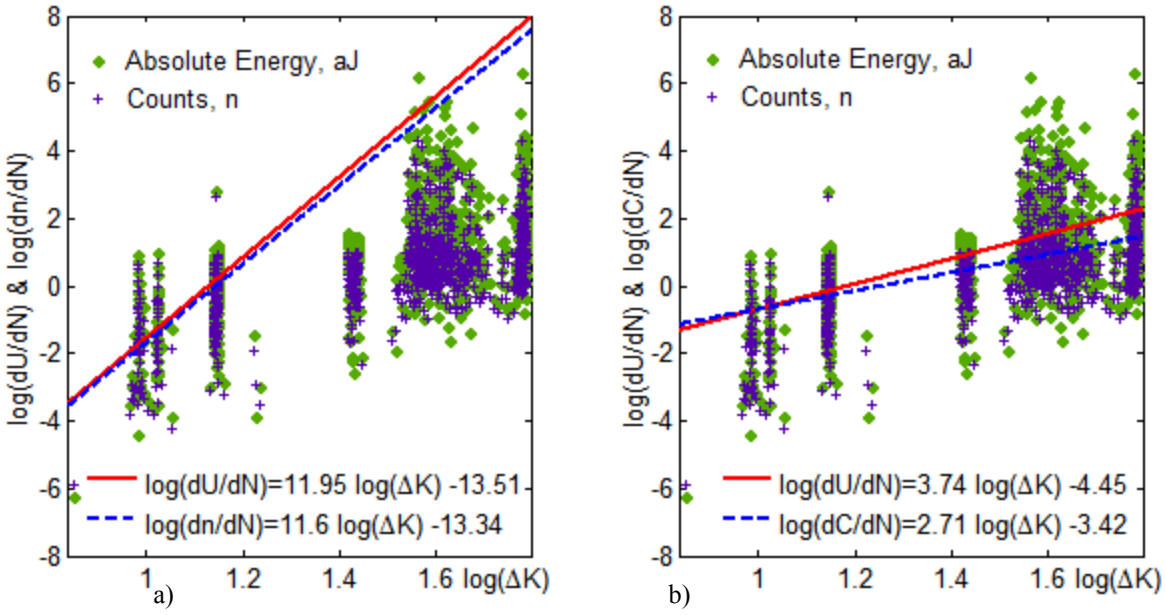

Figure 3-7. Absolute energy and count rate for a typical specimen with low *R* ratio, (ΔK in ksi-in.$^{1/2}$, 1 ksi-in.$^{1/2}$=1.1 MPa-in.$^{1/2}$): a) regression on plane stress valid band; b) regression on plane strain valid band (specimen S3)

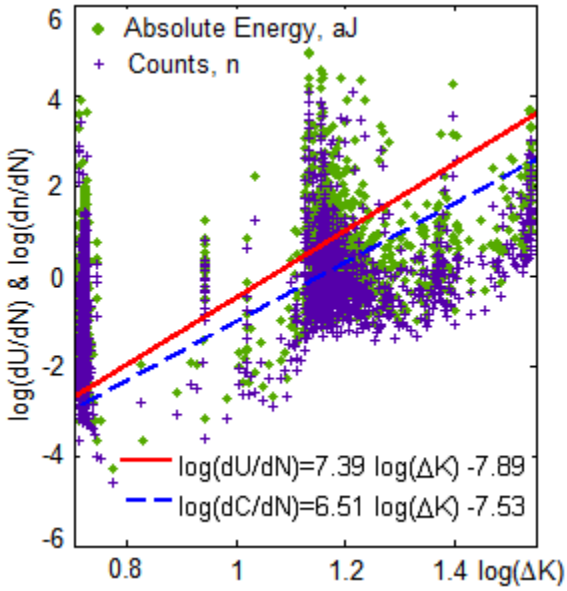

Figure 3-8. Absolute energy and count rate on plane strain valid band for specimen with high R ratio (ΔK in ksi-in.$^{1/2}$, 1 ksi-in.$^{1/2}$=1.1 MPa-in.$^{1/2}$, specimen S5)

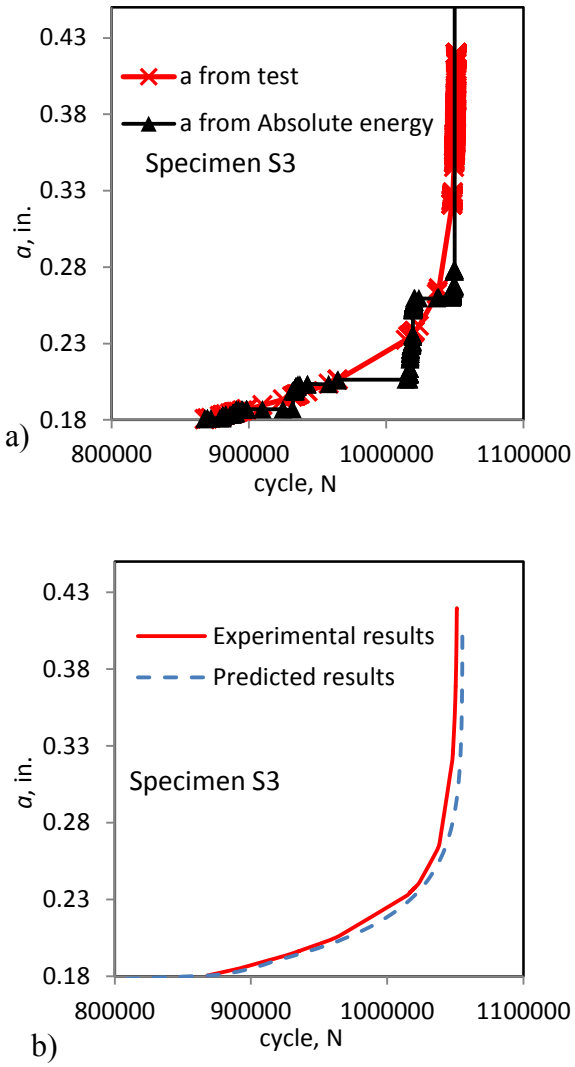

Figure 3-9. a) Crack size assessment based on AE absolute energy b) Crack propagation prediction based on AE absolute energy (1 in.=2.54e-2 m)

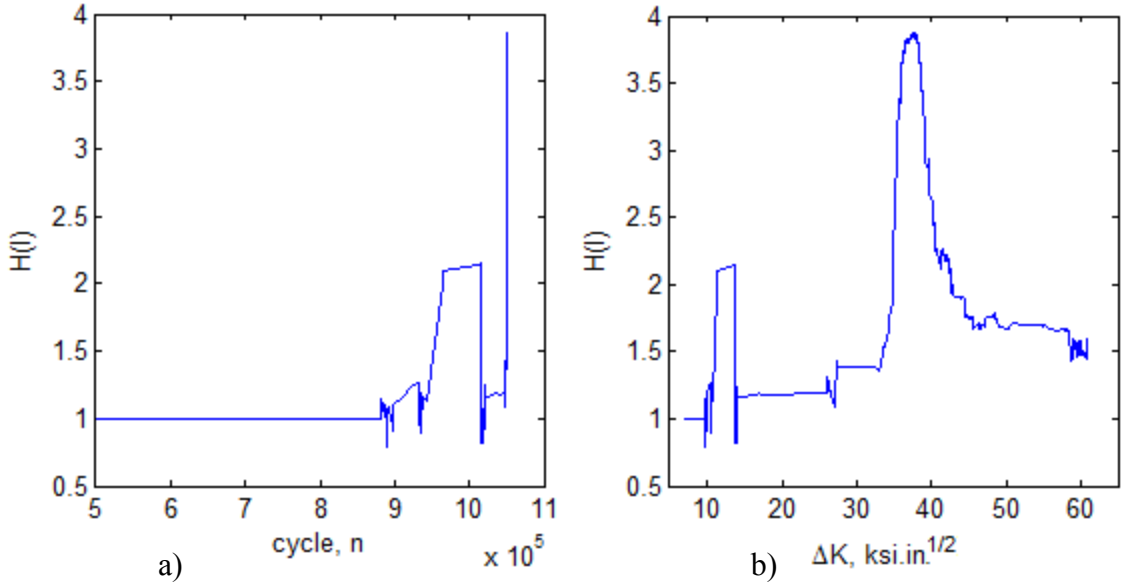

Figure 3-10. Typical specimen with A572-GR50 steel: a) *H(I)* vs. *n;* b) *H(I)* vs. *ΔK* (ΔK in ksi-in.$^{1/2}$, 1 ksi-in.$^{1/2}$=1.1 MPa-in.$^{1/2}$, specimen S3)

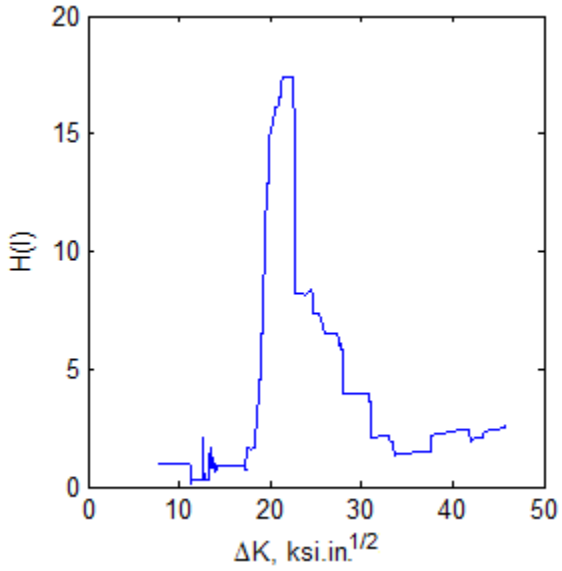

Figure 3-11. *H(I)* vs. *ΔK* for a typical specimen of A36 steel (ΔK in ksi-in.$^{1/2}$, 1 ksi-in.$^{1/2}$=1.1 MPa-in.$^{1/2}$, specimen S2)

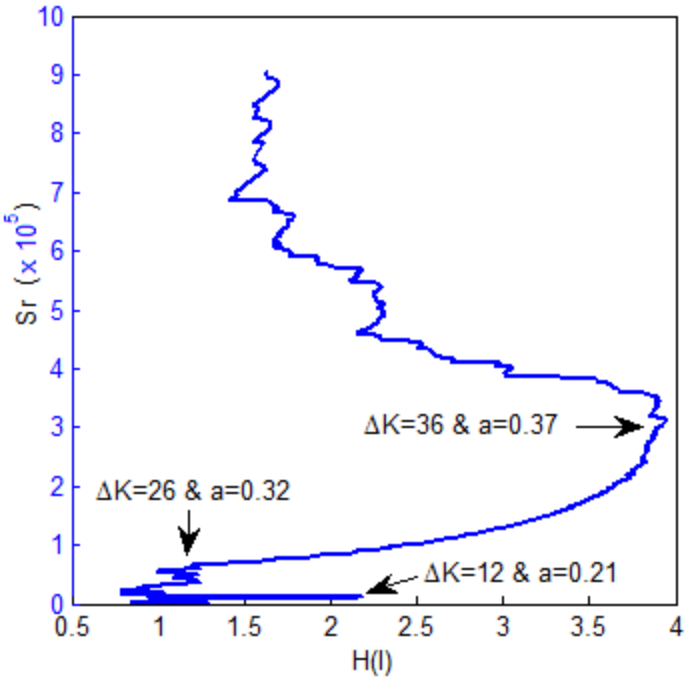

Figure 3-12. *Sr* vs. *H(I)* for a typical specimen (Sr in Pico-volt sec unit) (specimen S3)

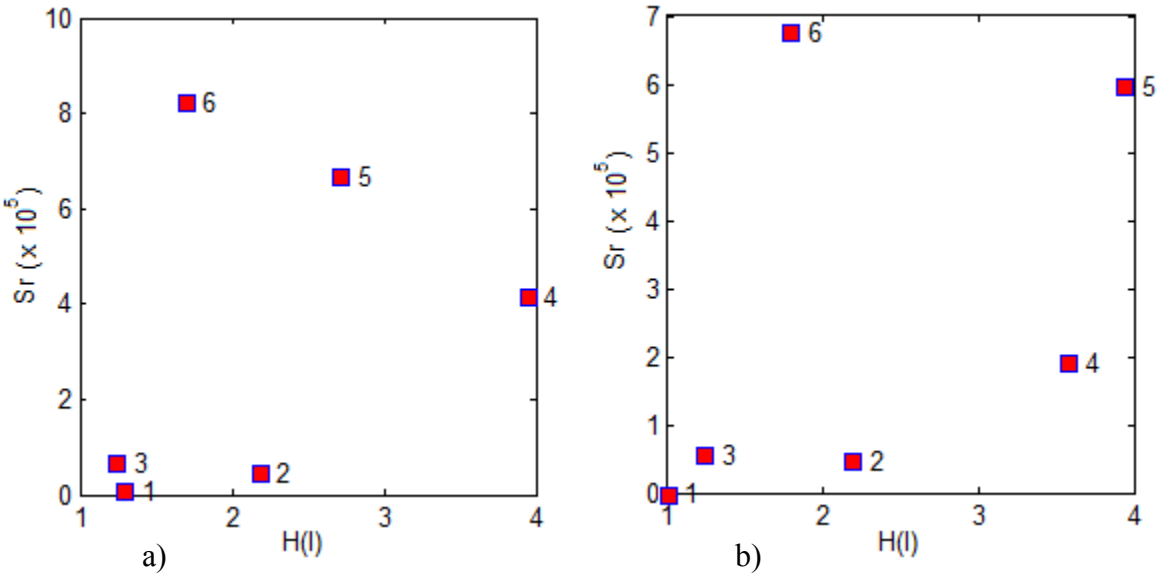

Figure 3-13. Intensity charts for a typical specimen: a) for test segments based on *ΔK*; b) for test segments based on K_{max} (*Sr* in Pico-volt sec unit, ΔK in ksi-in.$^{1/2}$, 1 ksi-in.$^{1/2}$=1.1 MPa-in.$^{1/2}$, specimen S3)

TABLES

Table 3-1. Applied load and geometry of specimens (1 in. =2.54e-2 m, 1 ksi= 6.89 MPa, 1 ksi-in.$^{1/2}$=1.1 MPa-in.$^{1/2}$)

Code	Gripping	Notch (in.)	σ_{min} (ksi)	σ_{Max} (ksi)	Initial ΔK (ksi-in.$^{1/2}$)	R	Material
S1	Wedge	0.15	0.71	6.97	7.04	0.10	A36
S2	Wedge	0.15	0.74	7.37	7.04	0.10	A36
S3	Wedge	0.15	0.75	7.46	7.04	0.10	A572-GR50
S4	Wedge	0.10	1.00	10.20	7.05	0.10	A572-GR50
S5	Wedge	0.10	10.00	16.70	5.13	0.60	A572-GR50
S6	Clevis	0.15	0.69	6.90	7.04	0.10	A572-GR50
S7	Clevis	0.15	6.3	10.50	4.76	0.60	A572-GR50

Table 3-2. Test thresholds and modified Swansong II filtering parameters

Code	Threshold, dB	Modified Swansong II filters in terms of Amplitude(A), dB and Duration(D), µs			
S1	34	A<36,D>100	36<A<38,D>150	38<A<41,D>250	41<A<45,D>500
S2	35	A<37,D>100	37<A<40,D>150	40<A<44,D>250	44<A<50,D>500
S3	35	A<40,D>100	40<A<44,D>150	44<A<50,D>350	
S4	38	A<40,D>100	40<A<42,D>250	42<A<45,D>350	45<A<50,D>750
S5	40	A<42,D>150	42<A<45,D>250	45<A<48,D>500	48<A<50,D>750
S6	41	A<45,D>250	45<A<54,D>350	54<A<60,D>500	
S7	41	A<45,D>250	45<A<54,D>350	54<A<60,D>500	

Table 3-3. Valid bands of crack growth and Paris constants calculated from regression (ΔK in ksi-in.1/2, 1 in.=2.54e-2 m, 1 ksi-in.1/2=1.1 MPa-in.1/2)

		Plane stress band			Plane strain band		
Code	ΔK after Initiation	Valid ΔK Limit	*log C*	*m*	Valid ΔK Limit	*log C*	*m*
S1	12.5	14.5	-11.2	4.36	22	-9.15	3.12
S2	10	15	-10.07	3.18	22.5	-9.8	3.43
S3	10	19	-10.79	3.77	29	-10.72	4.08
S4	11	21	-11.69	4.59	31	-9.94	3.92
S5	9.5	11	-10.74	3.93	15.5	-9.72	3.37
S6	10	19	-10.16	3.24	29.5	-9.5	2.93
S7	8	10	-9.48	2.81	15.5	-9.3	2.84

Table 3-4. LEFM valid bands (K in ksi-in.$^{1/2}$, 1 in. =2.54e-2 m, 1 ksi-in.$^{1/2}$=1.1 MPa-in.$^{1/2}$)

			Plane stress band			Plane strain band		
Code	ΔK Start	a_S (in.)	ΔK Valid Limit	a_v (in.)	K_{max} Valid Limit	ΔK Valid Limit	a_v (in.)	K_{max} Valid Limit
S1	10	0.18	14	0.24	15.5	22	0.30	24.5
S2	10	0.16	15	0.24	16.5	22.5	0.29	25
S3	8	0.17	19	0.27	21	29	0.32	32
S4	8	0.12	21	0.24	23	31	0.29	34
S5	6.5	0.13	11	0.2	27	15.5	0.24	37
S6	8	0.17	19	0.27	21	29.5	0.32	33
S7	8.5	0.18	10	0.24	23	15.5	0.28	34

Table 3-5. Regression results for valid test portion in plane strain (ΔK in ksi-in.$^{1/2}$, 1 in.=2.54e-2 m , 1 ksi-in.$^{1/2}$=1.1 MPa-in.$^{1/2}$)

Code	*Log(C)*	*m*	*Log(B_e)*	*p*	*Log(B_c)*	*q*
S1	-9.15	3.12	-4.64	4.83	-5.24	5.14
S2	-9.8	3.43	-6.64	5.55	-6.11	4.87
S3	-10.72	4.08	-4.45	3.74	-3.42	2.71
S4	-9.94	3.92	-2.84	2.83	-2.51	2.19
S5	-9.72	3.37	-7.89	7.39	-7.53	6.51
S6	-9.5	2.93	-4.79	3.84	-4.23	3.08
S7	-9.3	2.84	-15.78	12.95	-12.31	9.54

Table 3-6. Jump in H(I) curve for different specimens (1 in. =2.54e-2 m, 1 ksi= 6.89 MPa, 1 ksi-in.$^{1/2}$=1.1 MPa-in.$^{1/2}$)

Code	σ_y(ksi)	ΔK (ksi-in.$^{1/2}$)	K_{max} (ksi-in.$^{1/2}$)	*a*(in.)	r_y(in.)	*b-a*(in.)	σ_{net}/σ_y*100
S1	36	17	19	0.27	0.05	0.23	42.09
S2	36	17	19	0.26	0.05	0.24	42.67
S3	50	34	37.5	0.34	0.09	0.16	46.62
S4	50	36	40	0.31	0.10	0.19	53.68
S5	50	13	33	0.23	0.07	0.28	60.73
S6	50	31	34.5	0.33	0.08	0.18	39.43
S7	50	13.5	31.3	0.27	0.06	0.23	45.65

CHAPTER 4, STUDY 3 - ACOUSTIC EMISSION ASSESSMENT OF FATIGUE CRACK GROWTH FROM TRANSVERSE WELD TOE

SUMMARY

Acoustic emission (AE) has been increasingly used for assessment and prediction of fatigue cracks in steel bridge members. Fatigue cracks develop at the transverse weld toe of stiffeners, attachments, and cover plates in steel bridge members. Effectiveness of AE to assess fatigue crack initiation from weld toe is investigated in this study and an attempt is made to predict the crack growth behavior using AE signal features. Cruciform specimens consisting of a single tension pull plate with transverse fillet welded plates attached at midspan are tested in this study. The transverse plates represent stiffeners and/or short attachments typical of welded steel bridge details. The specimen provides realistic initial conditions of fatigue crack initiation and growth from high stress concentration regions. Consequently, AE waveform characteristics representative of those expected on bridge structures are produced. Accurate stress intensity factor values are difficult to obtain due to the small, non-uniform crack growth conditions at the weld toe. Finite Element Method analysis for welded geometries capturing stress fields at the weld toe of stiffener details is performed and numerical results are incorporated into an existing analytical stress intensity factor framework. Procedures for assessing the crack size and predicting remaining fatigue life of the specimen using absolute energy feature of AE signals are demonstrated.

OUTLINE

Fatigue cracks develop at the transverse weld toe of stiffeners, attachments, and cover plates in steel bridge members. The cracks initiate from a combination of conditions (e.g., weld toe geometry and discontinuities) that are difficult to accurately quantify, thus adapting fracture mechanics models for the prediction of fatigue crack growth is difficult without experimental verification (Metrovich and Fisher, 2005, 2006). Accurate assessment of the early fatigue crack growth characteristics is essential for the implementation of any rational prognostic methodology. Fatigue cracks, which are large enough to be detected by ordinary NDE inspection techniques, typically require extensive repair efforts (Fisher et al., 1979), (Roy et al., 2003). Thus, this level of crack detection is not suitable to develop efficient prognostic tools. Acoustic emission (AE) has been increasingly used for assessment and prediction of fatigue cracks in steel bridge members (Gong and Nyborg, 1992), (Martin, 1995), (Ziehl, 2008), (Yu et. al., 2011), (Nemati et al., 2011). AE fatigue crack monitoring has the potential of providing early fatigue crack detection and insight to assess structural integrity (Martin, 1995), (Ziehl, 2008). AE originates from defect-related sources such as crack extension and plasticization of material in the highly stressed zone adjacent to the crack tip (Roberts and Talebzadeh, 2003). Studies on well-defined fatigue crack shapes have shown good correlation between AE and crack growth parameters, indicating that AE can assist in understanding the state of the crack and predicting its behavior due to cyclic loads Roberts and Talebzadeh, 2003), (Yu et. al., 2011) .

In this study, the developed fundamental relationship between absolute energy rate of the AE signals and crack growth rate is evaluated and refined (study 2). The validity of the

Historic Index (*H(I)*) as an indicator of onset of significant damage is investigated. Historic Index is commonly used as a form of trend analysis with the objective of detecting significant changes in the slope of the cumulative signal strength versus time curve (Chotickai, 2001), (Nair and Cai, 2010), (Gostautas et al., 2005). This study aims to verify the ability of the AE method to locate and assess the size and severity of a crack initiating from the transverse weld toe of an attachment detail common in steel bridges. Cruciform specimens that consist of a single tension pull plate with transverse fillet welded plates attached at midspan are manufactured and fatigue tested. These specimens provide realistic initial conditions of fatigue crack initiation and growth from high stress concentration regions. Six specimens were tested to account for the statistical variability in weld discontinuities. The applied loading condition and load ratio (*R* ratio) is kept constant. The attachment was designed to be thicker than the base plate with the logic being that the further the spatial distance of weld toes, the easier it is to locate AE signals coming from weld toes on the two sides of the stiffener. Therefore, the probability of obtaining signals related to crack initiations in weld toes other than the one leading to failure is decreased. The use of larger stiffeners also produces fatigue cracks at lower nominal stress ranges.

4.1 EXPERIMENTAL PROCEDURE

The specimens are fabricated from ASTM A572 Grade 50 steel representative of materials widely used in steel bridge construction. Cyclic tension load was applied to the specimens using a servo-hydraulic mechanical testing machine under load-controlled mode with a constant amplitude cyclic load frequency of 2 Hz and an applied *R* ratio of 0.1. To account for both the probabilistic nature of fatigue crack growth from a weld toe

and to eliminate the effects induced by an edge on a weld, six specimens were cut from same assembly. The geometry of the specimens is shown in Figure 4-1. Table 4-1 shows the specifications of loading and geometry of the test specimens.

4.1.1 AE Setup

Acoustic noise is a significant issue when monitoring AE events during a fatigue test. Noise abatement precautions were implemented in the test setup by attaching modeling clay to the specimen as an acoustic damper. In addition, isolation shims between the grips and specimen were used. Before each fatigue test, a verification trial was performed to identify the extraneous noise level and to choose an appropriate threshold for AE signal recording. In this trial, the minimum load in the applied load cycle was increased while holding the maximum load constant, resulting in an insufficient stress range, $\Delta\sigma$, for crack growth ($\Delta\sigma$ = 6 ksi = 41.37 MPa). The frequent AE signals obtained under this loading condition were assumed to be due to non-relevant emission. The AE threshold was then set to a level higher than the frequent extraneous noise. Occasional extraneous noise with higher amplitudes was observed and filtered in post-processing. Sensors located nearest to the grips (numbered 1 and 4 in Figure 4-1) were used as guard sensors to discriminate the extraneous noise coming from the grips. The guard sensor technique is a commonly used way of filtering the non-relevant signals based on the sequence of arrival times for AE signals at different sensors.

The AE technology has the advantage that sensors together with appropriate algorithms are capable of spatially identifying active cracks. At least two sensors are required to locate an event on the line connecting the sensors. Each located AE event in a 1D case includes two signals captured by two sensors. Signals from events located further than 3

inches away from the weld toes were regarded as extraneous noise and filtered out. Only the AE events located on the specimen half which included the fatigue crack failure surface were used for AE to fatigue crack growth correlation in post-processing. Of the relevant AE events, only one of two signals composing each event was kept in the database, corresponding to the signal with first time of arrival.

Velocity of the acoustic wave was calculated with signals generated by standard Hsu–Nielsen pencil lead breaks located at specimen weld toes (ASTM E976, 2010). This data set was used in a location error minimization algorithm to calculate the optimal average velocity of wave propagation. Post-filtering protocol also included a modified Swansong II filtering procedure (Railroads, A. A., 1999). In this step, signals with low amplitude and high duration were filtered out using the amplitude and duration parameters described in Table 4-2.

AE data was recorded with a Sensor Highway II-Remote Asset Integrity Monitor system manufactured by Mistras Group. Four standard resonant sensors of type R15I-AST with integral 40 dB pre-amplification were utilized and the band pass of the analogue filter was set from 100 kHz to 300 kHz. The sensors were attached to each specimen using vacuum grease and clamps.

4.2 THEORETICAL PROCEDURE

Typical fatigue design of members in bridges utilizes the S_R-N curve approach (AASHTO, 1999). This is a graph of the logarithmic magnitude of a cyclic stress range (S_R) against the logarithmic scale of cycles to failure (N). Transverse cruciform fillet-welded joints are essential parts of welded structures and are generally classified into

load-carrying and non-load-carrying joints, and in the latter, fatigue cracks usually occur at the weld toes (Metrovich et al., 2012).. The specimen used in this study is considered a Category C' detail based upon the attachment's length in the direction of applied stress. (AASHTO, 1999) Constant-Amplitude Fatigue Limit (CAFL) of 12 ksi (82.74 MPa) was estimated for this detail (AASHTO, 1999).

4.2.1 Fatigue Life and Threshold

Expressions for relating the stress intensity factor K to crack length a for a crack propagating from 45- and 90-degree weld toes of a 1 in. attachment welded to an infinitely thick plate were derived by (Metrovich and Fisher, 2005, 2006) and (Metrovich et al., 2012). In order to propose a crack evolution model, the weld toe angle is assumed to be 90 degree to account for a lower bound, or worst case, solution for crack life. For 90-degree weld toe the expression that related K to a is presented in Eq. 4-1:

$$K = (0.445a^{0.0455} + 0.689a^{0.4085} + 0.9a)\sigma \quad \text{(ksi)} \qquad 4-1$$

To account for finite base plate thickness effects, existence of a stiffener on both sides, and crack front shape, two correction factors F_T (thickness and opposite stiffener) and F_S (curved crack front) are introduced as follows:

$$K = F_T F_S(0.445a^{0.0455} + 0.689a^{0.4085} + 0.9a)\sigma \quad \text{(ksi)} \qquad 4-2$$

A series of two dimensional Finite Element Method (FEM) analyses were performed to capture the stress field at the weld toe of 1 in. stiffeners with geometry replicating experimental specimens with 90-degree weld toe angle. Stress intensity factors were examined for 10 different crack depths covering the range of crack sizes expected through fatigue life of the specimen. The effect of limited thickness is shown in

Figure 4-2 and Table 4-3. Using the results of FEM analysis, the correction factor F_T is estimated by linear least square regression and is formulated in Eq. 4-3 as a function of a and t, the thickness of the base plate. This equation is valid over the range of crack sizes 0.0001" ≤ a ≤ 0.45".

$$F_T = \frac{-2.406\frac{a}{t} + ln\left(0.9738\frac{a}{t}\right)}{0.9612\ ln\left(0.9379\frac{a}{t}\right)} \qquad 4-3$$

The estimated values for F_T using Eq. 4-3 have an error of less than 0.7 percent as shown in Table 4-3. Fatigue cracks at fillet welds maintain a curved crack front as they propagate through the plate's thickness. For a uniform edge crack growth, F_S is equal to 1.0 and for an elliptical crack the shape correction factor F_S for stiffeners and short attachment details is defined as (Fisher et al., 1974):

$$F_S = \frac{1}{\sqrt{1 + 1.464\left(\frac{a}{b}\right)^{1.65}}} \qquad 4-4$$

where $2b$ is the crack width. The estimate of crack shape evolution for stiffener details have been developed from the experimental measurements by (Fisher et al., 1974) as:

$$b = 1.088a^{0.946} \qquad 4-5$$

Substituting Eq. 4-5 into Eq. 4-4 leads to:

$$F_S = \frac{1}{\sqrt{1 + 1.2738\ a^{0.0891}}} \qquad 4-6$$

This relationship was adopted for the current study.

4.2.2 Crack Evolution Model

No continuous measurement of crack size during the tests was possible. Based on experimental observations and empirical evidence it is confirmed that the crack growth is not a simple elliptical or uniform crack growth. This is due to simultaneous initiations that lead to multiple elliptical cracks that merge as they expanded due to cyclic fatigue loading. Observations from the crack surfaces indicate that several shear planes along the weld toe existed; where two or more independently growing cracks merged. On the other hand the elliptical crack shape (a to b) relationship (Eq. 4-5) suggests that the crack width along the weld toe ($2b$) would be 1.13 in. (2.87e-2 m) when the crack depth reaches the opposite surface of the base plate, while the visual crack surface indicates this is not the case. Therefore it is assumed that multiple elliptical cracks merged to form a uniform edge crack as the crack approached 0.1 in. in depth. Thus, for $a > 0.1$ in. (2.54e-3 m), Eq. 2 with F_S equal to 1 is used for the stress intensity factor K. For $a < 0.05$ in. (1.27e-3 m), simultaneous elliptical crack propagations are assumed. For this crack range the model follows Eq. 4-6 defined above assuming small crack shape evolution similar to results obtained from previous experimental studies. An intermediate stage was presumed between these two stages using a linear relation between a and K for $a = 0.05$ to 0.1 in. (1.27e-3 to 2.54e-3 m). The equation for this segment is derived as K=160.17a + 0.467 (K in ksi.in.$^{1/2}$ and a in in.).

Paris–Erdogan relationship (Paris and Erdogan, 1963), a commonly accepted method in practice for a wide range of mode I cracks, is used to predict fatigue crack propagation. This relationship is given as:

$$\frac{da}{dN} = C(\Delta K)^m \qquad 4-7$$

where a is a representative crack length, N is the number of fatigue cycles, and C and m are empirically obtained material constants. da/dN is increment in crack growth, da, per load cycle, dN.

Eq. 4-7 can be integrated as:

$$N = \int_{ai}^{af} \frac{da}{C(\Delta K)^m} \qquad 4-8$$

Where N is the number of load cycles required to grow a crack from the initial crack size a_i to final crack size a_f. As cross section at failure is available, final crack size, a_f, is measured directly from the specimen and used as final crack size in order to calculate the number of cycles required to grow the crack to failure. Implementing the crack shape model described above into stress intensity factor, and integrating Eq. 8 from an initial crack size of a_i = 0 in. to a_f = 0.41 in., provides an estimated fatigue life of N=661,962 load cycles for a constant applied stress range of $\Delta\sigma$=16 ksi. The material constants of C=3.6*10^{-10} and m=3 (ksi.in$^{1/2}$) are conservative estimates for fatigue crack growth in typical structural steels according to reference (Barsom and Rolfe, 1999). Material constants from a set of SE(T) specimen of the same steel tested under high R = 0.6 ratio (study 2) provided material constants of (C=1.905*10^{-10}, m=3.37). When these material constants were integrated in Eq. 8, the fatigue life was predicted to be 610,039 load cycles. The latter is used for this study as the lower bond of fatigue life. If the number of load cycles in experimental tests is larger than the predicted value, it is assumed the extra cycles are spent in initiation and only the final 610,039 cycles of the test is defined as propagation stage.

Figure 4-3 shows the crack growth behavior using the proposed crack evolution model compared with elliptical and uniform edge crack models assuming weld toe angles of 45 and 90 degrees. The proposed model accurately captured the lower bound fatigue life from experimental tests as seen in Figure 4-3. The proposed fatigue crack model is accurate enough to meaningfully correlate AE to fracture parameters in diagnostic and prognostic procedures. Ideally, accurate and continues crack size and shape measurements are required throughout the fatigue life in order to obtain an accurate correlation between K values and a. Beach marking, Ultrasonic Testing (UT) and penetrant testing (PT) were performed on the specimens but could not identify the crack shape continuously and the accuracy of the results were not certain.

4.2.3 LEFM Validity

In order to ensure that a calculated value of K is valid, the remaining uncracked ligament ahead of crack must remain predominantly elastic (study 2). This condition is considered to be met as long as the length of the remaining uncracked ligament at that point in the test is greater than or equal to eight plastic zone sizes (ASTM E561-10, 2010). Using the proposed crack evolution method the relationship between a and K is known and illustrated in Figure 4-4. Using the plane stress limit the value of maximum LEFM valid crack size, a, is considered to be 0.15 in. for these tests. Elastic-plastic FEM models will be required to fully verify the validity of the assumptions.

4.3 AE FATIGUE CRACK ASSESSMENT AND LIFE PREDICTION

The procedure for fatigue assessment and prediction using AE absolute energy (U) feature is thoroughly described in (study 2). In this study the same procedure is used to

assess the crack size without knowing the correlation between K and a. Using Eq. 4-9, crack size at any stage of fatigue life can be evaluated in real time by absolute energy rate of the AE signals.

$$\frac{da}{dN} = B_g \left(\frac{dU}{dN}\right)^r \qquad 4-9$$

where B_g and r are constants and dU/dN and da/dN are AE absolute energy rate and crack growth rate, respectively. In order to account for the effect of R ratio, the constants from the SET test with high R ratio are used to calculate the crack size in this study. (B_g and r are 7.55E-07 and 0.456 respectively).

When an AE signal is recorded after a certain number of cycles, the only unknown in Eq. 4-10 becomes the extension of a. Then, Eq. 4-9 can be used to predict the behavior of the crack using absolute energy rate of recorded AE signals.

$$\frac{dU}{dN} = B_e(\Delta K)^p \qquad 4-10$$

where B_e and p are constants derived from regression of the cruciform test data using the plane stress LEFM valid propagation band. For the crack growth prediction to be possible, the relationship between K and a need to be known. The proposed crack evolution model is used to provide this relationship.

Historic Index (*H(I)*) as indicator of onset of significant damage is investigated for the test. The Historic Index is used for identification of onset of significant emissions and is defined as a measure of the change in "signal strength" throughout the test (study 2) and it aims at comparing the signal strength of the most recent signals to all the signals.

4.4 RESULT AND DISCUSSION

Total fatigue life for all specimens is shown in Table 4-4. The results are plotted in S-N curves and appear to represent a category D detail (Figure 4-5), although they are consistent with the calculated fatigue model of Figure 4-3.

As fatigue crack initiation in a weld toe is expected anywhere along the weld toe line, some specimens had asymmetric crack growth and this could be confirmed by the yielded ligament at failure seen on the crack surface in Figure 4-6. This is due to the statistical nature of crack initiation at weld toe. If earlier crack initiation occurs near one side of the weld toe, it will grow from that side of the plate. As a result, a higher driving K can cause a faster growth on one side of the specimen with respect to another, producing an asymmetric crack growth (Figure 4-6). For most bridge details, large dimension plates most likely preclude this asymmetric crack shape. Hence, a typical specimen with symmetric crack growth (C1) is used for AE to fatigue correlation in this study.

Crack size, K_{max} and ΔK, for filtered AE hits were calculated knowing the cycle number at which each AE signal is recorded and using the proposed crack evolution model. The observations made in this study utilizing values of a and K are based upon the proposed crack evolution model.

AE was able to locate the crack at the weld toe of the specimen after less than 100,000 cycles when ΔK was about 5 ksi.in$^{1/2}$ (5.49 MPa.m$^{1/2}$). Few signals were observed at early stage of the test after filtering the data as described. AE location results indicated that simultaneous crack growth on the weld toes of the other side of the stiffeners existed (Figure 4-7). This may indicate the AE process could possibly identify initiation or small crack growth behavior.

Eq. 4-9 was used to assess the crack size assuming the correlation between K and a is unknown. The crack size at any stage of fatigue life was calculated by absolute energy feature of the AE signals using the constants calculated from high R ratio SE(T) test. The assessment of the crack size is shown in Figure 4-8. The approach clearly captures the crack growth trend. It is known that the approach does not provide a good resolution of crack growth behavior (study 2); however, given the fact that the specimen has complex crack growth pattern and applied R ratio compared to SE(T) specimen from which the constants were obtained, the result shows the capability of the approach for crack size assessment.

In the next step, Eq. 4-10 is used to predict the crack size for the specimen. B_e and p are calculated from linear least squares regression of the cruciform test data using the plane stress LEFM valid propagation band (Figure 4-9) therefore the crack propagation for the test was predicted using this band of the data. Even though the load was applied in a low R ratio it is expected that the residual stress at weld increases the mean stress thus the propagation is expected to be similar to the case of loading in high R ratio.

The calculated constants were used in a crack prediction routine using Eq. 4-9 and Eq. 4-10. The value of ΔK during the fatigue life is known by implementing the proposed crack evolution model. Consequently, dU/dN is predicted using Eq. 4-10. Then, assuming a crack size of a_i, after N_i number of cycles, dU/dN is numerically integrated over the segment a_i to a_{i+1} to calculate N_{i+1} using Eq. 4-9. The crack propagation prediction for the specimen is seen in Figure 4-10. The predicted curve closely follows the experimental curve. More experiments are necessary for field validation, yet the proposed

methodology with which the relationship between fatigue and AE is established and its prediction is of general use.

The capability of AE to pinpoint significant damage is investigated next. To do this, *H(I)* vs. K_{max} graph is developed in order to see if *H(I)* can be used as warning signal when a certain level of damage is reached. As stated before, a jump in *H(I)* is recognized as a clear indication of damage occurrence. *H(I)* shows a jump corresponding to a = 0.167 in. (4.24e-3 m) when K_{max} was about 28 ksi.in$^{1/2}$ (30.8 MPa.m$^{1/2}$) as seen in Figure 4-11. Assuming the uniform crack front at this stage, as proposed crack evolution model suggests, the stress in net cross section is 27 ksi (186.16 MPa) which is about half of the yield capacity of the section. This observation is significant noting that the jump in *H(I)* in SE(T) specimens took place at same level of stress in net cross section (study 2).

4.5 CONCLUSION

Specimens with transversely welded plates representing stiffeners typical of steel bridge details were fatigue tested. The specimen provided realistic initial conditions of fatigue crack initiation and growth from high stress concentration regions. The purpose of these tests was to understand the capability of AE technique in assessing, locating and predicting through-thickness crack growth in a typical steel bridge detail. Guard sensor, location and modified Swanson II techniques were used to filter the extraneous noise. AE proved to be able to identify and locate the crack at early stage of initiation and propagation. However, in the early propagation stage, limited numbers of signals were recorded.

AE absolute energy feature was used to assess the crack size after the test assuming that the correlation between *K* and *a* is unknown. The crack size during the fatigue life was calculated by absolute energy rate of the AE signals using the constants calculated from high *R* ratio SE(T) test. The procedure closely captures the crack growth trend and the capability of the approach for crack size assessment shows promise. FEM analysis was used to implement the effect of limited thickness and opposite face attachment into existing *K* to *a* models. A fatigue crack evolution model was proposed assuming evolution of simultaneous cracks from elliptical to uniform edge crack from the weld toe during the fatigue life of the specimen. Procedure for predicting crack length and remaining fatigue life of the specimen using absolute energy rate of AE signals were demonstrated.

The validity of *H(I)* for fatigue crack propagation was evaluated and it is observed that *H(I)* can be used as an alarm when the applied stress is about half of the yielding capacity of the net cross section of crack plane.

FIGURES

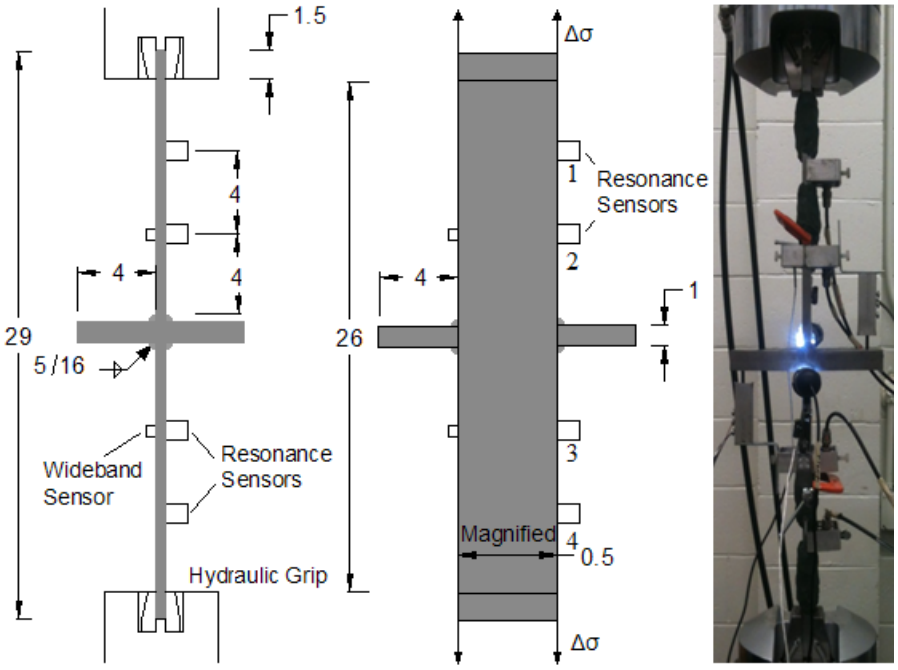

Figure 4-1- Cruciform specimens test setup (dimensions in)

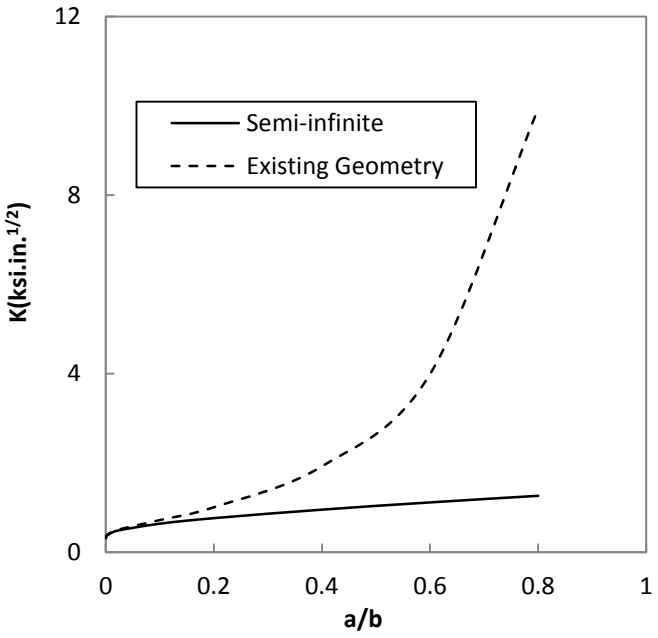

Figure 4-2- FEM models to corelate *K* to *a* in 2D analysis

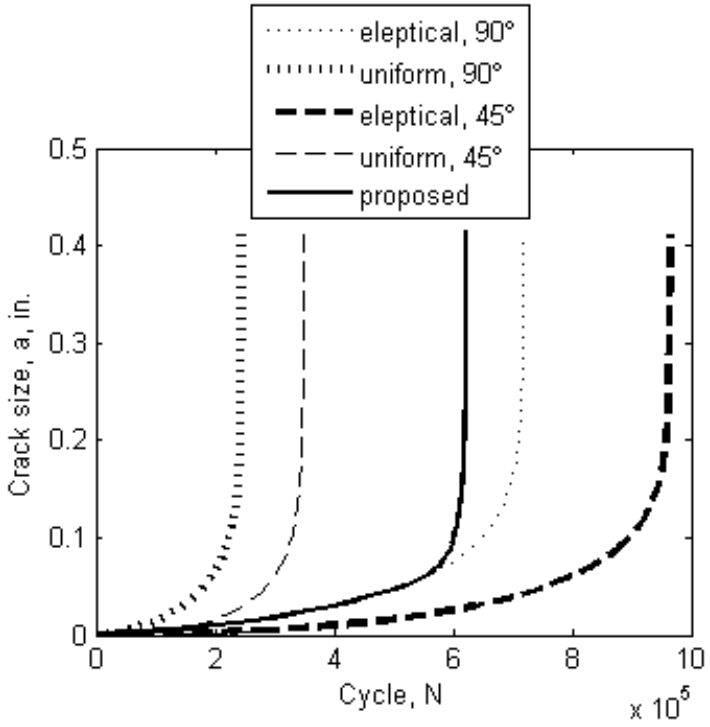

Figure 4-3- Proposed model compared to eleptical and uniform cracks growing from 45 and 90 degrees weld toe angles

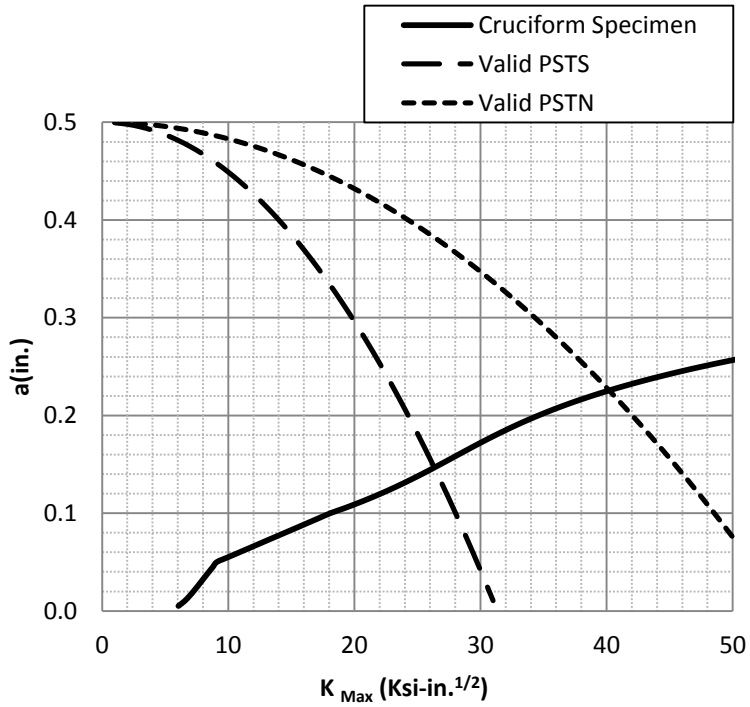

Figure 4-4- Validity of LEFM in plane stress and plane strain conditions

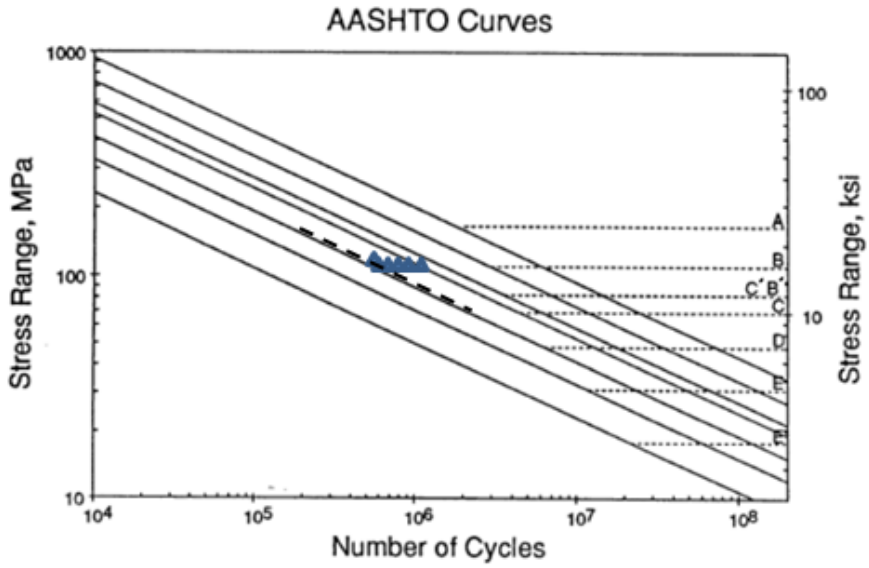

Figure 4-5- Stress range versus number of cycles (AASHTO Fig. C6.6. 1.2.5-1) [20]

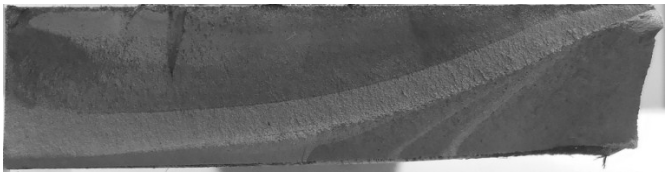

a) Non symmetric crack growth

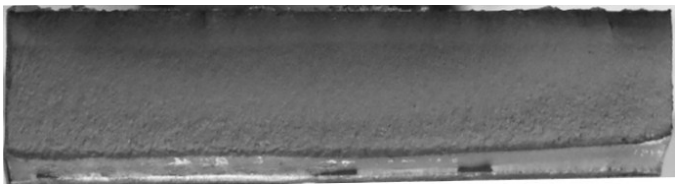

b) Symmetric crack growth

Figure 4-6- Crack plane surface

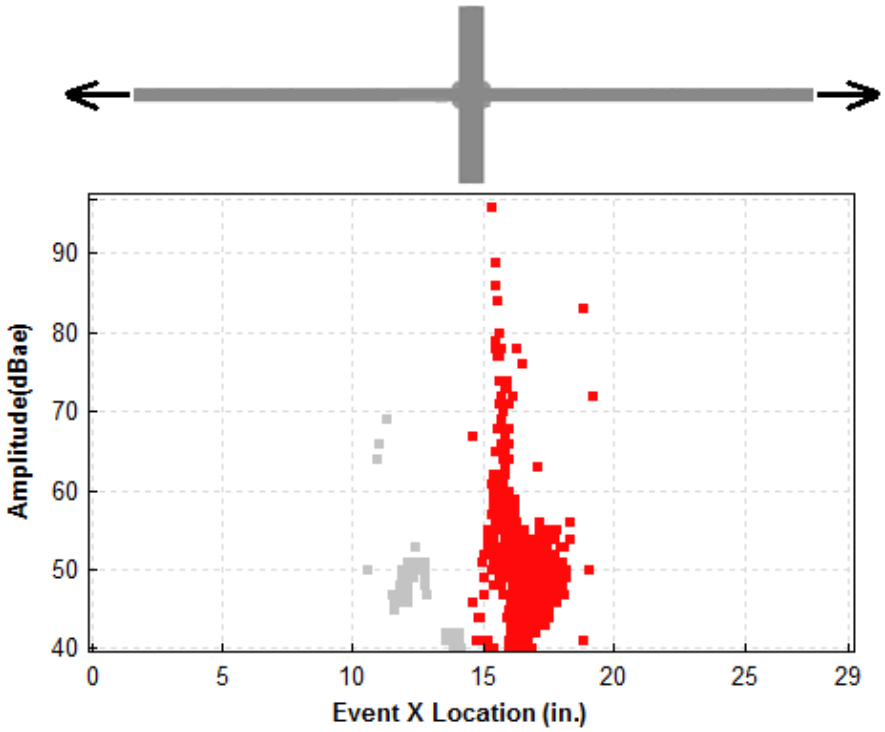

Figure 4-7- AE crack location technique (specimen C1)

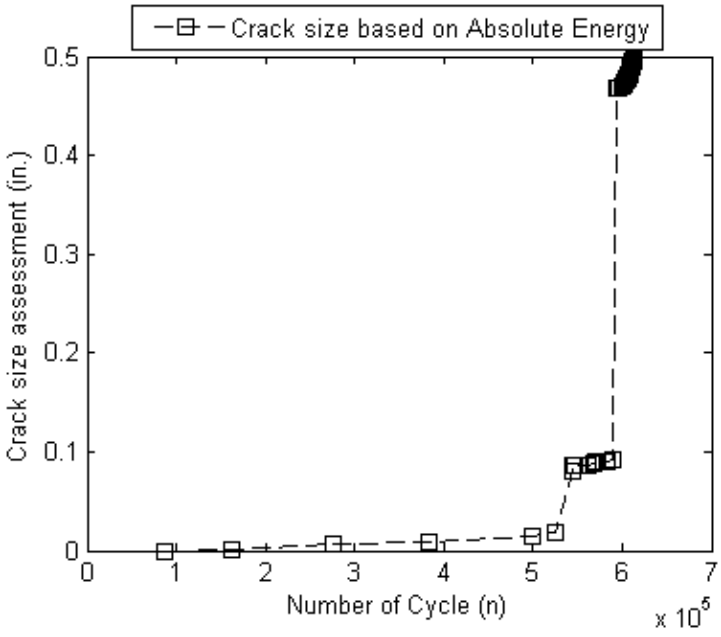

Figure 4-8- Crack size assessment based on absolute energy rate of AE signals

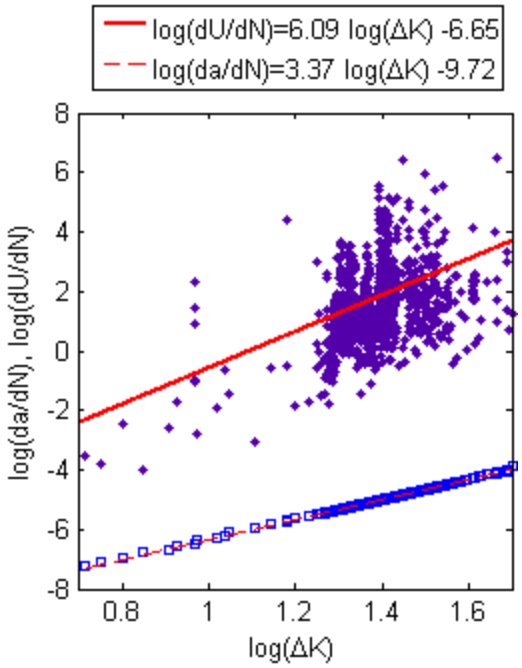

Figure 4-9- Absolute energy rate for a typical cruciform specimen

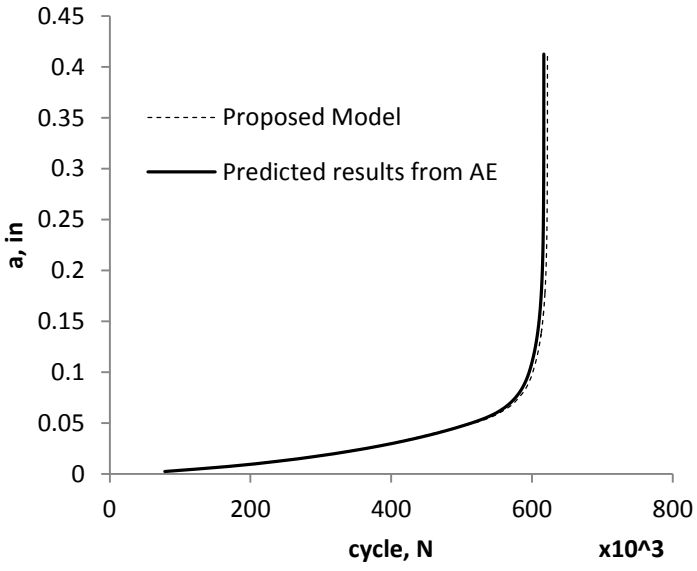

Figure 4-10- Crack growth prediction using AE absolute energy rate (crack evolution model and predicted model using AE both assuming the proposed crack evolution model)

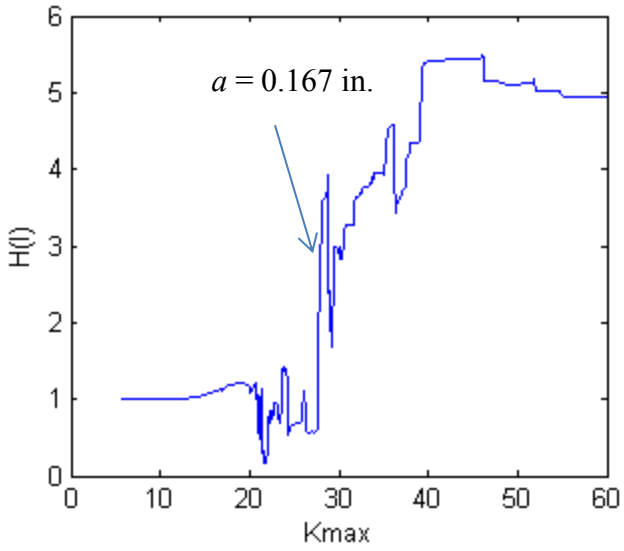

Figure 4-11- H(I) as an alarm mechanism

TABLES

Table 4-1- Cruciform specimens

Code	Width (in)	Thickness (in)	Length (in)	Stiffeners Thickness (in)	Load Min (kip)	Load Max (kip)	$\Delta\sigma$ (ksi)	R	Freq. (Hz)
C1-C6	2	0.5	29	1	2	18	16	0.1	2

Table 4-2- Modified swansong II filter parameters

Modified Swansong II filters in terms of Amplitude(A), dBae and Duration(D), µs			
$A<A_{th}$*+2,D>150	A_{th}+2<A< A_{th}+5,D>250	A_{th}+5<A< A_{th}+8,D>500	A_{th}+8<A< A_{th}+10,D>750

*A_{th} = threshold amplitude dBae

Table 4-3- FEM and curve fitting results

a/t	K_{FEM} (from FEM with limited thickness)	K_{Eq2} (from Eq 2, Ft=1 with semi-infinite base plate)	$F_{t\text{-}FEM}$ (K_{FEM} / K_{Eq2})	$F_{t\text{-}Eq3}$ (from Eq 3)	% error ($F_{t\text{-}Eq3}$ and $F_{t\text{-}FEM}$)
0.0002	0.322	0.309	1.040	1.036	0.413
0.002	0.380	0.367	1.035	1.035	0.004
0.02	0.493	0.475	1.036	1.043	-0.654
0.1	0.718	0.636	1.128	1.130	-0.187
0.2	1.005	0.760	1.322	1.316	0.437
0.4	1.922	0.951	2.021	2.022	-0.055
0.6	3.990	1.113	3.584	3.585	-0.012
0.8	9.933	1.261	7.875	7.875	-0.006

Table 4-4- Fatigue test results

Specimen	Cycles to failure
C1	691,353
C2	639,356
C3*	1108107+592,965
C4	659,021
C5	1,017,765
C6	671,026

* No sign of growth $\Delta\sigma$ increased to 18 ksi

CHAPTER 5, CONCLUSIONS

The objective of this research was to develop a prognostic model that relates acoustic emission (AE) data to crack growth rate for steel specimens that are representative of details prone to fatigue and fracture in steel bridges. To be able to develop a viable solution for AE assessment and prognosis of fatigue cracks initiated from transverse weld toes in steel bridge details, as a first step, a single edge notched specimen is designed to provide ideal situation in which AE and fracture mechanics parameters could be associated. Initially, a modified version of the SE(T) specimen has been examined in order to maintain similitude with the orientation of crack propagation with reality. The specimen provides a crack with through thickness growth that simulates fatigue cracks through the flanges or early stage of crack growth in webs of steel bridge members. In order to properly understand the correlation between AE and fracture mechanics features for the modified SE(T) specimen, the effect of test parameters on the stress state of the crack was addressed. Equations to include the effects of fix boundary condition on K and CMOD of the crack were developed and a framework was proposed to map the crack front evolution in high cycle fatigue tests for the modified SE(T) specimen with initial crack inclination. Modified SE(T) specimens then were tested under high cycle fatigue load while AE activity was monitored. Applicability of AE to capture, locate and predict the behavior of the growing crack was positively verified for SE(T) specimens. AE absolute energy was used to predict the crack size after the test and the prediction results were compared to the experimental results. AE and crack growth constants were obtained based on the experimental data and procedures for assessing the current crack size and predicting the remaining fatigue life of the crack were demonstrated. R ratio showed to

have a significant effect on evolution of AE data captured during the test. This is important when considering that High R ratios exist in welded members. This also implies that K_{max} has an important role in fatigue assessment of cracks using AE. In the performed tests, the AE signals after filtering were not necessarily created close to peak loads. The validity of Historic Index (*H(I)*), as indicator of onset of significant damage using AE data, for fatigue crack propagation was evaluated and it is observed that regardless of initial crack size, R ratio and gripping condition, *H(I)* significantly increases when the applied stress was about half of the yielding capacity of the net cross section of crack plane.

In order to understand the capability of AE technique in assessing, locating and predicting through-thickness crack growth in a more realistic detail typical to steel bridges, cruciform specimens with transversely welded plates representing stiffeners were fatigue tested. The specimen provided realistic initial conditions of fatigue crack initiation and growth from high stress concentration regions. AE proved to be able to identify and locate the crack at early stage of propagation. However, in early propagation stage, limited numbers of signals were recorded.

AE absolute energy feature was then used to assess the crack size after the test assuming that the correlation between *K* and *a* is unknown. The crack size during the fatigue life was calculated by absolute energy rate of the AE signals using the constants calculated from high *R* ratio SE(T) test. The procedure was able to closely capture the crack growth trend and the capability of the approach for crack size assessment shown promising. In order for life prediction to be possible, the *K* to *a* relationship describing the crack evolution has to be known. FEM analysis was used to implement the effect of limited

thickness and opposite face attachment into existing *K* to *a* models. A crack evolution model was proposed assuming evolution of simultaneous cracks from elliptical to uniform at weld toe during the fatigue life of the specimen. Knowing the crack evolution model, procedure for predicting crack length and remaining fatigue life of the specimen using absolute energy rate of AE signals were demonstrated.

The validity of *H(I)* for fatigue crack propagation was evaluated and it is observed that similar to SE(T) specimen tests, *H(I)* can be used as an alarm when the applied stress is about half of the yielding capacity of the net cross section of crack plane.

The core outcomes of the research are as follow:

- AE is able to capture, locate and predict the behavior of the growing crack in steel details.
- Knowing the fatigue and AE crack evolution constants, the current crack size can be evaluated using AE data even when the correlation between *K* and *a* is unknown.
- To be able to predict the crack growth behavior, the relationship between *K* and *a* has to be known.
- *H(I)* can be used as an alarm when the applied stress is about half of the yielding capacity of the net cross section of crack plane.
- Limited numbers of signals are recorded (located) in initiation and early propagation stages.

FUTURE WORK

High scatter was observed in *dU/dN* vs. *ΔK* curve. This can affect the validity of the crack propagation. Lower bound *dU/dN* vs. *ΔK* data appears to have a more reliable behavior compared to regression of all AE data as seen in Figures 3-7, 3-8 and 4-9. Implications and viability of using the lower bound AE data in the relationship between absolute energy rate and stress intensity range needs to be verified.

An AE signal feature sensitive enough to show the difference between low energy signals but not too sensitive to high energy signals, as "Signal Strength" feature, might prove to be a better fit for the proposed method for propagation prediction. This may potentially help in arriving to a material constant rather than a case based constant for AE crack propagation equations. A more extensive test matrix is required for the test results to be statistically verified. Mid-scale specimens are needed to capture the residual stress, constraint and stress field observed in as-built structures. These specimens provide a 3 dimensional environment in which the fatigue crack grows at a slower pace similar to the field environment. Also, the higher *K* values can be reached for a crack growing through the thickness of a flange and net cross section yielding is less of a factor. In these specimens, the crack evolution is more likely to follow fracture mechanics models of weld toe cracks that have been developed that provide accurate solutions over the range of small initial defect sizes expected at the weld toe.

APPENDIX 1, STUDY 1

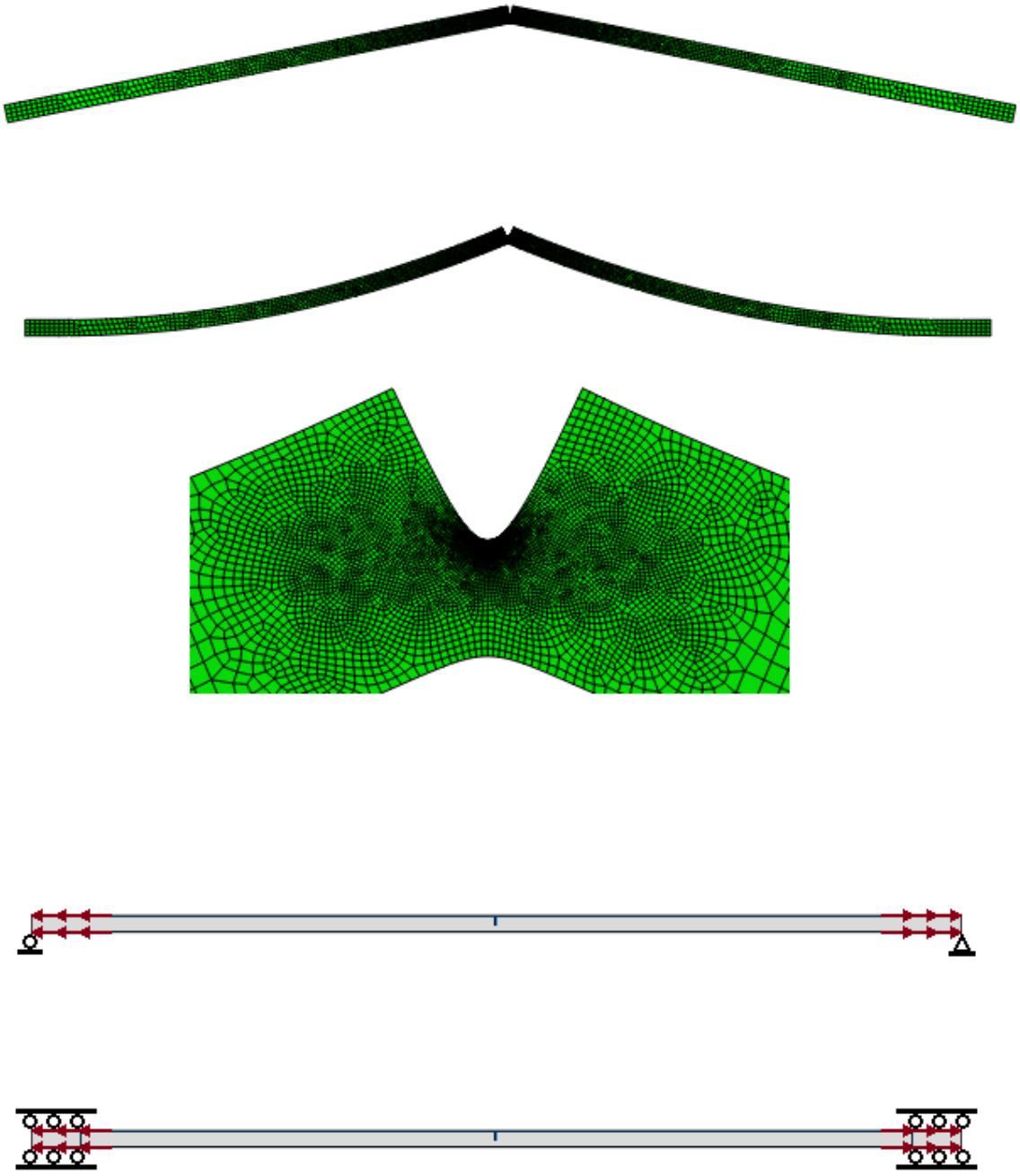

Figure A1-1 Effect of gripping condition

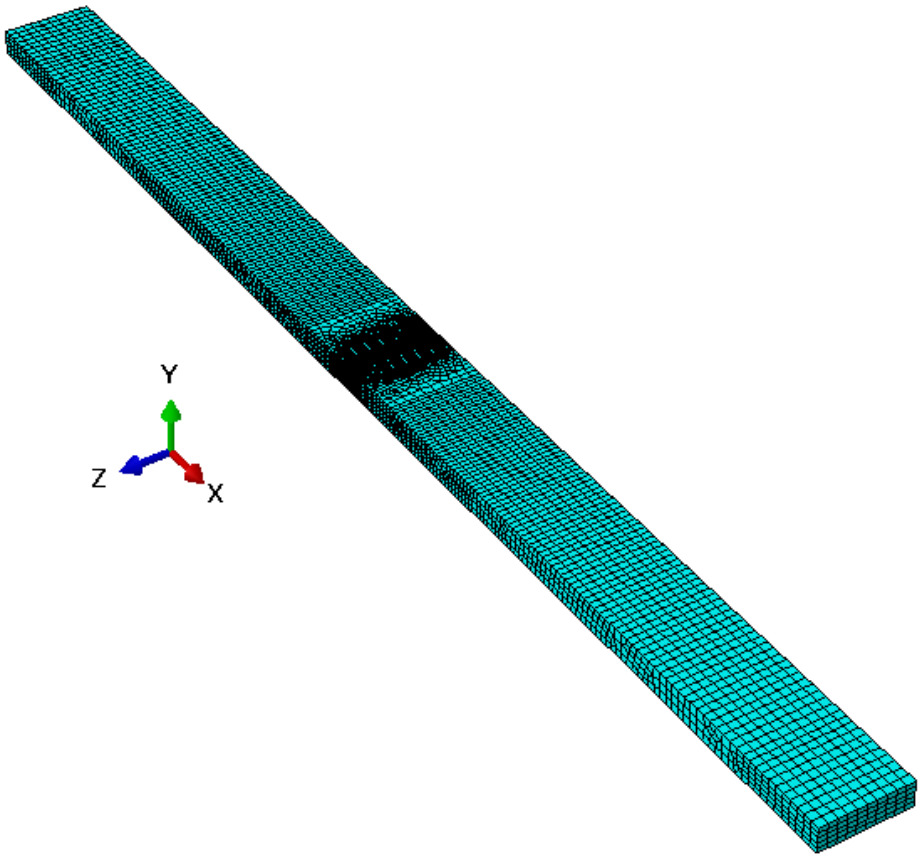

Figure A1-2 3D FEM is performed to assess the misalignment effects

APPENDIX 2, STUDY 2

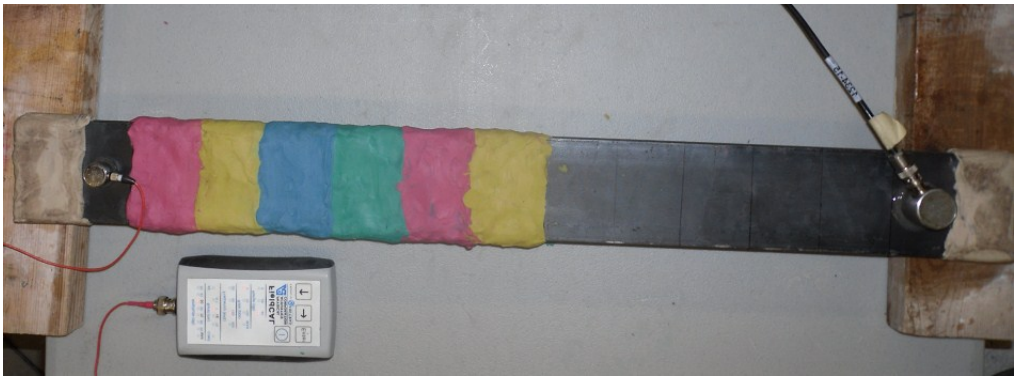

Figure A2-1 assessing the drop in Amplitude (Attenuation) in the specimen due to use of modeling clay

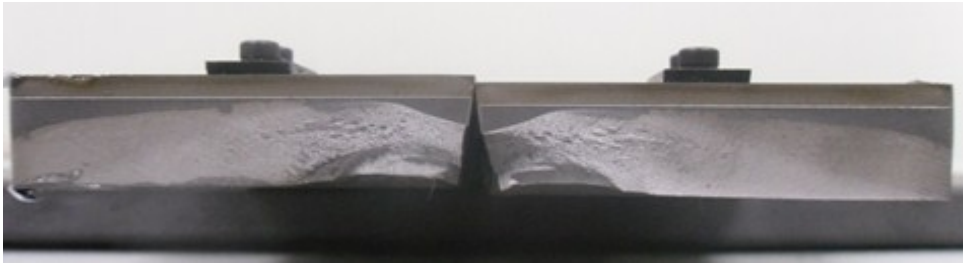

Figure A2-2 Low applied stress range leading to initiation problem

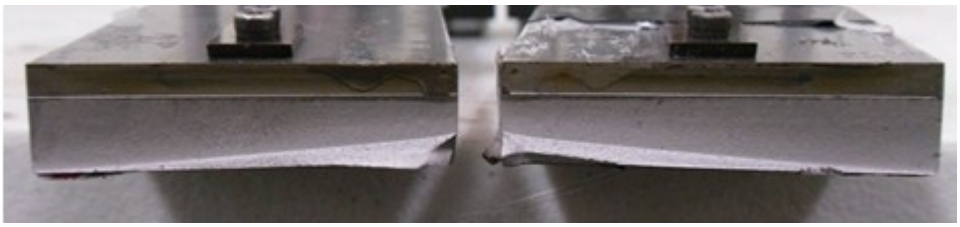

Figure A2-3 Inclined crack growth

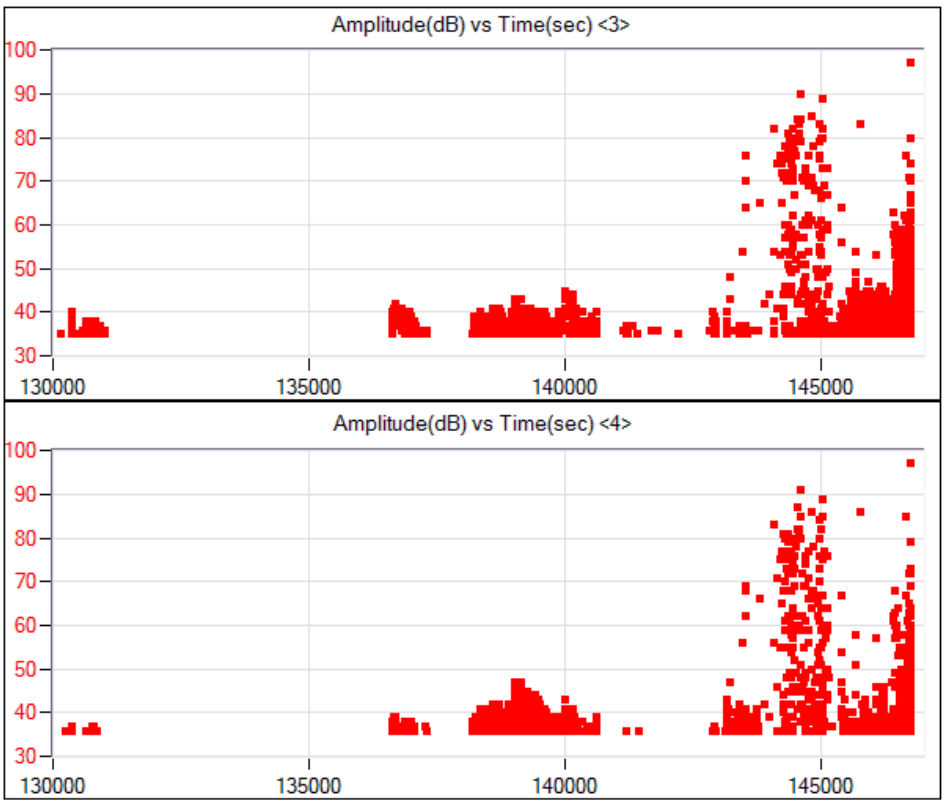

Figure A2-4 Amplitude vs. time for data sensors specimen S1 (unfiltered data)

Figure A2-5 Notch and hair line crack in SE(T) specimens

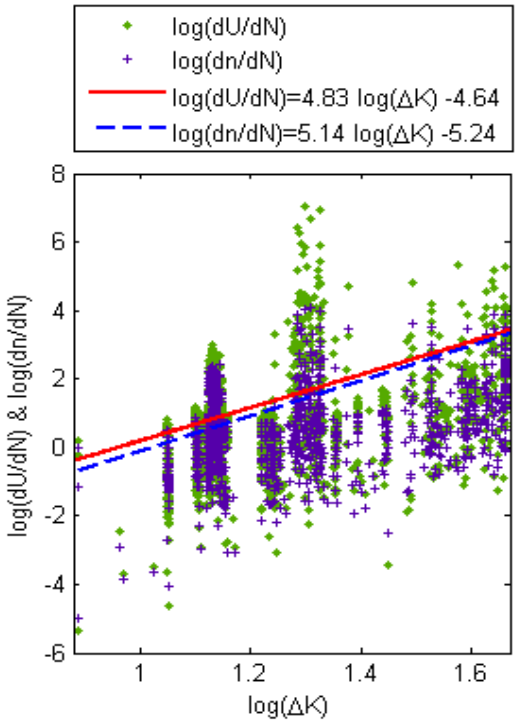

Figure A2-6 Absolute energy and count rate for specimen S1

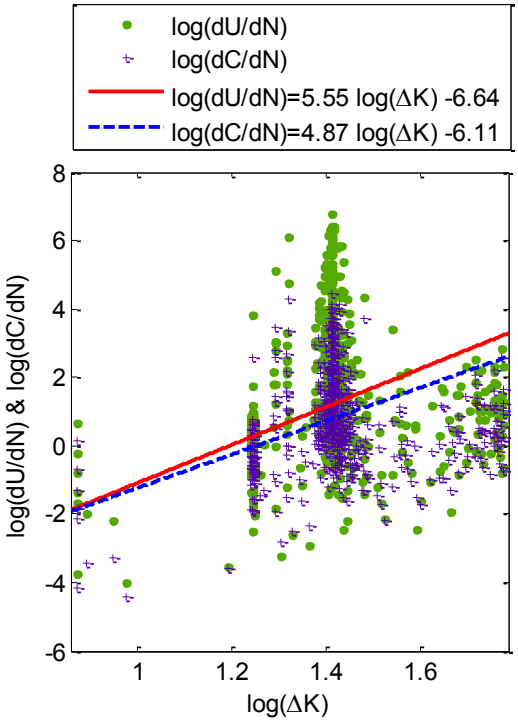

Figure A2-7 Absolute energy and count rate for specimen S2

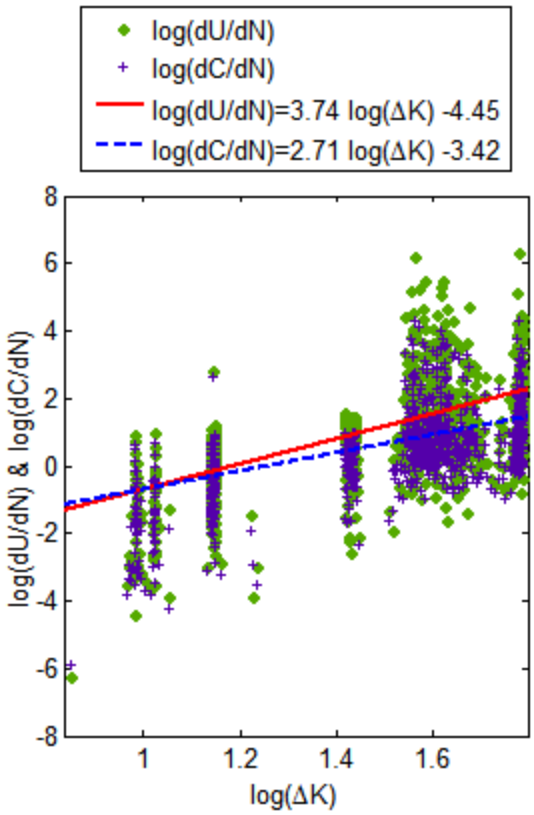

Figure A2-8 Absolute energy and count rate for specimen S4

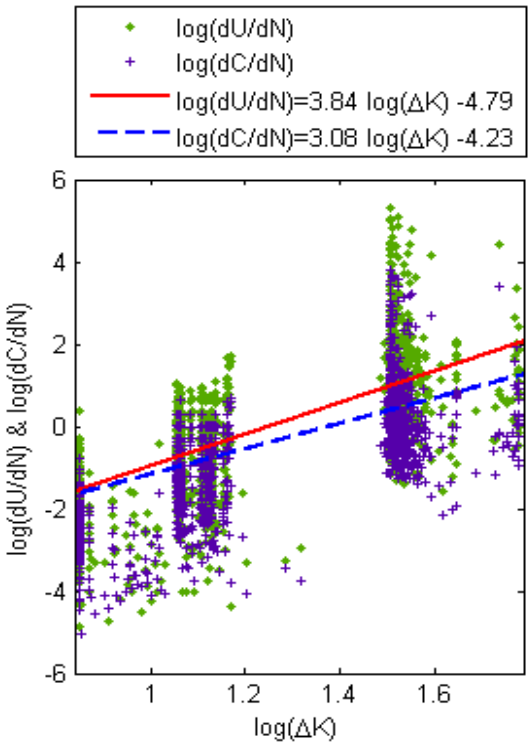

Figure A2-9 Absolute energy and count rate for specimen S5

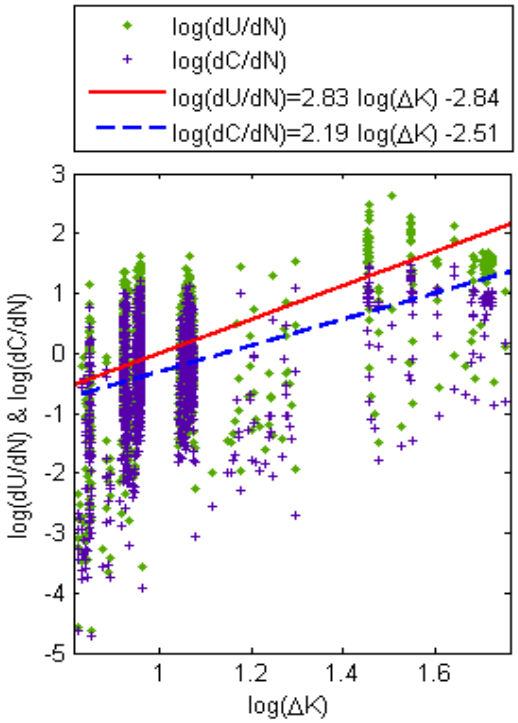

Figure A2-10 Absolute energy and count rate for specimen S6

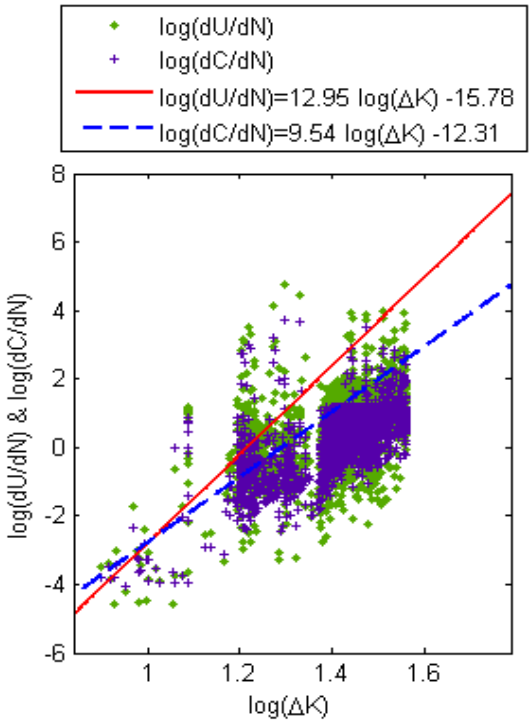

Figure A2-11 Absolute energy and count rate for specimen S7

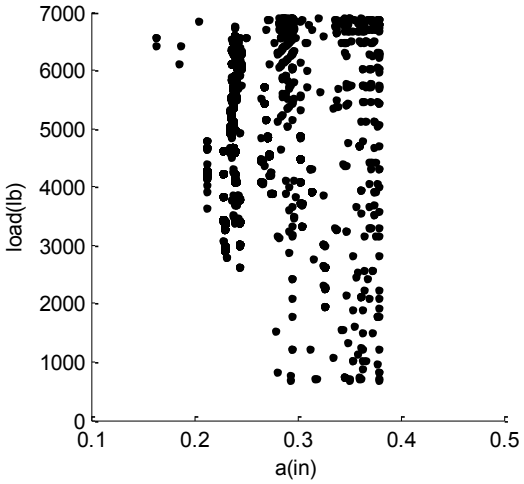

Figure A2-12 load levels at which AE is recorded during the test Specimen S1

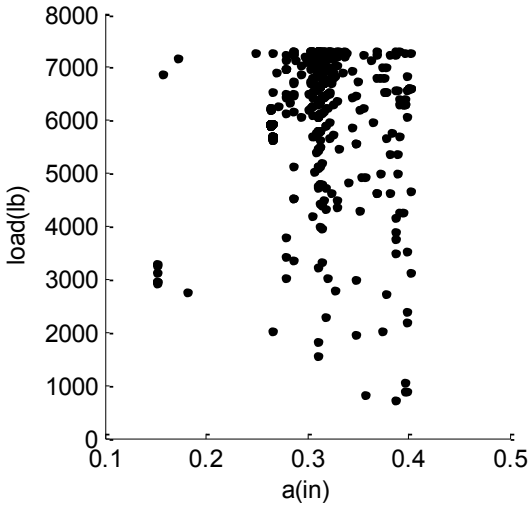

Figure A2-13 load levels at which AE is recorded during the test Specimen S2

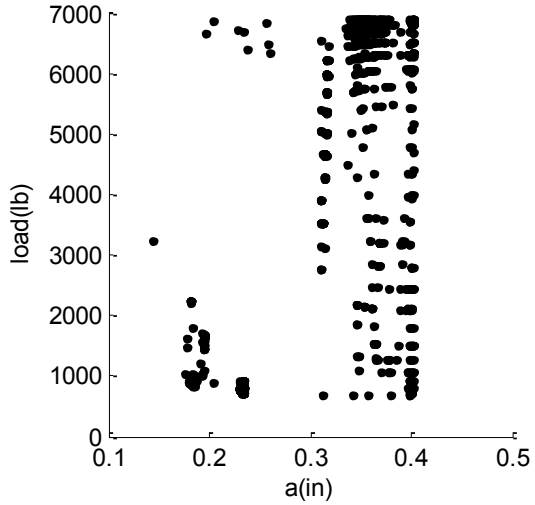

Figure A2-14 load levels at which AE is recorded during the test Specimen S3

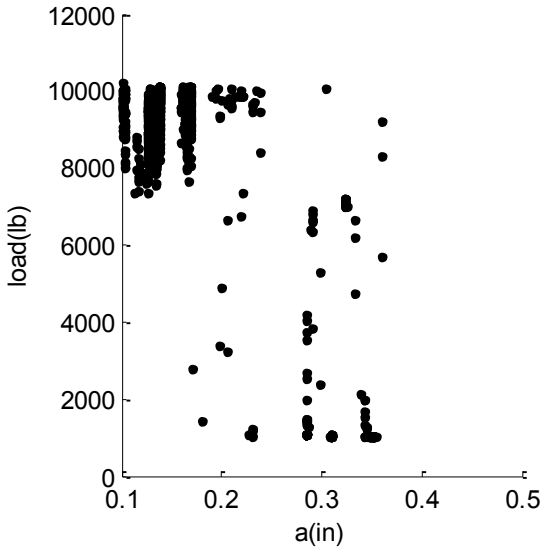

Figure A2-15 load levels at which AE is recorded during the test Specimen S4

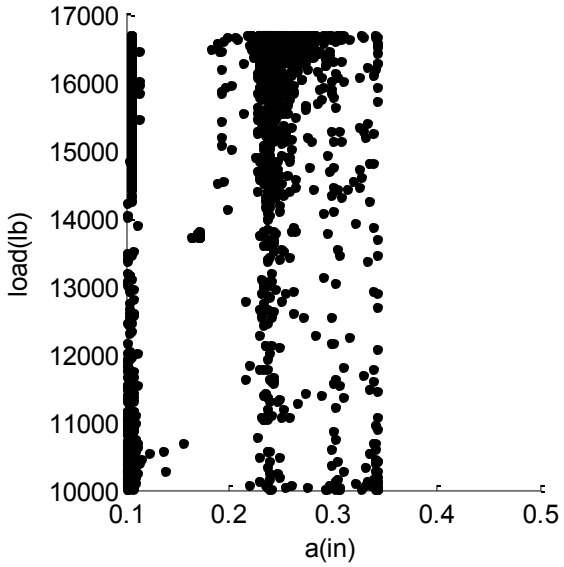

Figure A2-16 load levels at which AE is recorded during the test Specimen S5

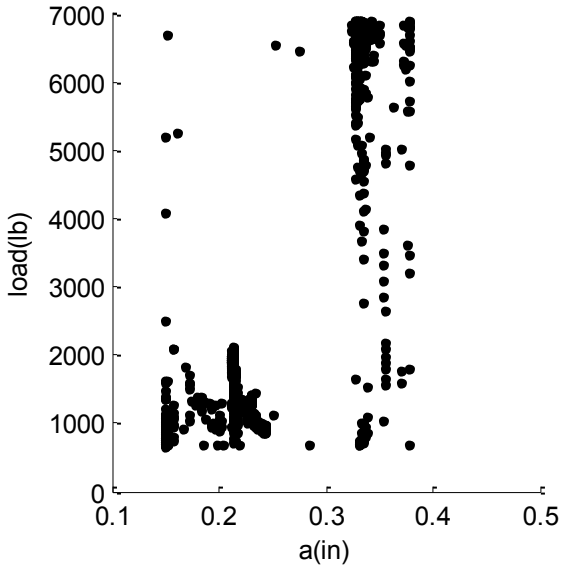

Figure A2-17 load levels at which AE is recorded during the test Specimen S6

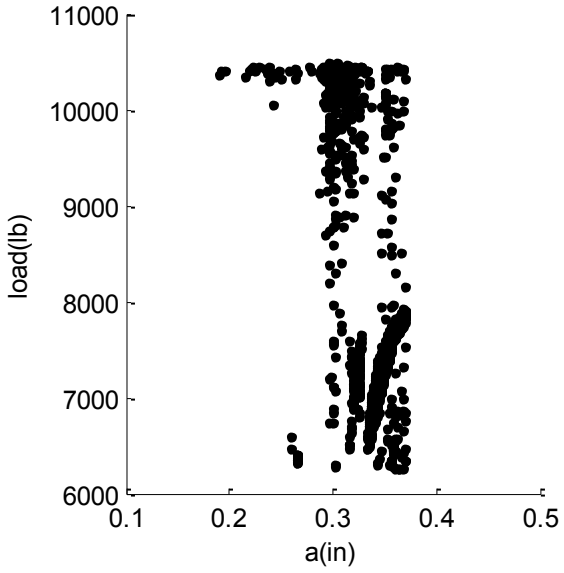

Figure A2-18 load levels at which AE is recorded during the test Specimen S7

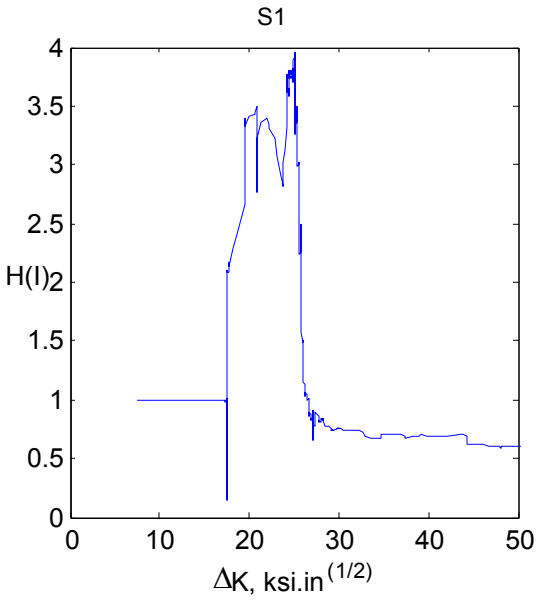

Figure A2-19 H(I) vs. ΔK for Specimen S1

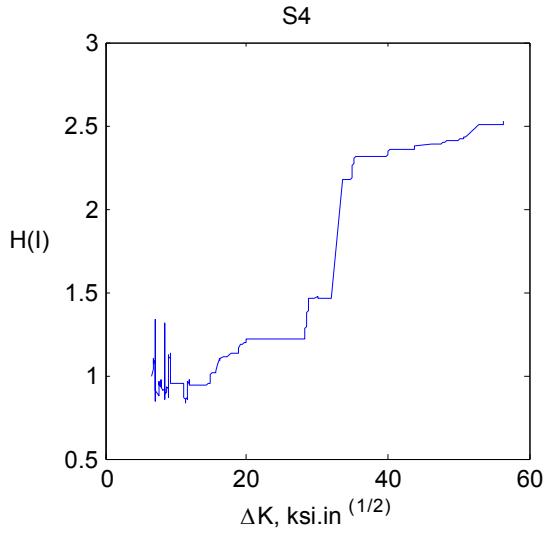

Figure A2-20 H(I) vs. ΔK for Specimen S4

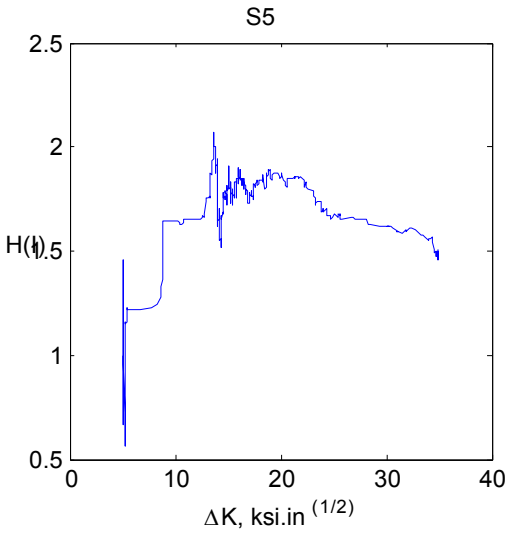

Figure A2-21 H(I) vs. ΔK for Specimen S5

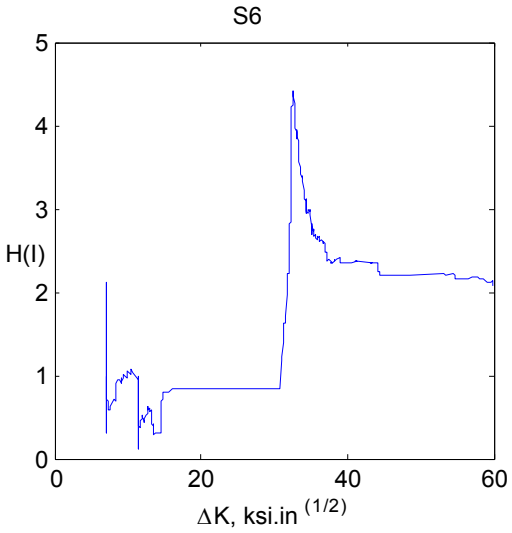

Figure A2-22 H(I) vs. ΔK for Specimen S6

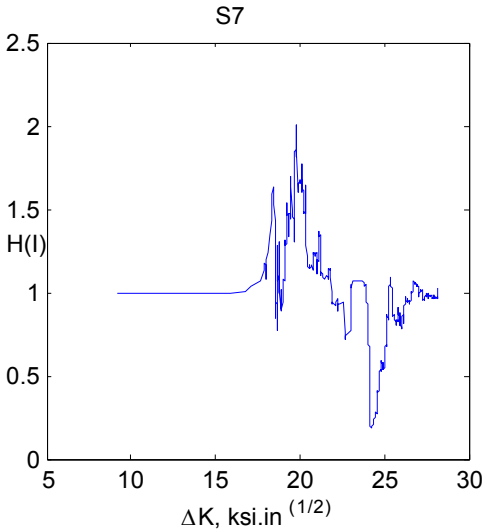

Figure A2-23 H(I) vs. ΔK for Specimen S7

APPENDIX 3, STUDY 3

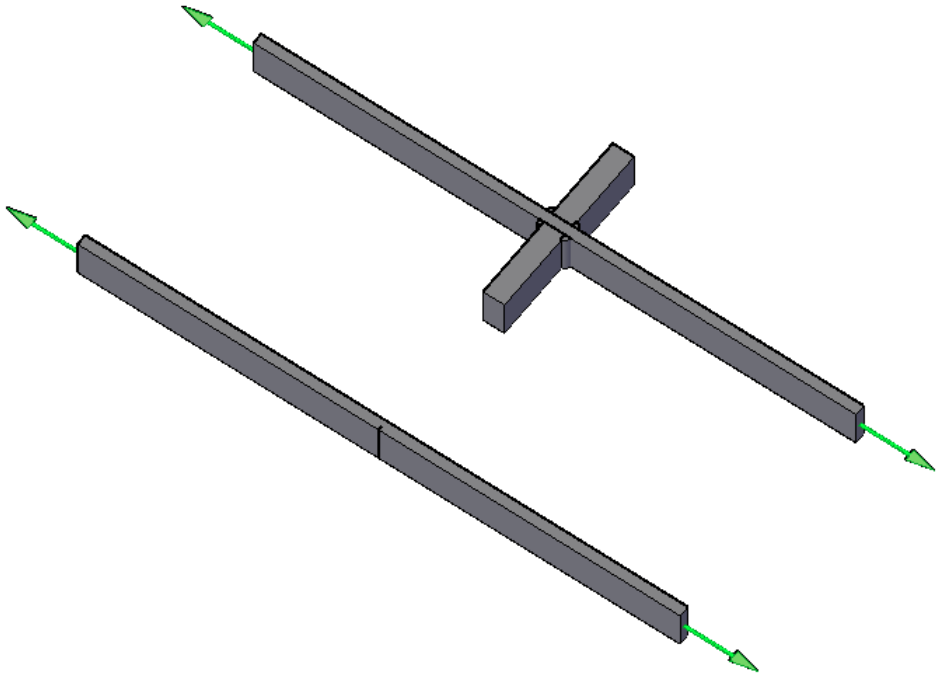

Figure A3-1 Geometry of cruciform vs. SE(T) specimen

Table A3-1 FEM modeling in order to calculate K vs. a

Crack Depth, in.	90 Deg weld (ABA)	90 Deg weld (ANA)	45 Deg weld (ABA)	45 Der weld (ANA)
0	0	0	0	0
2.00E-05	0.273	0.281	0.1451	1.45E-01
0.0001	0.3008	0.309	0.192	0.192
0.0005	0.3379	0.346	0.2548	0.254
0.002	0.383	0.392	0.3265	0.325
0.005	0.4253	0.433	0.3866	0.384
0.01	0.4676	0.475	0.4418	0.439
0.1	0.7625	0.760	0.7611	0.761
0.2	0.9611	0.951	0.9603	0.968
0.5	1.422	1.400	1.422	1.467
1	2.02	2.034	2.021	2.2

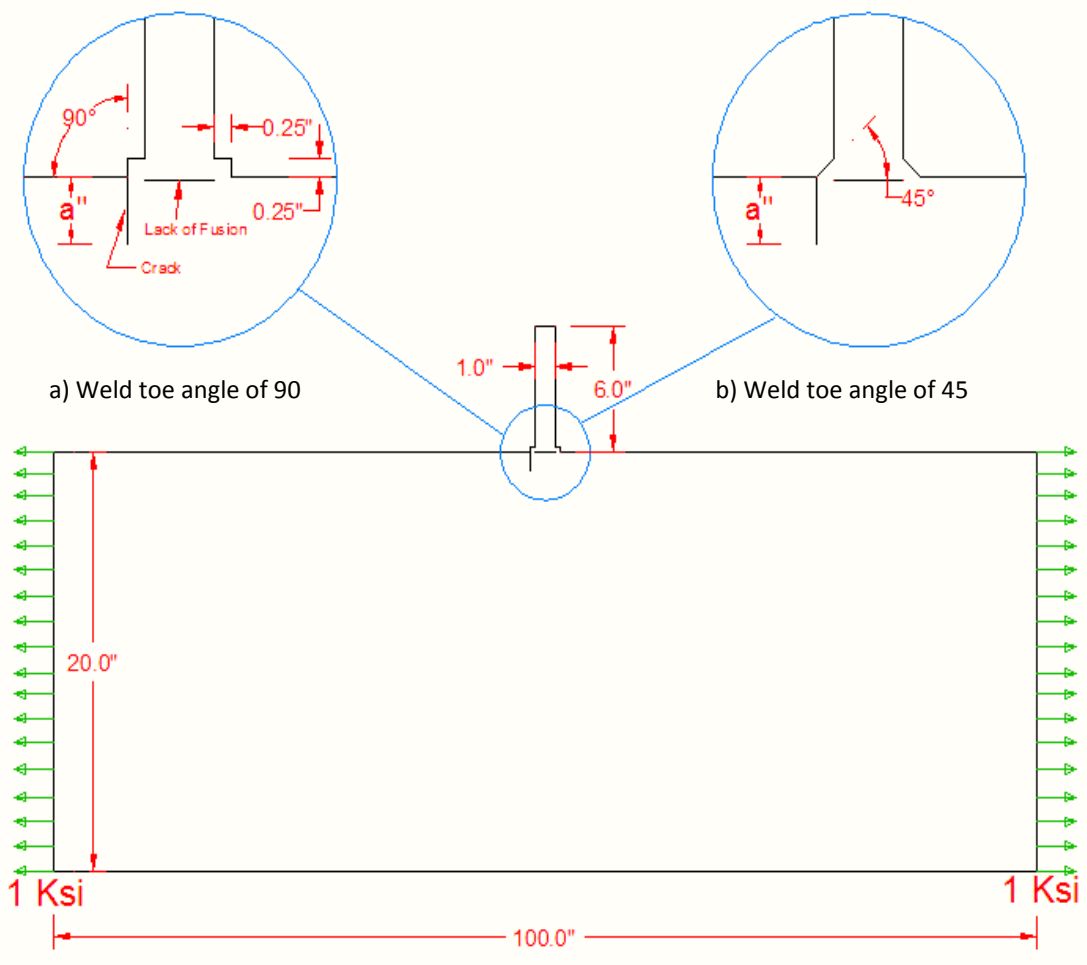

Figure A3-2 Geometry of the FEM model

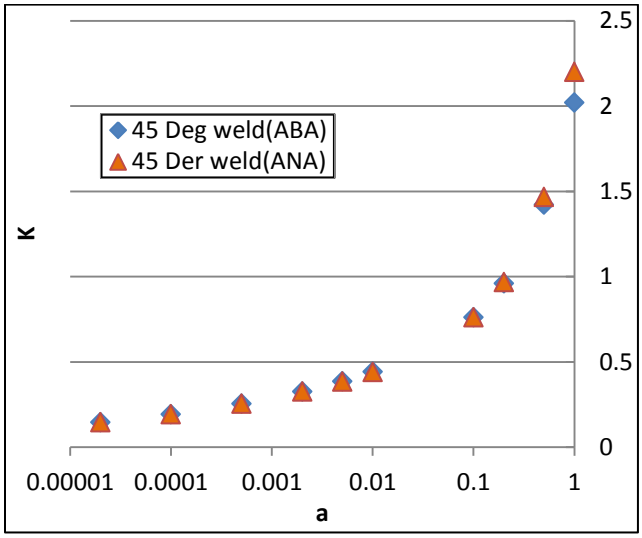

a) Results for 90 degrees weld toe

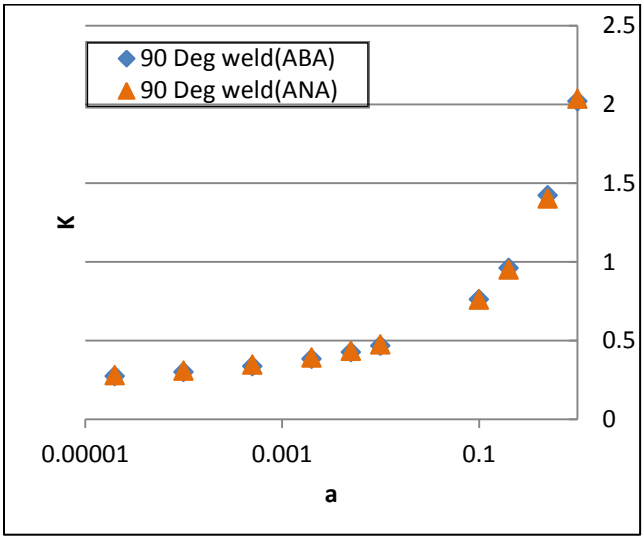

b) Results for 45 degrees weld toe

Figure A3-3 Numerical(ABA) vs. analytical(ANA) stress intensity factors for semi-infinite case

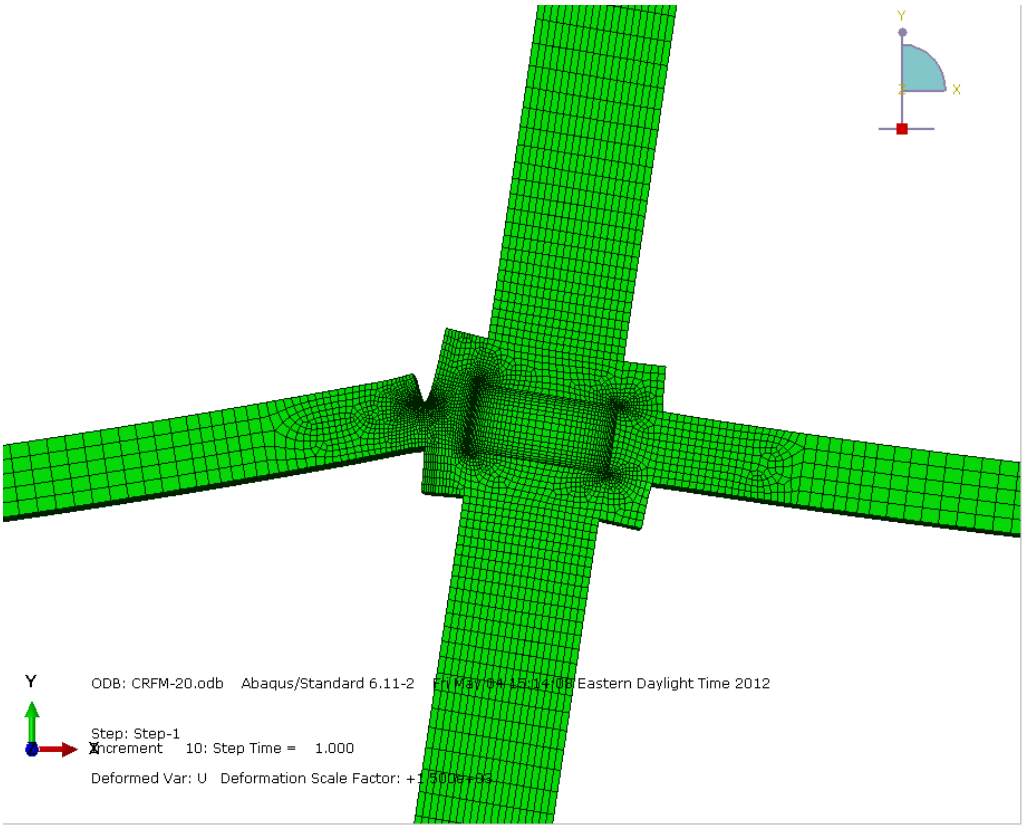

Figure A3-4 FEM model with limited thickness and 90 Degrees weld toe

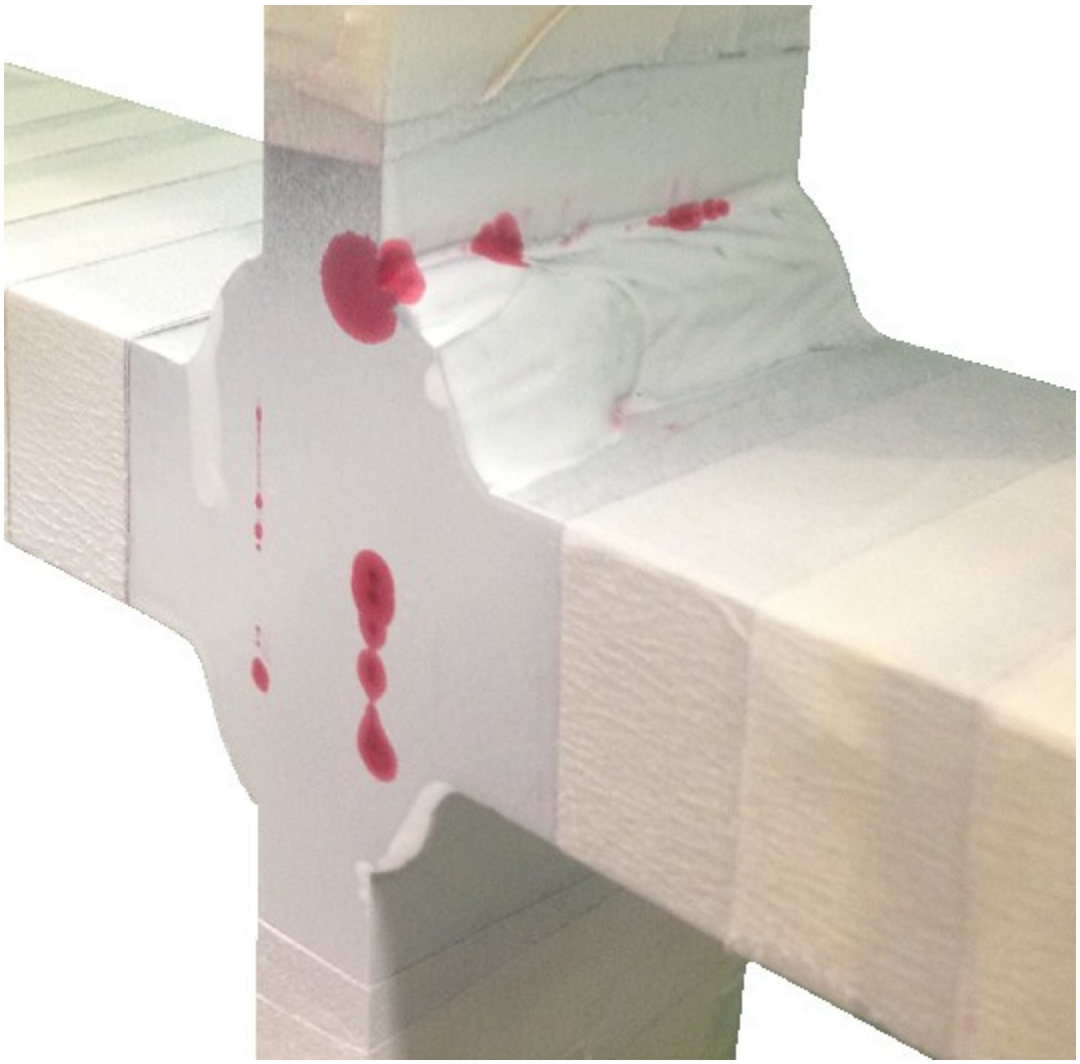

Figure A3-5 Specimen C6 - PT test 1

Figure A3-6 Specimen C6 - PT test 2

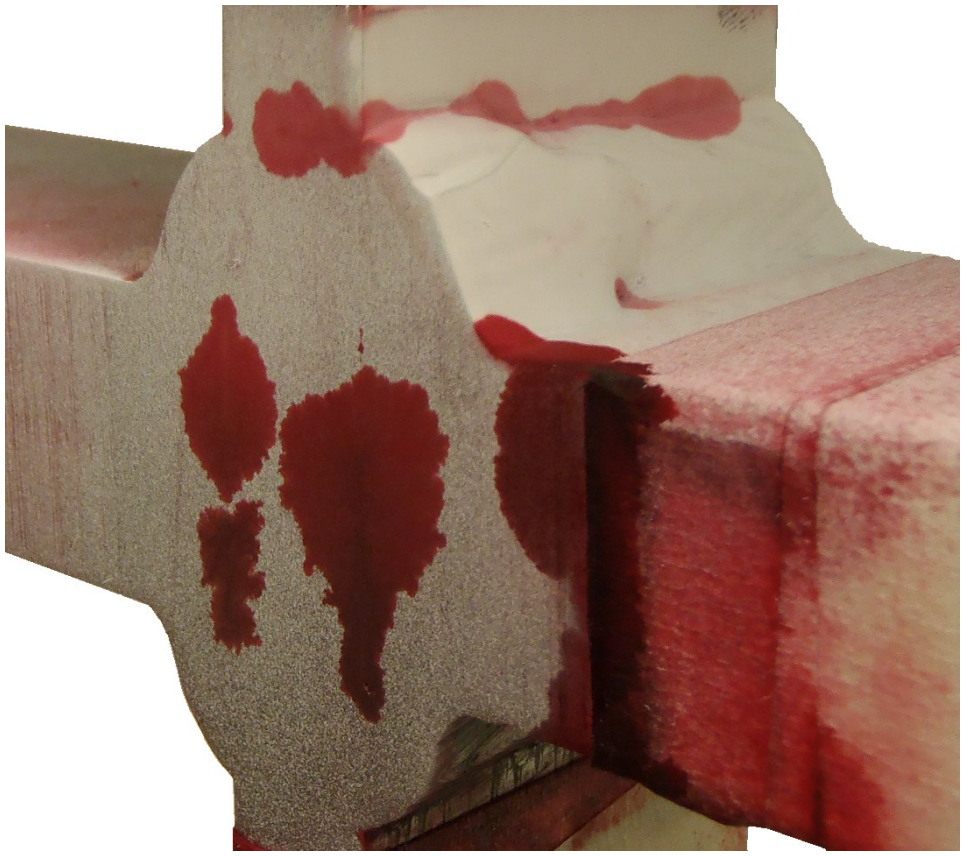

Figure A3-7 Specimen C6 - PT test 3 before UT

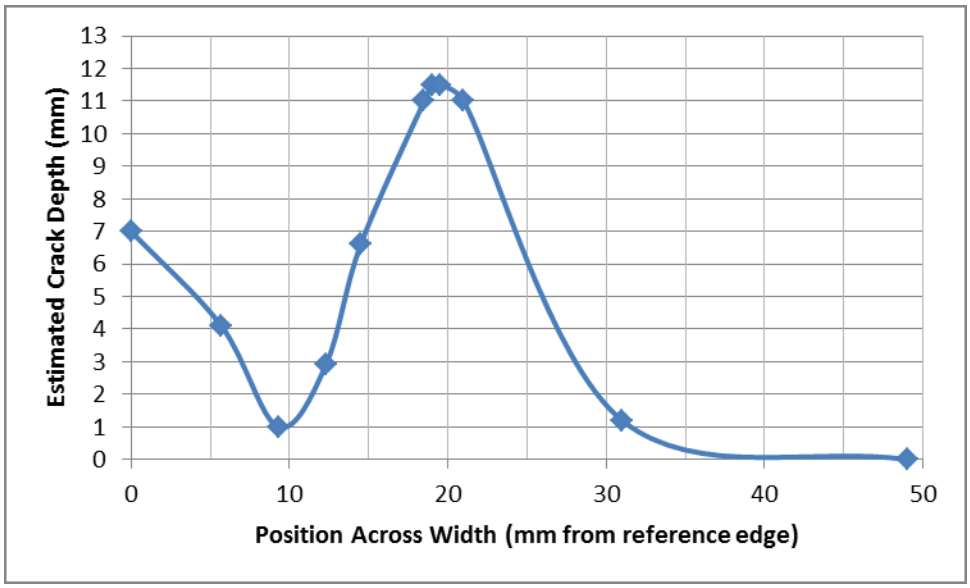

Figure A3-8 UT crack depth estimation (Done at Mistras by Dr. Adrian Pollock)

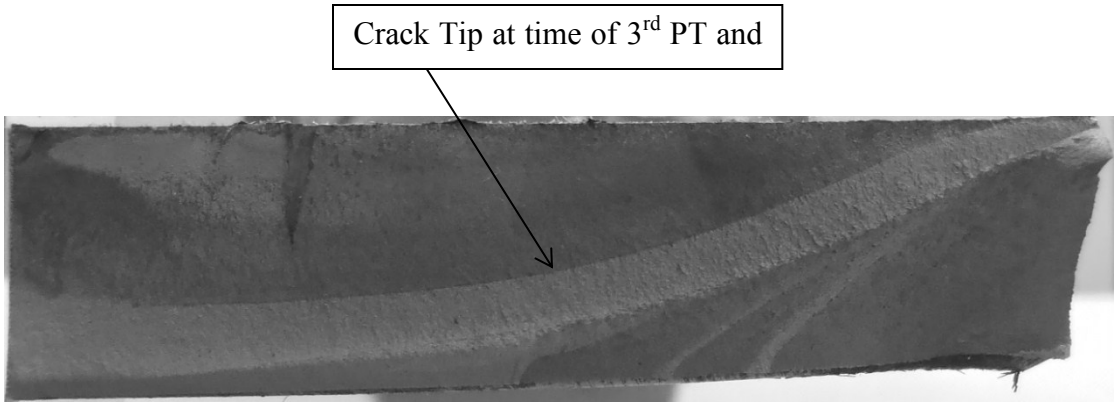

Figure A3-9 Crack profile after the test

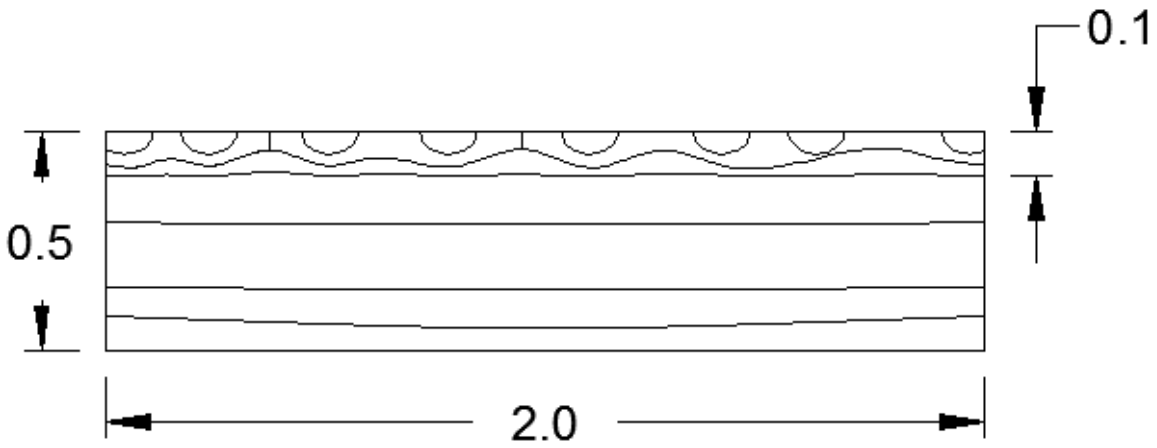

Figure A3-10 Proposed crack evolution model

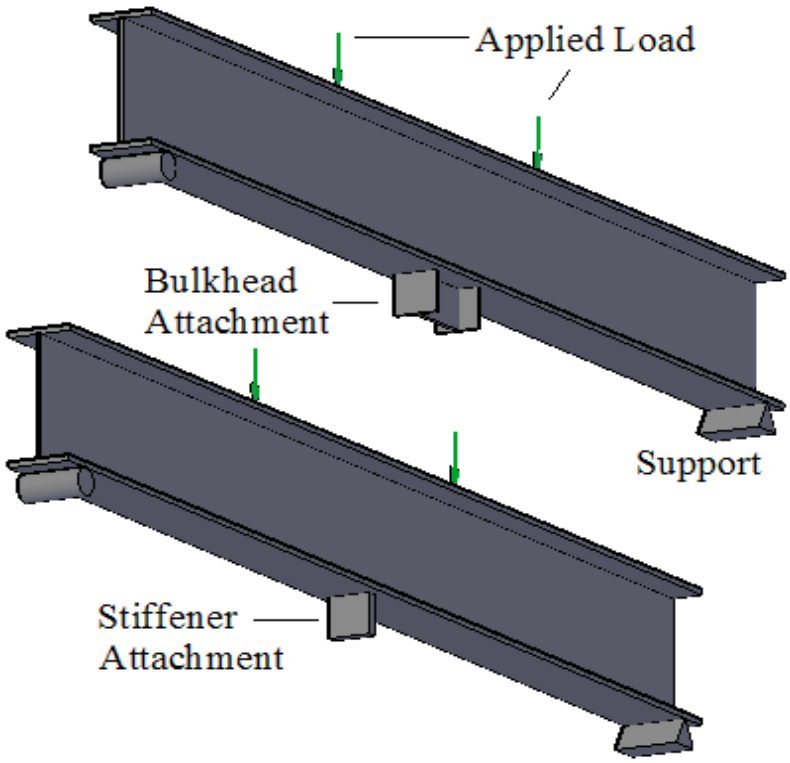

Figure A3-11 Proposed specimens for future work

BIBLIOGRAPHY

AASHTO. (1999). LRFD bridge design specifications. Washington, D.C.

ASTM E1316-11b, (2011). Standard Terminology for Nondestructive Examinations, ASTM International, West Conshohocken, PA, USA.

ASTM E976. (2010). Standard Guide for Determining the Reproducibility of Acoustic Emission Sensor Response. 1–7.

ASTM Standard E561-10e1. (2010). Standard test method for K–R curve determination, ASTM International, West Conshohocken, PA, USA.

ASTM Standard E647-11e1. (2011). Standard Test Method for Measurement of Fatigue Crack Growth Rates. ASTM International, West Conshohocken, PA, USA.

Barsoum, R. S. (1975). "Further application of quadratic isoparametric finite elements to linear fracture mechanics of plate bending and general shells." International Journal of Fracture, 11(1), 167–169.

Bassim, M. N., Lawrence, S. S., and Liu, C. D. (1994). "Detection of the onset of fatigue crack growth in rail steels using acoustic emission." Engineering Fracture Mechanics, 47(2), 207–214.

Chen, H.L., Choi, J. H.(2004). "Acoustic emission study of fatigue cracks in materials used for AVLB". Journal of Nondestructive Evaluation. 23(4):133-51.

Chotickai, P. (2001). "Acoustic emission monitoring of prestressed bridge girders with premature concrete deterioration." University of Texas.

Committee on Fatigue and Fracture Reliability of the Committee on Structural Safety Reliability of the Structural Division Fatigue reliability. (1982). 1–4 Journal of Structural Division, Proceedings of ASCE, 108 (ST1), 3–88

Daniel, I. M., Luo, J.-J., Sifniotopoulos, C. G., and Chun, H.-J. (1998). "Acoustic Emission Monitoring OF Fatigue Damage in Metals." Nondestructive Testing and Evaluation, 14(1-2), 71–87.

DiSP User's Manual, Rev.1. (2001). Physical Acoustics Corporation. Princeton Junction, NJ, USA.

Federal Highway Administration. (2011). National Bridge Inventory, Available: http://www.fhwa.dot.gov/bridge/britab.cfm

Fisher, lW., Hausammann, H., Sullivan, M.D., and Pense, A. W. (1979). Detection and repair of fatigue damage in welded highway bridges. NCHRP Report 206, Transportation Research Board, Washington, D.C., USA.

Forman, R., Kearney, V., and Engle, R. M. (1967). "Numerical analysis of crack propagation in cyclic-loaded structures." Journal of basic Engineering, 89, 459–464.

Fowler, T. J., Blessing, J. A., and Conlisk, P. J. (1989a). "New directions in testing." Acoustic Emission From Composite Materials, American Mathematical Society, 3, 16–27.

Fowler, T., Blessing, J., Conlisk, P., and Swanson, T. (1989b). "The MONPAC system." Journal of Acoustic Emission, 8(3), 1–8.

Golaski, L., Gebski, P., Ono, K. (2002). "Diagnostics of reinforced concrete bridges by acoustic emission". Journal of Acoustic Emission. 20: 83-98.

Gong, Z., and Nyborg, E. (1992). "Acoustic emission monitoring of steel railroad bridges." Materials Evaluation, 50(7), 883–7.

Gostautas, R. S., Ramirez, G., Peterman, R. J., and Meggers, D. (2005). "Acoustic emission monitoring and analysis of glass fiber-reinforced composites bridge decks." Journal of Bridge Engineering, 10(6), 713–721.

Hamel, F., Bailon, J. P., and Bassim, M. N. (1981). "Acoustic emission mechanisms during high-cycle fatigue." Engineering Fracture Mechanics, 14(4), 853–860.

Hamstad, M. A., and Mccolskey, J. D. (1997). "Wideband and narrowband acoustic emission waveforms from extraneous sources during fatigue of steel samples." Journal of Acoustic Emission Y, Acoustic Emission Group, 15(1), 1–18.

Harris, D. O., and Dunegan, H. L. (1974). "Continuous monitoring of fatigue-crack growth by acoustic-emission techniques." Experimental Mechanics, 14(2), 71–81.

Henshell, R. D., and Shaw, K. G. (1975). "Crack tip finite elements are unnecessary." International Journal for Numerical Methods in Engineering, 9(3), 495–507.

John, R., and Rigling, B. (1998). "Effect of height to width ratio on K and CMOD solutions for a single edge cracked geometry with clamped ends." Engineering Fracture Mechanics, 60(2), 147–156.

John, R., Kaldon, S., and Johnson, D. (1985). "Weight function for a single edge cracked geometry with clamped ends." International Journal of Fracture, 72, 145–158.

Lindley, T. C., Palmer, I. G., and Richards, C. E. (1978). "Acoustic emission monitoring of fatigue crack growth." Materials Science and Engineering, 32(1), 1–15.

Martin, C., Way, C. V., Lockyer, A., Kudva, J., and Ziola, S. M. (1995). “Acoustic emission testing on an F/A-18 E/F titanium bulkhead.” Proceedings of SPIE, 204–211.

Metrovich, B. and Fisher, J.W. (2005), "Fatigue strength of stainless steel weldments," International Journal of Steel Structures, 5(3), 189-198.

Metrovich, B. and Fisher, J.W. (2006), "Use of weld toe stress singularities in evaluating stress intensity factors for welded details," Bridge Structures-Assessment, Design and Construction, 2(4), 199-206.

Metrovich, B., Fisher, J., Yen, B. (2012). “Theoretical development of lower bound s-n fatigue curves”. Journal of Bridge Engineering. 17(5):747–53.

Nair, A., and Cai, C. S. (2010a). “Acoustic emission monitoring of bridges: Review and case studies.” Engineering Structures, Elsevier Ltd, 32(6), 1704–1714.

Oh, K. H., Jung, C. K., Yang, Y. C., and Han, K. S. (2004). “Acoustic emission behavior during fatigue crack propagation in 304 stainless steel.” Key Engineering Materials, 261-263, 1325–1330.

Ohira, T., Kishi, T., Horiuchi, R. (1980). “Acoustic emission during fatigue crack propagation in structural materials”, International Acoustic Emission Symposium. 5: 137-45.

Paris, P C, and Erdogan, F. (1963). “A critical analysis of crack propagation laws.” Journal Of Basic Engineering, 85(4), 528–534.

Paris, P C, Gomez, M. P., and Anderson, W. E. (1961). “A rational analytic theory of fatigue.” The Trend in Engineering, 13(1), 9–14.

Railroads, A. of A. (1999). “Procedure for Acoustic Emission Evaluation of Tank Cars and IM101 Tanks.” Association of American Railroads, Washington, DC.

Roberts, T., and Talebzadeh, M. (2003a). “Fatigue life prediction based on crack propagation and acoustic emission count rates.” Journal of Constructional Steel Research, 59(6), 679–694.

Roberts, T., and Talebzadeh, M. (2003b). “Acoustic emission monitoring of fatigue crack propagation.” Journal of Constructional Steel Research, 59(6), 695–712.

Roy, S., Fisher, J W, and Yen, B. T. (2003). “Fatigue resistance of welded details enhanced by ultrasonic impact treatment (UIT).” International Journal of Fatigue, Th International Society of Offshore and Polar Engineering Conference, 25(9-11), 1239–1247.

Sinclair, A. C. E., Connors, D. C., and Formby, C. L. (1977). "Acoustic emission analysis during fatigue crack growth in steel." Materials Science and Engineering, 28, 263 – 273.

Tada, H., Paris, Paul C., and Irwin, G. R. (2000). The stress analysis of cracks handbook, Third Edition. ASME, Three Park Avenue New York, NY 10016-5990.

Yu, J., Ziehl, P., Zárate, B., and Caicedo, J. (2011). "Prediction of fatigue crack growth in steel bridge components using acoustic emission." Journal of Constructional Steel Research, Elsevier Ltd, 67(8), 1254–1260.

Ziehl, P. H. (2008). "Applications of acoustic emission evaluation for civil infrastructure." Proceedings of SPIE, SPIE, 69340I–69340I–8.

Ziehl, P. H., Engelhardt, M. D., Fowler, T. J., Ulloa, F. V., Medlock, R. D., and Schell, E. (2009). "Design and field evaluation of hybrid frp/reinforced concrete superstructure system." Journal of Bridge Engineering, 14(5), 309–318.

VITA

Navid Nemati was born in a small town by the Caspian Sea and worked in industry as a structural design engineer for over three years after obtaining a MS from the University of Tehran, Iran. While a Masters Student, he was part of a team researching FRP applications as strengthening materials for concrete and masonry structures and his thesis focused on "Numerical and experimental evaluation of shear strengthening in concrete beams using CFRP L-shaped plates". This work was done in collaboration with EMPA, the Swiss Federal Laboratories for Material Sciences and Technology. With his industrial experience in designing public and private buildings and structures, Navid chose to return to academia to conduct research on the international level. At the University of North Dakota, as a PhD student, he began his research on "Cyclic Buckling Behavior of Compression Members with Initial Out-of-flatness". When he learned the University of Miami's CAE department had just been awarded a five-year research project awarded by the NIST Technology Innovation program, he pursued his studies there. As a part of this department's team, his research focuses on Acoustic Emission Behavior of Steel Members Subjected to High Cycle Fatigue Loads, an almost completely new research area. He is a member of ASCE and ACI and has 3 submitted journal papers and 7 published conference proceedings. He was granted a Ph.D. degree from University of Miami in December 2012.